

**CHARACTERIZING THE PHYSICAL
AND CHEMICAL MASS TRANSPORT
OF DISSOLVED SALTS IN
LAYERED OIL SANDS WASTE
UNDERGOING RECLAMATION**

A Thesis Submitted to the College of
Graduate and Postdoctoral Studies
In Partial Fulfillment of the Requirements
For the Degree of Master of Science
In the Department of Geological Sciences
University of Saskatchewan
Saskatoon

By

CARLO ROSARIO CASANOVA CILIA

© Copyright Carlo Rosario Casanova Cilia, December 2017. All rights reserved.

PERMISSION TO USE

In presenting this thesis in partial fulfillment of the requirements for a Postgraduate degree from the University of Saskatchewan, I agree that the Libraries of this University may make it freely available for inspection. I further agree that permission for copying of this thesis in any manner, in whole or in part, for scholarly purposes may be granted by the professor or professors who supervised my thesis work or, in their absence, by the Head of the Department or the Dean of the College in which my thesis work was done. It is understood that any copying or publication or use of this thesis or parts thereof for financial gain shall not be allowed without my written permission. It is also understood that due recognition shall be given to me and to the University of Saskatchewan in any scholarly use which may be made of any material in my thesis.

Requests for permission to copy or to make other use of material in this thesis in whole or in part should be addressed to:

Head of the Department of Geological Sciences
University of Saskatchewan
114 Science Place
Saskatoon, Saskatchewan, Canada
S7N 5E2

ABSTRACT

This research aims to characterize the physical and chemical transport processes driving the distribution of dissolved salts in experimental reclamation scenarios that layer centrifuged fine tailings, petroleum coke, and reclamation material. Six field lysimeters were constructed at an oil sands mine near Fort McMurray, Alberta to assess various layering scenarios under both saturated and unsaturated conditions. Physical characteristics (temperature, water content), pore water geochemistry, and bulk mineralogy were characterized through collection of samples via multi-level monitoring wells, cores, and data loggers. Complimentary laboratory column experiments were set up to monitor the migration of dissolved ions over time, and conservative transport models developed as a means of assessing the major mass transport processes controlling salt distribution. Logger data and pore water chemistry revealed that self-weight consolidation and seasonal freeze-thaw cycles facilitate a volume change in the CFT that translates to an advective release of pore water toward the surface. Depth profiles of major ions and electrical conductivity consistently demonstrate that dissolved salt concentrations become elevated at the surface of saturated systems without a reclamation cover due to evaporation. Data suggests evaporative solute concentration has a larger influence on pore water chemistry in saturated systems. Measurable analyte concentrations were not observed near the surface of unsaturated systems with petroleum coke, due to a lack of available pore water to act as a vehicle for salt movement. Column experiments support the field data, suggesting that the saturated arrangements are at greater risk of surface salt accumulation than unsaturated complements. Both field and column experiments demonstrate that petroleum coke cannot host exchange reactions that mitigate dissolved salt migration. Modeling results support the idea that advection - hydrodynamic dispersion is the primary transport regime in early time due to initially rapid settlement of CFT. In the long-term, transport transitions to primarily diffusion dominated.

ACKNOWLEDGEMENTS

First and foremost, I would like to thank my supervisor Dr. Matthew Lindsay. Your infinite patience, gentle guidance, and unwavering support have been instrumental to the completion of this degree. I am grateful for the mentorship you have provided me throughout this journey. I would also like to thank Dr. Joyce McBeth and Dr. Lee Barbour for all the constructive feedback and guidance to improve this thesis. Special thanks to Lee Barbour for all the support and advice throughout the development of my transport models.

My eternal thanks to Lawrence Swerhone for being the most unbelievable field and lab partner throughout this entire process. Your friendship and support have meant the world to me from the moment we started this project and beyond. Thank you for listening to me talk for 9 hours straight on the way to Fort McMurray, for all the lab and field assistance, and for always encouraging visits to Sweet Basil (best Pho in Canada!). To the rest of the Environmental Geochemistry Research Group, especially: Noel Galuschik, Mattea Cowell, Colton Vessey, Jake Nesbitt, Qingyang Liu, Sarah Rudderham. You have all become a family to me in Saskatoon, and I will always cherish our lab socials, all the encouragement and chats in the lab and field, and the endless support you have shown me. A huge thank you to Dr. Kathryn Dompierre for all the phone calls helping me understand GeoStudio and contaminant transport modeling. This thesis would not have been completed without your patience and friendship. You have my most sincere gratitude.

Special thank you to Dr. Jing Chen, Fina Nelson, Erin Schmeling, and Thomas Bonli for all the support with sample analysis at the University of Saskatchewan, the Reclamation and Closure Research Team at Syncrude Canada Ltd., specifically Richard Kao, Wendy Kline, Janna Lutz, Jessica Percy, and Lori Cyprien, and ConeTech, Kevin Boyer, and Kelly Malo.

Thank you to the University of Saskatchewan, NSERC, and Syncrude Canada Ltd. for providing the funding that made this research possible.

And last but not least, thank you to my friends and family for all the unconditional love and support throughout the last two years. It has meant the world to me through this journey.

DEDICATION

To Anne Coady:

‘A teacher affects eternity;
he can never tell where his influence stops.’

– Henry Adams

TABLE OF CONTENTS

PERMISSION TO USE.....	i
ABSTRACT	ii
ACKNOWLEDGEMENTS	iii
DEDICATION	iv
LIST OF TABLES	vii
LIST OF FIGURES	viii
LIST OF ABBREVIATIONS	ix
Chapter 1: INTRODUCTION	1
1.1 Alberta Oil Sands Deposits	1
1.2 Bitumen Extraction and Upgrading.....	2
1.3 Fluid Fine Tailings	4
1.4 Oil Sands Process-Affected Water	5
1.5 Centrifuged Fine Tailings	6
1.6 Petroleum Coke.....	8
1.7 Transport Processes in Tailings.....	9
1.8 Layered Waste Scenarios	12
1.9 Reclamation Considerations	13
Chapter 2: RESEARCH SCOPE	15
2.1 Research Hypotheses and Objectives.....	15
Chapter 3: METHODOLOGY	17
3.1 Site Description	17
3.2 Field-Scale Lysimeter Experiments.....	18
3.2.1 Lysimeter Construction and Instrumentation.....	18
3.2.2 Pore-Water Sampling and Analysis	21
3.2.3 Core Sampling and Pore-Water Extraction.....	23
3.2.4 Solid-Phase Geochemical Characterization	23
3.3 Geochemical Modeling and Statistical Analysis.....	24
3.4 Laboratory Column Experiments	25
3.4.1 Column Setup	25
3.4.2 Pore-Water Sampling.....	27
3.4.3 Estimating Settlement Rates	28
3.4.4 One-Dimensional Solute Transport Modeling.....	28
Chapter 4: RESULTS	33

4.1	Field Experiments	33
4.1.1	Settlement	33
4.1.2	Pore-Water Geochemistry	33
4.1.3	Solid-phase analyses	57
4.1.4	PHREEQCi Modeling and Statistical Analysis	60
4.2	Column Experiments	61
4.2.1	Settlement Measurements	61
4.2.2	Column Water Chemistry	62
4.2.3	Transport Modeling	68
4.2.4	Sensitivity Analyses	70
Chapter 5:	DISCUSSION	73
5.1	Water and Salt Transport	73
5.2	Ion Exchange Reactions	76
5.3	Biogeochemical Processes	79
5.4	Conceptual Model	80
5.5	Model Limitations and Sensitivity	83
Chapter 6:	CONCLUDING REMARKS	86
6.1	Conclusion	86
6.2	Recommendations and Future Work	87
REFERENCES		89
APPENDIX A:	LYSIMETER SAMPLE LIST AND SAMPLE TYPE	100
APPENDIX B:	FIELD LYSIMETER PORE WATER GEOCHEMISTRY	105
APPENDIX C:	SOLID PHASE GEOCHEMISTRY	113
APPENDIX D:	COLUMN EXPERIMENT PORE WATER CHEMISTRY	114
APPENDIX E:	PHREEQC OUTPUT AND CORRELATION ANALYSIS	135

LIST OF TABLES

Table 3-1: Lysimeter fill arrangement and approximate thickness of waste layers.....	19
Table 3-2: Location of matric potential sensors and reflectometers in lysimeters	20
Table 3-3: Model input parameters.....	31
Table 4-1: Measured settlement in field lysimeters	33
Table 4-2: Measured settlement data in experimental columns	62
Table 4-3: RMSE calculated for changes in the rate of settlement parameter.....	71
Table 4-4: RMSE determined for varying values of coke porosity	72

LIST OF FIGURES

Figure 1-1: Schematic representation of bitumen extraction and upgrading	3
Figure 1-2: Schematic diagram of cation exchange on clays	8
Figure 3-1: Syncrude site map and the Deep Cake site	18
Figure 3-2: Schematic diagram of lysimeter construction.....	20
Figure 3-3: Schematic and photograph of laboratory column experiments.....	27
Figure 4-1: Temporal and spatial temperature profiles in lysimeters	35
Figure 4-2: Temporal and spatial conductivity profiles in lysimeters	36
Figure 4-3: Crossplots of bulk EC and temperature in CFT layers of field systems	38
Figure 4-4: Depth profiles of temperature through lysimeters at select times	40
Figure 4-5: Bulk EC and VWC depth profiles in unsaturated lysimeters	42
Figure 4-6: Bulk EC and VWC depth profiles in saturated lysimeters	43
Figure 4-7: Comparison of EC bulk and pore water EC in field lysimeters.....	44
Figure 4-8: Correlation between Cl and $\delta^{18}\text{O}$, and sample characterization on the LMWL	47
Figure 4-9: Depth profiles of Cl and $\delta^{18}\text{O}$ in field lysimeters	48
Figure 4-10: Depth profiles of pore water pH, alkalinity, and Eh in field lysimeters	50
Figure 4-11: Major cation concentrations with depth in the lysimeters	54
Figure 4-12: Comparison of relative concentrations of Na, Ca, and Cl in field systems	52
Figure 4-13: Ammonia and sulfate depth profiles in field lysimeters	56
Figure 4-14: XRD spectra from unsaturated lysimeters.....	58
Figure 4-15: XRD spectra from saturated lysimeters	59
Figure 4-16: Saturation indices for minerals of interest	61
Figure 4-17: pH, alkalinity, and EC depth profiles in laboratory columns	63
Figure 4-18: Depth profiles of Cl, Na, and Ca within laboratory column experiments	65
Figure 4-19: Depth profiles of Mg, K, and $\text{NH}_3\text{-N}$ within laboratory column experiments	67
Figure 4-20: Comparison of Na and Cl profiles in the saturated column.....	67
Figure 4-21: One-dimensional transport model results	69
Figure 4-22: Temporal change in the Peclet number within the saturated column	70
Figure 4-23: Sensitivity test of various rates of settlement	71
Figure 5-1: Conceptual model of layered systems.....	83

LIST OF ABBREVIATIONS

AER	Alberta Energy Regulator
AOSR	Athabasca Oil Sands Region
CBE	Charge Balance Error
CEC	Cation Exchange Capacity
CFT	Centrifuged Fine Tailings
EC	Electrical Conductivity (pore water)
EC _{bulk}	Bulk Electrical Conductivity (solids and solution)
FFT	Fluid Fine Tailings
HDPE	High Density Polyethylene
IC	Ion Chromatography
ICP-MS	Inductively Coupled Plasma – Mass Spectroscopy
ICP-OES	Inductively Coupled Plasma – Optical Emission Spectroscopy
L1	Lysimeter 1; Unsaturated with CFT, PC, and RM
L2	Lysimeter 2; Unsaturated with CFT and PC
L3	Lysimeter 3; Unsaturated with TS and CFT
L4	Lysimeter 4; Saturated with CFT, PC, and RM
L5	Lysimeter 5; Saturated with CFT and PC
L6	Lysimeter 6; Saturated with TS and CFT
LEL	Local Evaporation Line
LMWL	Local Meteoric Water Line
MFT	Mature Fine Tailings
OSPW	Oil Sands Process-Affected Water (or PW = Process Water)
PC	Petroleum Coke
PES	Polyestersulfone
PVC	Polyvinylchloride
RM	Reclamation Material
RMSE	Root Mean Square Error
SMP	Soil Matric Potential
SSA	Specific Surface Area
Syncrude	Syncrude Canada Ltd.

TDR	Time Domain Reflectometry
TMF	Tailings Management Framework
TS	Tailings Sand
VWC	Volumetric Water Content
WCR	Water Content Reflectometers
XRD	X-Ray Diffraction

CHAPTER 1: INTRODUCTION

1.1 Alberta Oil Sands Deposits

Oil sands development in Canada represents both a significant, positive stimulant for the economy and a source of environmental and health issues, posing risks for air, water, and soil quality as a byproduct of production and waste generation (Gosselin et al., 2010). Canadian oil sands represent the third largest reserve of extractable hydrocarbons in the world, following Saudi Arabia and Venezuela (Chen et al., 2013), facilitating a significant interest in the extraction of viable bitumen and production of synthetic crude oil. The majority of these oil sand deposits are located in Alberta, Canada, and are divided amongst three regions: the Peace River, Cold Lake, and Athabasca (Masliyah et al., 2004). The Athabasca Oil Sands Region (AOSR) represents the largest deposit of surface mineable oil sands in Canada, covering a total area of 50,000 km² and containing an estimated 171 billion barrels of recoverable bitumen reserves (CAPP, 2017). However, as extraction technology continues to improve, the quantity of recoverable bitumen and production potential in the AOSR is expected to grow substantially.

The AOSR geologic framework consists of three main formations: the deeper Waterways Formation, Wabiskaw-McMurray Formation and Clearwater Formation (Hein & Cotterill, 2006; Gibson et al., 2013). The bulk of the bitumen is hosted in Cretaceous aged sand with interbedded shales, sands, and silts of the Wabiskaw-McMurray Formation (Hein & Cotterill, 2006; Gibson et al., 2013). Underlying this formation is the deeper Waterways Formation of Devonian age, containing evaporite deposits within carbonate rock (Gibson et al., 2013). The near surface Clearwater Formation, which represents an approximately 10 m shale unit that grades from silt to fine-grained sand downward, overlies the Wabiskaw-McMurray Formation (Gibson et al., 2013). These units are overlain by a thin layer of Quaternary age glacial till sediment (Gibson et al., 2013). As a result of these near surface bitumen deposits (~60 – 80 m below the surface), surface mining methods remain the most efficient way to exploit large quantities of oil sands (Kasperski and Mikula, 2011). Based on current production and increasing global demand for oil, the amount of bitumen produced from mined oil sands ore is expected to climb to over 5.1 million barrels per

day by 2030 (CAPP, 2017). However, with increasing production comes the generation of large quantities of oil sands tailings waste, creating approximately 1 million m³ of fine tailings per day with a reported total volume of greater than 920 million m³, as of 2014 (Siddique et al., 2014). Due to the massive quantities of mine wastes and upgrading byproducts produced on site and limited space to store these materials, there is increasing pressure to reduce inventories and promote progressive reclamation.

1.2 Bitumen Extraction and Upgrading

Oil sands in the AOSR are composed of silt, clay, sand, water, and bitumen. Oil sand ore, by weight, contains approximately 85% mineral solids, 5% water, and 10% bitumen (Zubot et al., 2012). Bitumen is a high molecular weight, viscous hydrocarbon that requires treatment and further upgrading before it is in a usable form fit for distribution (Masliyah et al., 2004). To begin the bitumen extraction process, surface mining removes surficial sediments to expose the bitumen-rich Wabiskaw-McMurray formation sediment and facilitate extraction of oil sands ore. This ore is then crushed, mixed with recycled process water, and transported as slurry to an extraction plant. The Clark hot water process is used to begin separation of bitumen from the ore; hot water (as high as 75°C), caustic soda (NaOH), and solvent such as naphtha are added to aid in the liberation of bitumen through a reduction in bitumen viscosity (Masliyah et al., 2004). Addition of NaOH creates an alkaline environment suitable for production of surfactants in the slurry, which aid in bitumen release (Masliyah et al., 2004). Surfactant production is a natural, pH dependent process where high pH promotes release of asphaltic acids from bitumen and facilitates a three-phase contact point that relieves surface and interfacial tension for removal of bitumen from sand grains (Chalaturnyk et al., 2002; Masliyah et al., 2004). Elevated Na concentrations in the slurry from the caustic soda enhance the dispersal of clays within the water film surrounding the sand grains, helping to break down the ore and release bitumen (Chalaturnyk et al., 2002). Aeration of the slurry further enhances bitumen release from sand grains. The resulting bitumen slurry is then passed into a primary separation vessel where aerated bitumen is skimmed off the top as bitumen froth, which contains approximately 60% bitumen, 30% water, 10% solids (Masliyah et al., 2004). At this point, the addition of naphtha solvent helps separate the remaining water and solids from the bitumen. A byproduct of the bitumen extraction and treatment process is creation of tailings waste streams containing unrecovered bitumen and organics, oil sands process-affected water (OSPW), solids, and solvent.

Bitumen recovered from oil sands ore remains highly viscous and requires upgrading in order to produce marketable synthetic crude oil. Oil sands operators employ a complex coking and hydro-treatment process that produces lighter hydrocarbon compounds through thermal cracking of long-chain bitumen molecules, and subsequent exposure to hydrogen which saturates the molecules (Shah et al., 2011; Puttaswamy and Liber, 2012). This process creates a solid, carbonaceous, heterogeneous product known as petroleum coke that contains elevated sulfur and metal contents (Puttaswamy and Liber, 2012). The result of the upgrading process is synthetic crude oil that is ready for transport to refineries that will further refine the product to produce usable petroleum products to meet global demand (Figure 1-1). Currently, petroleum coke waste production and stockpiling is occurring at a rate of 20,000 tonnes per day in the AOSR, with projected production to reach a total of 1 billion m³ coke waste over the lifespan of oil sands exploitation (Puttaswamy et al., 2010; Yuan et al., 2010).

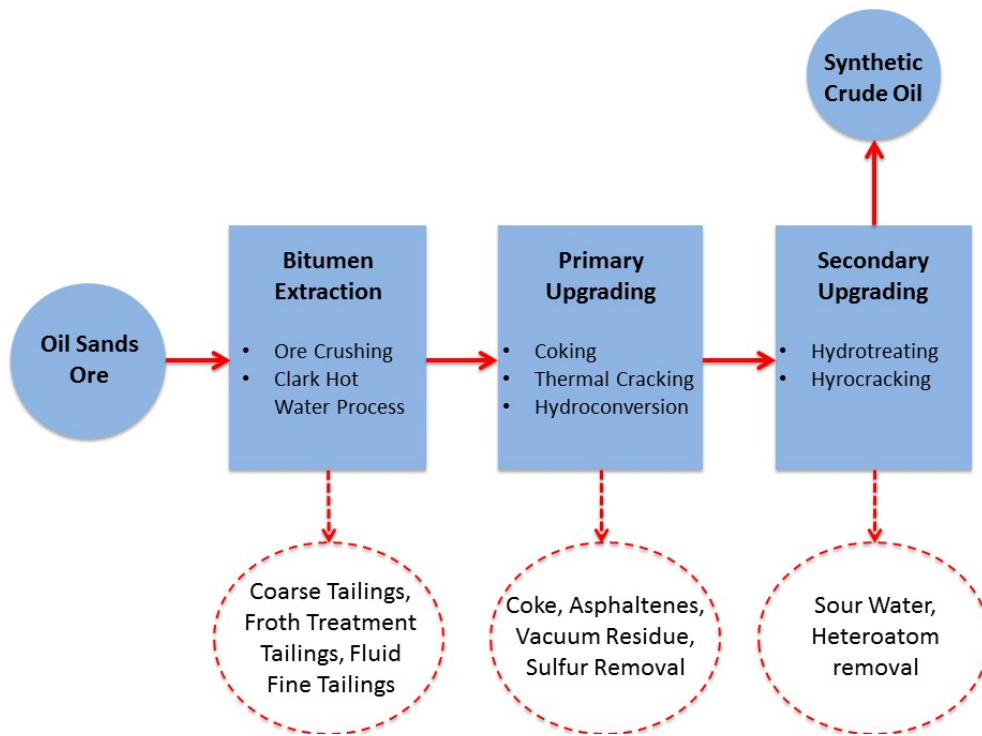


Figure 1-1: Schematic representation of the bitumen extraction and upgrading process to produce crude oil. Solid arrows represent subsequent steps in the production process. Dashed arrows and lines represent waste products produced at each step (adapted from Gray 2015).

1.3 Fluid Fine Tailings

Commercial production of synthetic crude oil generates large quantities of fluid fine tailings (FFT). For every 1000 m³ of synthetic crude oil produced, approximately 5000 m³ of overall mine waste and upgrading byproducts are generated, with 2500 m³ being associated with fine tailings waste (Luna Wolter and Naeth, 2014). Each day, approximately 1 million m³ of FFT are produced during bitumen extraction, with waste being stored in artificially constructed tailings ponds (Siddique et al., 2014). Fluid fine tailings are composed of a mixture of OSPW and solids, with the solid fraction containing 82% sand, 17% dispersed fines, and 1% residual bitumen, by weight (Chalaturnyk et al., 2002; Kasperski and Mikula, 2011). The fines fraction of FFT is composed primarily of quartz and clay minerals, with particle size being characteristically less than 44 µm (Kasperski and Mikula, 2011). By weight, the mineralogy of the fines can vary between 20-80% clays depending on the ore (Kasperski and Mikula, 2011). Disposal of FFT in tailings ponds begins the process of natural consolidation of tailings particles, with the coarser tailings sand settling first. This leaves a slurry of fines and OSPW in suspension with initial settling at approximately 10% solids by weight (Siddique et al., 2014). Literature reports that consolidation of fines after approximately three to five years reaches about 30 wt% solids (Kasperski and Mikula, 2011; Siddique et al., 2014), at which point it is referred to as mature fine tailings (MFT). However, natural consolidation to greater than 30 wt% can take tens to hundreds of years due to the interaction of negatively charged clay particles associated with the fines. As a result, FFT clay mineralogy plays an important role in the settling behaviour of oil sands tailings waste.

The clay mineralogy of FFT is consistent with that of bulk Athabasca oil sand deposits, composed primarily of kaolinite (40-70 wt%) and illite (28-45 wt%), with minor smectite (montmorillonite, 1-15 wt%) and chlorite (Omotoso and Mikula, 2004; Kasperski and Mikula, 2011; Hooshar et al., 2012). Montmorillonite is an expanding 2:1 clay, with a high specific surface area that undergoes isomorphic substitution within tetrahedral and octahedral layers resulting in a net negative charge. The highly negative surface charge can be balanced by cations present in the surrounding pore fluid, resulting in a high cation exchange capacity (CEC; Liu et al., 2004). In contrast, kaolinite is a non-swelling, 1:1 with a lower specific surface area and less isomorphic substitution, which results in a lower CEC. Additionally, illite is a 2:1 non-expanding clay with characteristics intermediate to that of kaolinite and montmorillonite. Large quantities of interlayered clay deposits have been reported in FFT, being predominantly interlayered kaolinite-

smectite and illite-smectite. This interlayered smectite arrangement explains the high surface area and cation exchange capacity of tailings solids (Omotoso and Mikula, 2004; Botha and Soares, 2015). Kaminsky et al. (2009) reports specific surface area and cation exchange capacity (as methylene blue index) in the clay fraction of tailings as high as 319 m²/g and 38 meq/100 g, respectively.

Clay composition has important implications for the settling behaviour of FFT deposits, due to the overall negative surface charge and size of the diffuse double layer of clay particles. The negative surface charge is balanced by a variety of cations adsorbed onto the clay surface, usually sodium (Na⁺), calcium (Ca²⁺), magnesium (Mg²⁺), and potassium (K⁺). Additions of NaOH during the bitumen extraction process introduce large quantities of Na⁺ into FFT, facilitating exchange of Na⁺ in solution with other cations bound to the clay surface. Sodium increases the thickness of the electrical double layer of these clays, increasing dispersion and causing a significant decrease in the rate of consolidation. Currently, oil sands operators are attempting to find solutions that will increase consolidation rates in an economical, efficient, and sustainable manner. As production and tailings waste inventories increase, greater pressure will be placed on industry to deal with excess waste storage and water reuse issues. Enhanced settling of fines in tailings ponds is critical to the implementation and success of future reclamation plans, and requires greater attention.

1.4 Oil Sands Process-Affected Water

With the production of FFT waste streams comes the simultaneous generation of oil sands process-affected water (OSPW): a mixture of water, unrecovered bitumen, hydrocarbons, and inorganic salts that are concentrated during the extraction process. Currently, 2.2 barrels of Athabasca river water are required to produce one barrel of bitumen, with the remaining water requirements satisfied from recycled process water (COSIA, 2017). This results in the creation of 4 m³ of OSPW per m³ of oil sands ore extracted (Giesy et al., 2010). Tailings waste streams are stored in on-site tailings ponds where solids settle over time and concomitantly release OSPW. Once OSPW naturally separates from the solids fraction, it can be pumped from tailings ponds for reuse in the bitumen extraction process. This recycling of OSPW in oil sands operations alleviates the need to extract freshwater from the nearby Athabasca River, reducing the water requirement of producing a barrel of oil. However, continual cycling of OSPW through the Clark hot water process concentrates OSPW with increasing amounts of contaminants creating brackish, alkaline water with elevated toxicity (Abolfazlzadehdoshanbehbazari et al., 2013). This poses a substantial

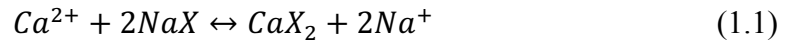
problem for reclamation efforts as dewatering of tailings waste, implemented in closure landscapes, releases OSPW trapped in pores facilitating migration of water into overlying vegetation layers.

Existing research conducted in oil sands environments has extensively covered the impacts of naphthenic acids (NA) and inorganic salts associated with OSPW, as these contaminants have proven toxic for a wide variety of flora and fauna (Frank et al., 2009; Han et al., 2009; Luna Wolter and Naeth, 2014). The elevated salinity of OSPW is of particular concern due to Na, which has the potential to impact the pore water chemistry of tailings waste and are toxic to vegetation and some invertebrates. Ions such as Ca^{2+} , Mg^{2+} , Na^+ , chloride (Cl^-), ammonium (NH_4^+), and sulfate (SO_4^{2-}) are all present at concentrations that exceed what is found in most near-surface groundwater systems (Abolfazlzadehdoshanbehbazari et al., 2013).

1.5 Centrifuged Fine Tailings

As a means of addressing the issue of increasing waste production and recycling of OSPW, the Alberta Energy Regulator (AER) implemented Directive 074 in September of 2009. Directive 074 mandated that oil sands operations reduce FFT inventories on site by 50% over 5 years. To accomplish this, operators aimed to create more trafficable waste deposits and enhance recycling of generated OSPW (AER, 2009). This would encourage progressive reclamation efforts and help decrease the quantity of natural water taken from the surrounding Athabasca River. In response to this directive, oil sand operators have begun investigating a number of technologies to enhance dewatering and facilitate out-of-pit deposition of trafficable fine tailings. Large-scale centrifugation of FFT waste streams have demonstrated promising ability to enhance consolidation of tailings up to 70% solids content through rapid acceleration several times the force of gravity (Rima and Azam, 2015). Application of decanter centrifugation technology has proven to create a more consolidated, dry stackable tailings deposit while simultaneously reducing the water requirements of producing a barrel of bitumen through increased recycling of process-water (Mikula et al., 2009).

Before fine tailings are centrifuged, they are amended with gypsum ($\text{CaSO}_4 \cdot 2\text{H}_2\text{O}$) and polyacrylamide in order to assist in consolidation. Fine tailing have been previously amended with 1 kg of gypsum per m^3 of fine tailings in order to achieve desired geotechnical characteristics for use in dry reclamation landscapes (Matthews et al., 2002). Dissolution of gypsum releases Ca^{2+} that readily exchanges with Na^+ and other cations at the clay mineral surfaces (Equation 1):



where X represents an exchange site at a clay-mineral surface. When Na^+ replaces Ca^{2+} on the mineral surface, hydraulic conductivity is decreased as increased Na^+ increases the repulsive barrier between particles and hinders clay particle aggregation, reducing water infiltration. Conversely, when Ca^{2+} replaces Na^+ on the mineral surface there is a decrease in the size of the electrical double layer of clays, as fewer Ca^{2+} ions are required to satisfy the net negative charge, therefore promoting the consolidation of negatively charged tailings (Figure 1-2; Brown et al., 2013). This exchange reaction decreases the electrical double layer thickness, increasing consolidation and dewatering of tailing solids. Addition of polyacrylamide, with an optimal anionicity of 20-30%, assists in flocculating clays and allows for greater packing (Sworska et al., 2000). The resulting waste product, referred to here as centrifuged fine tailings (CFT), has a lower water content making it more trafficable for direct use in dry reclamation initiatives. Little is known regarding pore-water chemistry and solute transport within CFT deposits, which could have implications for mine reclamation. Seasonal freeze-thaw of CFT can facilitate release of OSPW within pores, potentially inducing upward migration of this water through soil cover. Currently, Directive 074 has been suspended by the AER and replaced by Directive 085 (AER, 2015), in response to the release of a Tailings Management Framework for Mineable Athabasca Oil Sands (TMF) by the Government of Alberta, in order to better align tailings management goals (Government of Alberta, 2015). The aim of the TMF is to provide a framework for the management and reduction of FFT inventories, with sights set on reclamation within 10-years of mine closure (Government of Alberta, 2015). The momentum provided by Directive 074, Directive 085, and the TMF is continually demonstrated through the outpouring of research currently being conducted on technologies for effective management and reduction of FFT waste stockpiled on active mining sites.

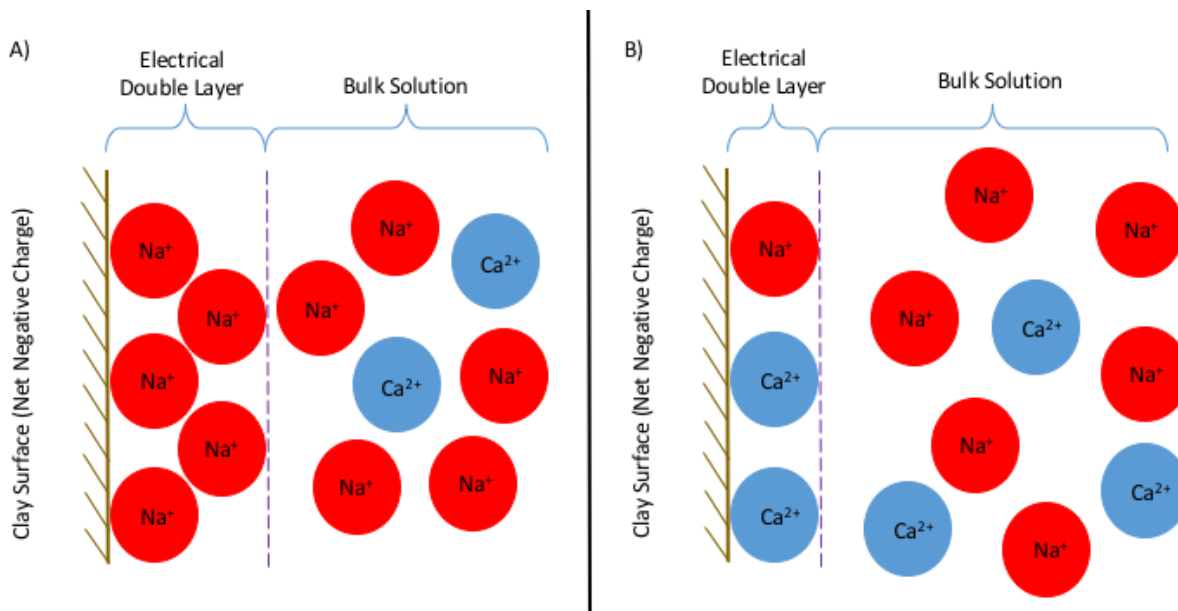


Figure 1-2: Schematic diagram illustrating: (A) clay equilibrated with a Na^+ dominated solution and (B) clay equilibrated with a Na^+ - Ca^{2+} solution. Ca^{2+} is able to exchange with Na^+ , decreasing the thickness of the electrical double layer of the clay particle.

1.6 Petroleum Coke

On-site inventories of petroleum coke waste have grown as oil sands operations expand, placing pressure on operators to deal with increasing storage considerations. Despite its carbon rich content, petroleum coke contains high levels of sulfur and heavy metals and a low combustibility, making it a poor energy source with current technologies (Puttaswamy and Liber, 2012; Nesbitt et al., 2017). As a means of decreasing petroleum coke stockpiles and encouraging progressive reclamation, operators have begun implementing petroleum coke into dry reclamation scenarios, usually involving placement of coke underneath vegetative soil cover (Nakata et al., 2011). This technique poses problems for reclamation due to the potential release of heavy metals from coke grains, and uptake of these toxic metals by plants and aquatic invertebrates (Nakata et al., 2011; Baker et al., 2012). Nickel and vanadium have been identified as the primary metals responsible for toxicity of coke leachate, and are released from the asphaltene fraction of petroleum coke (Baker et al., 2012; Puttaswamy and Liber, 2012). Vegetation roots may extend from reclamation cover downward into the petroleum coke layer, facilitating uptake of vanadium and nickel rich coke pore water and inducing phytotoxic effects. Nakata et al. (2011) reports that plant exposure to both capped and uncapped coke layers causes visual signs of plant stress such as leaf

chlorosis, leaf tip necrosis, stunted growth, and decreased physiological functions (i.e. transpiration and stomatal conductance) due to uptake of leached metals from coke. Alternatively, coke has been reported to adsorb NA and organics from OSPW, enhancing the remediation of ingressing process water (Zubot et al., 2012).

Petroleum coke has the potential to leach other potentially-hazardous metals such as Mo, Zn, Al, and Mn, which may accumulate in leachate and enhance pore water toxicity over time (Kessler and Hendry, 2006; Puttaswamy et al., 2010; Puttaswamy and Liber, 2011). Numerous studies have shown that exposure to petroleum coke and petroleum coke leachate places vegetation, organisms, and even human health at risk of toxic effects due to elevated metal concentrations (Singh, 1971; Ward, 1978; Puttaswamy et al., 2010; Nakata et al., 2011; Puttaswamy and Liber, 2011; World Health Organization, 2011; Tchounwou et al., 2012). Leachate or pore-water concentrations of Zn (1 to 125 $\mu\text{g L}^{-1}$), As (3.2 to 4.6 $\mu\text{g L}^{-1}$), Mo (82 to 3576 $\mu\text{g L}^{-1}$), Ni (16 to 62 $\mu\text{g L}^{-1}$), Se (9 to 26 $\mu\text{g L}^{-1}$), and V (1079 to 2950 $\mu\text{g L}^{-1}$) have been reported for oil sands petroleum coke (Puttaswamy et al., 2010; Puttaswamy and Liber, 2012; Nesbitt, 2016; Nesbitt and Lindsay, 2017). Overall, these issues have raised concerns about the use of petroleum coke as a substrate in active reclamation environments. Further studies are, therefore, required to understand the long term, in-situ impacts of petroleum coke in reclamation environments.

1.7 Transport Processes in Tailings

Contaminant transport represents a potential long-term risk to the sustainability of mine closure landscapes. The success of oil sands mine closure depends on an in-depth understanding of the transport mechanisms controlling the mass distribution of dissolved salts in reclamation substrates. In both natural and anthropogenically altered systems, contaminant transport is attributed to three main processes: diffusion, advection, and hydrodynamic dispersion. Mass transport theory has been well established (Freeze and Cherry, 1979; Fetter, 1999; Fetter, 2001; Appelo and Postma, 2005; Cussler, 2009), with current research focused on applications to more complex and poorly understood systems such as the case of oil sands tailings systems.

Molecular diffusion is the process by which dissolved ions and aqueous species move across a concentration gradient, independently of water movement. Contaminated systems that do not experience a hydraulic gradient are still at risk of contaminant plume migration due to the process of diffusion. Fick's first law (Equation 1.2) expresses the relationship between the mass flux of solute and the concentration gradient in a porous medium, in one dimension:

$$J_d = -D^*n_e \left(\frac{dC}{dx} \right) \quad (1.2)$$

where J_d is the diffusive mass flux of solute ($M L^{-2} T^{-1}$), D^* is the effective coefficient of molecular diffusion ($L^2 T^{-1}$), n_e is the effective porosity, and $dC dx^{-1}$ is the concentration gradient ($M L^{-3} L^{-1}$). Moreover, in groundwater flow regimes advective transport becomes an important mechanism distributing solutes. Advection is the process by which solutes are physically moved along the flow of groundwater. In one dimension, the mass flux can be related to the quantity of water flowing through the following relationship (Equation 1.3):

$$J_a = vn_e C \quad (1.3)$$

where J_a is the advective mass flux of solute ($M L^{-2} T^{-1}$), v is the average linear pore water velocity ($L T^{-1}$), n_e is the effective porosity, and C is the solute concentration ($M L^{-3}$). This can be written in terms of the Darcy flux (q) which shares the same units as v (Equation 1.4).

$$J_a = qC \quad (1.4)$$

In a very fine grained porous medium, the average linear pore water velocity may be negligible such that, despite there being a hydraulic gradient, diffusion becomes the dominant transport process.

Additionally, variations in the average linear pore water velocity exist at the macroscopic scale due to the intrinsic properties of the porous media, which include the pore size, path length, and friction induced by the grains (Fetter, 1999). As a result of these variations in groundwater movement through the pores, mixing of the solute is induced at the leading front of flow and is known as mechanical dispersion. This mixing can occur both along the flow path and perpendicular to flow, and are termed longitudinal dispersion and transverse dispersion, respectively. Diffusion plays a crucial role on the mixing of solutes, and thus the diffusion coefficient is included in the definition of the coefficient of hydrodynamic dispersion (Equation 1.5):

$$D_H = \alpha v + D^* \quad (1.5)$$

where D_H is the hydrodynamic dispersion coefficient ($L^2 T^{-1}$), α is the longitudinal or transverse dispersivity (a property of the medium), v is the average linear pore water velocity ($L T^{-1}$), and D^* is the effective diffusion coefficient ($L^2 T^{-1}$). Therefore, the coefficient of hydrodynamic dispersion can be related to the hydrodynamic dispersive mass flux (Equation 1.6):

$$J_H = -D_H n_e \left(\frac{dc}{dx} \right) \quad (1.6)$$

where J_H is the hydrodynamic dispersive mass flux ($M L^{-2} T^{-1}$). Derivation of a one-dimensional advective-hydrodynamic dispersive flow expression was accomplished using these equations and the idea of conservation of mass flux through a representative elementary volume (Equation 1.7):

$$\frac{\partial c}{\partial t} = D_H \left(\frac{\partial^2 c}{\partial x^2} \right) - v \frac{\partial c}{\partial x} \quad (1.7)$$

which is changed to a diffusion only transport equation (Equation 1.8) given that there is no water flow:

$$\frac{\partial c}{\partial t} = D^* \left(\frac{\partial^2 c}{\partial x^2} \right) \quad (1.8)$$

It is possible to evaluate the extent of solute transport that occurs due to advection, dispersion, and diffusion by utilizing a dimensionless number known as the Peclet number. The Peclet number is given by a ratio of the general form:

$$\frac{v_x d}{D_d}$$

where v_x is the average linear pore water velocity, d is some characteristic flow length, and D_d is the coefficient of molecular diffusion. Understanding the evolution of the Peclet number in a given flow system can reveal the main mechanisms governing contaminant distribution at a specific point in time.

A large body of literature exists that succinctly characterize mass transport of solutes through fine grained porous media, including research that discusses natural clay aquitard systems,

mechanisms of ion distribution in clay tills, and semi-permeable clay membranes, to name a few (Hendry and Wassenaar, 2000; Malusis et al., 2003; Hendry and Wassenaar, 2011; Barbour et al., 2012). Additionally, research investigating the migration of dissolved salts into reclamation covers and out of tailings ponds, in oil sands environments, have been well defined (Kelln et al., 2008; Kessler et al., 2010; Abolfazlzadehdoshanbehbazari et al., 2013; Dobchuk et al., 2013; Holden et al., 2013). However, the majority of studies done on mass transport in oil sands environments have not focused on reclamation landscapes that incorporate tailings waste. An initial study completed by Dompierre and Barbour (2016) was the first attempt to elucidate the complex processes governing the movement of dissolved ions through FFT undergoing active reclamation in the oil sands. This investigation revealed that the release of water by FFT settling decreases over time, facilitating a diffusion dominated transport regime over time (Dompierre and Barbour, 2016). In this system, it is expected that advection-driven solute migration will be predominant in the early stages of reclamation, facilitating the release of contaminants to the overlying water cover of the experimental end-pit lake (Dompierre et al., 2016). Despite the best efforts of preliminary research, little is known regarding mass transport processes in most oil sands waste streams, specifically CFT. Moreover, application of wastes in multi-layer arrangements in preparation for mine closure has not been studied extensively, resulting in a gap in knowledge surrounding the mechanisms controlling migration of contaminants through these systems. An in depth understanding of chemical mass transport in CFT is crucial for its implementation into closure landscapes, as contaminant transport holds significant risks for the future of reclamation initiatives.

1.8 Layered Waste Scenarios

Natural consolidation of CFT and seasonal freeze-thaw cycles are important processes governing tailings dewatering and solute transport. As the air temperature drops below 0°C during winter months, water in the CFT pore space freezes and expands. The onset of spring facilitates melting of ice in the pore space, resulting in the expulsion of pore water upward. The advective release and migration of CFT pore water provides an opportunity for the highly saline water to interact with cover material and vegetation. Rooney et al. (1998) identify that the successful growth of cover vegetation in reclaimed areas continues to be jeopardized by the capillary rise of contaminated pore water. To address this issue, layered waste containing materials with different grain sizes have been considered and implemented as a capillary break and preventative measure for landscapes undergoing active reclamation. Capillary barriers function by imposing coarse

grained material overtop layers with a finer pore structure. The smaller pore structure of the fine grained material holds water at a higher tension than the coarse grained material, preventing water from entering the coarse material (Ho and Weber 1998; Naeth et al., 2011). Research studies investigating the in-situ reclamation of mine waste have determined that the use of coarse grained material to impose a capillary break between a vegetative cover and waste has been successful in isolating plants from contaminated groundwater (Tordoff et al., 2000; Lottermoser et al., 2009). Careful consideration is necessary when making decisions regarding the materials used to reclaim disturbed landscapes, as these carry important implications for its success post mine closure.

The oil sands industry aims to deal with inventories of all waste products on site before bitumen mining is complete in the AOSR. This has sparked interest and research into the implementation of various waste streams in reclamation design. The coarse, well-sorted nature of petroleum coke grains create a deposit with superb drainage and poor water retention (Nakata et al., 2011), making this material an ideal candidate for use as a capillary barrier between underlying tailings waste deposits and overlying reclamation material. The use of petroleum coke as an intermediary layer may accommodate release water volumes and prevent dissolved solutes from reaching reclamation covers. Moreover, the geochemical properties of petroleum coke may aid in the mitigation of dissolved analyte distribution into surface layers. An investigation conducted by Baker et al. (2012) assessed the potential of implementing petroleum coke overtop various substrates, including composite tailings, in preparation for wetland reclamation. Their findings suggested that further research was necessary to discern whether or not reclamation was possible using petroleum coke, as coke pore water exhibited elevated metal concentrations that poses risks to water quality and wetland health (Baker et al., 2012). The effectiveness of petroleum coke as a reclamation substrate is still uncertain, and very little is known regarding its long-term interaction with tailings streams, including CFT.

1.9 Reclamation Considerations

As a means of decreasing the volume of tailings waste stored on-site and addressing future mine closure requirements, various dry reclamation scenarios are being considered by oil sand operations. Implementation of dewatered, stackable CFT is currently being explored for long-term reclamation scenarios, due to the consolidated, dry, and trafficable nature of these deposits. According to Allen (2008), typically dry reclamation landscapes would consist of a base layer of dewatered FFT, overlain by a material with a different physical structure (i.e. sand), and capped

by a vegetative soil layer. However, due to the amendments of gypsum and polyacrylamide added to CFT during centrifugation, the pore water chemistry of CFT differs drastically than that of FFT deposits. As a result, little is known regarding the release and migration of high salinity pore water from CFT and the concomitant geochemical reactions that could take place within overlying materials. In addition, implementation of layered, multi-waste systems is being considered to deal with growing quantities of various waste streams on site. Specifically, petroleum coke is being considered as a cap above the CFT waste, due to its sand-like grain size and porous nature and the desire to reclaim growing stockpiles of this waste byproduct. However, the direct interactions between CFT and petroleum coke have not been studied, and it is unclear whether this arrangement has the potential to facilitate growth of a healthy reclamation cover over long periods. Furthermore, mass transport processes in tailings systems undergoing active reclamation are poorly defined, and it is unclear whether layered waste arrangements will mitigate both the rate of salt migration and quantity of salts to reclamation covers. Therefore, the geochemical interactions and mass transport processes occurring within and between these layered waste deposits need to be constrained in order to assess whether the use of these waste streams are viable options for long-term mine closure plans.

CHAPTER 2: RESEARCH SCOPE

Oil sands operators are currently exploring the implementation of CFT in various closure scenarios, as its production reduces the volume of waste that requires storage. Coupled with a cap of petroleum coke waste, this arrangement may allow the industry to deal with stockpiled waste products, while achieving reclamation goals for mine closure. However, natural settling and dewatering of CFT, combined with seasonal freeze-thaw cycles, can promote the release of toxic OSPW. The elevated salinity of released OSPW is a major concern to reclamation initiatives as upward migration of salts, at elevated concentrations, will impose toxic effects on establishing vegetation and organisms, and degrades reclamation soil structure. Currently, little is known about salt migration through layered waste systems containing CFT. Release and transport of Na^+ from CFT pore water may drive ion exchange reactions within and between deposits of these multi-layered systems; however, the geochemical and ion exchange reactions within these layered waste systems are poorly constrained, and may hold critical implications on future reclamation design. Furthermore, the use of petroleum coke as a cap above CFT deposits has not been attempted and, therefore, its ability to act as a capillary barrier and useful reclamation substrate, in this setting, is not well defined. Therefore, this thesis aims to understand the release and physical transport of salt from CFT deposits and identify the resulting geochemical and ion exchange reactions that occur, within and between layers in these multi-waste systems. Additionally, the chemical mass transport processes governing dissolved salt distribution will be characterized using field lysimeters and laboratory column experiments to elucidate the key controls on contaminant migration throughout multi-layered waste systems in a reclamation context.

2.1 Research Hypotheses and Objectives

Research hypotheses tested through this thesis include:

- (1) self-weight consolidation and freeze-thaw cycles drive upward vertical advective transport of OSPW and associated salts from CFT layers;

- (2) salt transport within adjacent petroleum coke and cover soil layers is largely conservative; and
- (3) evaporation promotes salt accumulation within shallow CFT, petroleum coke and soil cover layers.

The specific objectives of this study were to:

- (1) evaluate the extent of salt release and migration from underlying CFT deposits into overlying petroleum coke and reclamation cover;
- (2) elucidate the geochemical reactions occurring within individual waste layers and at layer interfaces, in various multi-layer systems; and
- (3) assess the potential of a petroleum coke to mitigate salt transport in multi-layered waste systems

CHAPTER 3: METHODOLOGY

3.1 Site Description

The Mildred Lake mine represents one of the largest surface mining operations in the world, covering an expansive 1000 km² (Dompierre et al., 2016). Operated by Syncrude Canada Limited (Syncrude), the Mildred Lake site is located approximately 35 km north of Fort McMurray, in northern Alberta, Canada. The climate at the Mildred Lake mine is consistent with a continental environment that is sub-humid in nature (Carey, 2008). Maximum and minimum mean daily temperatures were determined to be 18.9°C (July) and -16.6°C (January), respectively, over an eighteen-year period (1997 – 2016) at the Mildred Lake weather station (57°02' N, 111°33' W; Environment Canada, 2016) located near the active mine site. Mean annual precipitation reported from daily total precipitation data over sixteen-years (1999 – 2015) is reported as 373.9 mm at this site (57°02' N, 111°33' W; Environment Canada, 2016), with rainfall events occurring more frequently between the months of June and August and averaging 50 mm (Carey, 2008; Environment Canada, 2016). Snowfall contributes about one third of the annual precipitation from September to May, which is common considering the extended winters experienced at this climate (Carey, 2008; Dompierre et al., 2016).

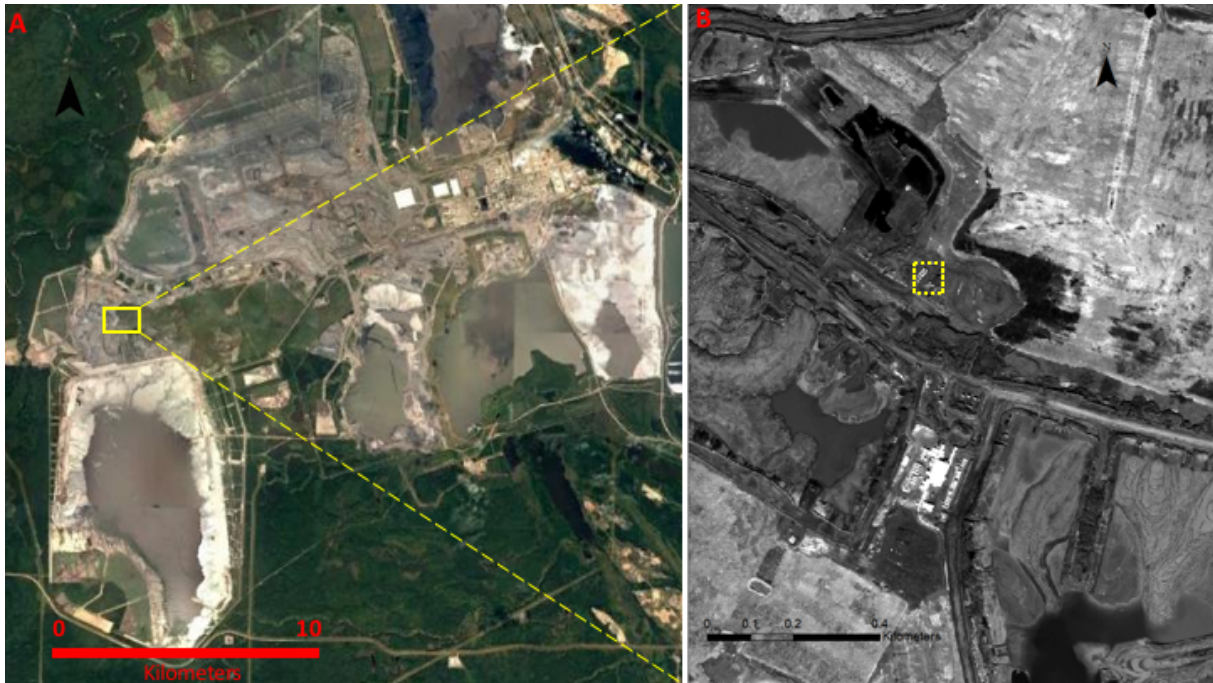


Figure 3-1: (A) Site map of Syncrude's Mildred Lake Mine, with highlighted study area. (B) Aerial photograph of the Deep Cake site with the specific study area outlined by the yellow, dashed line (Photos provided by Synrude).

3.2 Field-Scale Lysimeter Experiments

Research was focused on a set of field-scale lysimeters located in close proximity to the Deep Cake Research Facility ($57^{\circ}0'42.02''$ N, $111^{\circ}46'37.50''$ W) at the Mildred Lake Mine (Figure 3-1).

3.2.1 Lysimeter Construction and Instrumentation

Six field lysimeters were constructed and installed at the Mildred Lake Mine in the spring of 2015. Each cylindrical lysimeter measured 2.92 m in diameter and 3 m in height, and were uncovered at the top. Prior to placement of fill material and instrumentation, lysimeters were partially buried to 1.8 m below the ground surface to focus seasonal freezing at surface. Lysimeters were filled with different layers of CFT, petroleum coke, tailings sand, and soil cover material to mimic potential mine closure scenarios (Table 3-1). The three scenarios used for the six lysimeters were: (1) CFT, petroleum coke, reclamation material consisting of a peat-mineral mix; (2) CFT, petroleum coke; (3) CFT, tailings sand. These materials were placed in each lysimeter using an excavator in early October 2015, at specific thicknesses chosen to imitate potential reclamation decisions (Table 3-1). Fresh water from Syncrude's water treatment plant, sourced from the Mildred Lake reservoir, was used to maintain saturated conditions within three of the lysimeters

(L4, L5, L6), whereas water was not added to the other three unsaturated lysimeters (L1, L2, L3). The lysimeters were constructed without a basal drain and therefore precipitation and evaporation determined the degree of saturation maintained throughout the year in the unsaturated lysimeters. Fresh water was again added in July 2016 and again in August 2016 to ensure the water-saturated conditions were maintained in the saturated lysimeters. It is important to note that tailings sand in L6 was not directly saturated, as the cap CFT layer prevented infiltration of fill water into the base.

Table 3-1: Lysimeter fill arrangement and approximate thickness of waste layers (in parentheses) in each lysimeter at the end of filling (reported in meters); RM = Reclamation Material, PC = Petroleum Coke, CFT = Centrifuge Fine Tailings, TS = Tailing Sand.

Layering	Lysimeter					
	Unsaturated			Saturated		
	1	2	3	4	5	6
Cover	RM (0.5)	-	-	RM (0.5)	-	-
Layer 1	PC (1)	PC (1)	CFT (2)	PC (1)	PC (1)	CFT (2)
Layer 2	CFT (1.5)	CFT (2)	TS (1)	CFT (1.5)	CFT (2)	TS (1)

Lysimeters were instrumented with: (1) water content reflectometer (WCR) probes (Campbell Scientific, model CS655-L), which use the time-domain reflectometry (TDR) method; and (2) soil matric potential (SMP) sensors (Campbell Scientific, model CS229-L), which utilize the heat dissipation method. The WCRs measured electrical conductivity (EC) and temperature in addition to volumetric-water content. Four SMP sensors and six WCR probes were installed in each lysimeter. These instruments were placed during filling within individual material layers and material interfaces in order to capture a suite of geochemical and hydrological data that would provide key insight into the movement of salts and pore water (Figure 3-2; Table 3-2). The instruments were connected to two data loggers (Campbell Scientific, model CR1000), containing channel-relay multiplexors (Campbell Scientific, model AM16/32B), that were programmed to be accessed remotely. Both data loggers were connected to solar panels (Campbell Scientific, model MSX10) mounted to instrument tripods, allowing for continuous power supply and data collection. All sensors were calibrated prior to installation by O’Kane Consultants (Saskatoon, SK), and associated calibration equations were determined so that values could be converted into

meaningful data. Measurements are ongoing and are made every four hours, and began October 28, 2015.

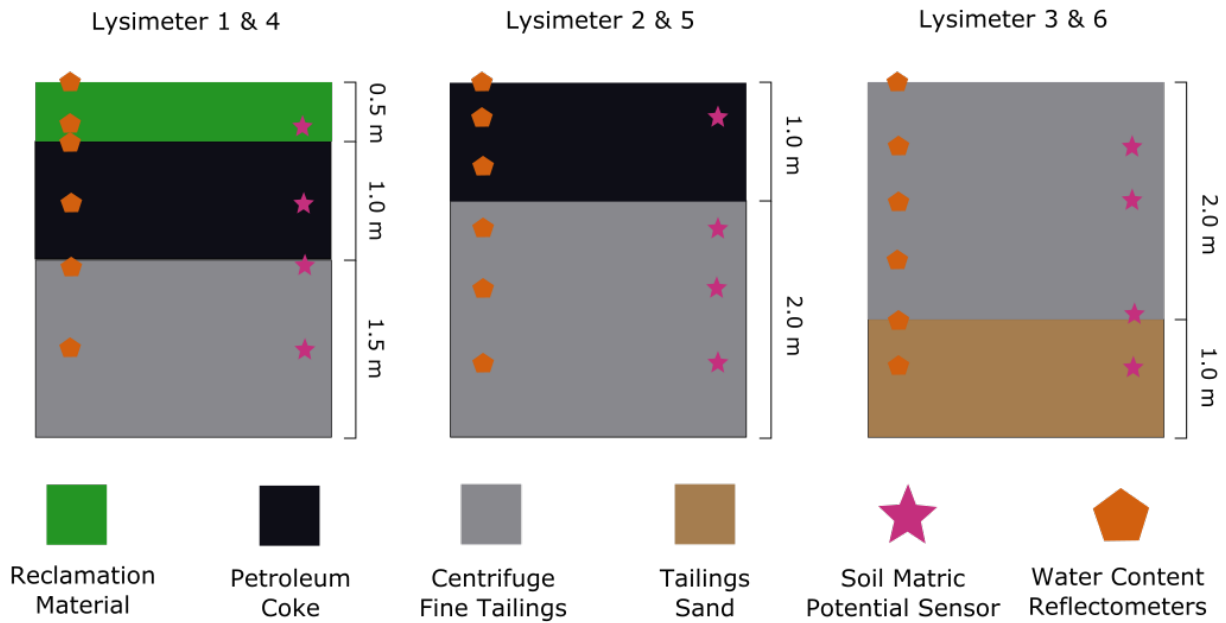


Figure 3-2: Schematic diagram of lysimeter fill arrangement and relative placement of probes/sensors. Lysimeters 1, 2, and 3 were kept unsaturated and lysimeters 4, 5, and 6 were saturated.

Table 3-2: Location of CS655-L probes and CS229-L sensors in each lysimeter in October 2015, reported as cm below lysimeter surface.

Lysimeter	Instrumentation									
	Soil Matric Potential Sensors (CS229-L)				Water Content Reflectometers (CS655-L)					
	1	2	3	4	1	2	3	4	5	6
L1	225	150	90	36	225	150	90	50	36	0
L2	238	172	125	30	238	172	125	70	30	0
L3	240	195	100	55	240	200	152	100	55	0
L4	226	145	85	30	226	145	85	47	30	0
L5	239	175	115	40	239	175	115	68	40	0
L6	245	178	93	50	245	200	115	93	50	0

Multi-level monitoring wells were constructed from polyethylene tubing with a $\frac{1}{4}$ inch outer diameter, varying in length from 2.75 (surface) to 5.5 m (bottom) depending on their location in the lysimeter. V-shaped notches were cut into the bottom of each piezometer over a length of 10 cm and covered with a 125 μm porous Nitex mesh to exclude solids during pumping. Twelve wells were bundled to a 1.9 cm outer diameter by 3 m long polyvinyl chloride (PVC) tube such that the screened sections were spaced 25 cm apart on center. The bundles were positioned vertically within the center of each lysimeter prior to filling.

Measurements of material settlement within each lysimeter were made 9 months and 13 months after initial construction. The initial depth to the material surface from the top of the lysimeters was measured immediately following lysimeter construction. No method was put in place to collect frequent settlement data, and measurements were limited to site visits.

3.2.2 Pore-Water Sampling and Analysis

Initial sampling was conducted in August 2016, approximately 10 months after lysimeter construction. This timing ensured the materials underwent one complete seasonal freeze-thaw cycle prior to sampling. Water sampling was attempted at each depth for each of the six the multi-level wells. Due to limitations on the quantity of pore water available, 1.5 well volumes (150 mL) were purged prior to sampling each well to ensure that representative samples were being drawn. Pore water sample were drawn from each well using a peristaltic pump (Geotech Environmental Equipment Inc.). Clean 0.6 cm silicone tubing (Masterflex) was attached to each polyethylene sampling well and guided through the peristaltic head to begin sample collection.

Pore water pH, reduction-oxidation potential (Eh), electrical conductivity (EC), and temperature were measured immediately following pore water extraction, due to the time-sensitive nature of these analyses. Measurements of pH and Eh were completed on unfiltered water samples, while EC was measured on samples filtered through 0.45 μm polyestersulfone (PES) syringe filter membranes (Pall Corporation, USA) using sterile 30 mL syringes (HSW GmbH, Germany). The pH electrode (Thermo Scientific, model 8172BNWP) was calibrated before each sampling period with a 3-point calibration using NIST-traceable pH 4, 7, 10 buffer solutions (Thermo Scientific). Prior to sampling, the Eh electrode (Thermo Scientific, model 9678BNWP) was checked using Zobell's (Nordstrom, 1977) and Light's (Light, 1972) solutions (Ricca Chemical) to ensure that the electrode was functioning optimally. The conductivity probe (Thermo Scientific,

model 011050MD) was calibrated using a standard 1413 $\mu\text{S}/\text{cm}$ NaCl solution (Thermo Scientific), and corrected for temperature. Similarly, analysis of pore water alkalinity, sulfide (S^{2-}), and ammonia ($\text{NH}_3\text{-N}$) were carried out directly after sample collection – to minimize oxidation and degassing of samples – on water passed through 0.45 μm PES syringe filter membranes. Alkalinity was determined by titrating sample to the bromocresol green-methyl red endpoint using 1.6 and 0.6 N H_2SO_4 . Both dissolved sulfide and ammonia were measured spectrophotometrically with a portable spectrophotometer (HACH Company, model DR2800) using the methylene blue method (HACH Method 8131) and salicylate method (HACH Method 10031), respectively.

Samples were also collected for determination of dissolved major cation, anion, and trace element concentrations present in lysimeter pore water. Preservation of samples for major cation and trace element analysis required passing samples through 0.2 μm PES syringe filter membranes into 15 mL high-density polyethylene (HDPE) bottles, and acidification to $\text{pH} < 2$ with trace metal grade nitric acid (HNO_3 ; Omnitrace, EMD Millipore, USA). Inorganic anion samples were filtered through a 0.45 μm PES syringe filter membrane into 15 mL HDPE bottles and did not require acidification for preservation. All samples were kept in coolers on ice, transported back to the University of Saskatchewan, and stored in a 4°C fridge until analysis. Major cations, anions, and trace elements were quantified by inductively coupled plasma – optical emission spectroscopy (ICP – OES; EPA Method 200.7), ion chromatography (IC; EPA Method 300.0), and inductively coupled plasma – mass spectrometry (ICP – MS; EPA Method 200.8), respectively. Analysis of major cations were carried out at the University of Saskatchewan, while trace element and inorganic anion samples were shipped to Edmonton, AB to be analyzed by Syncrude’s research and development lab.

The stable isotopes of water were also quantified in lysimeter pore water by determining the $\delta^2\text{H}$ and $\delta^{18}\text{O}$ values. The δ notation delineates the ratio between the heavy and light isotope of that element as they relate to both a standard and specified sample (Appelo and Postma, 2005). Water isotope samples were filtered through a 0.45 μm PES filter membrane and stored in 15 mL HDPE bottles with no headspace. All samples were kept over ice in a cooler, transported to the University of Saskatchewan, and kept at 4°C until analysis. Analysis was completed at the University of Saskatchewan using a $\text{H}_2\text{O}_{\text{liquid}} - \text{H}_2\text{O}_{\text{vapor}}$ equilibration method that employs off-axis integrated cavity output spectroscopy (OA-ICOS) as described by Wassenaar et al. (2008).

Identifying the isotopic signature of lysimeter pore water samples is important to the understanding of the water provenance and its geochemical evolution (Appelo and Postma, 2005).

3.2.3 Core Sampling and Pore-Water Extraction

Coring of unsaturated and saturated lysimeters occurred November 2016 using a drive-point, piston technique that allowed for continuous core samples to be retrieved at 0.6 m intervals over the entire depth of each lysimeter. Cores were collected and stored in aluminum casings that measured 7.2 cm in diameter. Immediately following recovery, the cores were sealed on one end with paraffin wax and polyethylene caps at both ends, and sealed with electrical tape to limit exposure to oxygen. The aluminum core tubes were then transported back to the University of Saskatchewan and kept in a freezer at -20°C until analysis. Compaction during core collection was assumed to be linear; therefore, the actual length recovered was divided by the push length in order to calculate a compression factor that was used to determine the interval at which cores were cut. Each 0.6 m core sample was subsampled into 0.15 m intervals, corrected with the predetermined compression factor, in preparation for pore water extraction and solids analysis. The cores were sectioned using a reciprocating saw, and subsamples were labelled with the appropriate depth range, capped and kept frozen at -20°C until analysis.

Subsampled cores were transferred into an anaerobic chamber ($<5\%$ H_2 gas, balance N_2 gas), left to thaw for 3 to 4 hr, and then extruded. Plastic, sterile scoopulas were used to extract sample, excluding sample at the top and bottom as well as around the outer layer due to possible contamination and oxidation. Samples were collected in 50 mL polypropylene centrifuge tubes for both pore water and solids analyses. Three to seven centrifuge tubes were filled for each core, depending on sample availability. Collected sediment samples were placed in a centrifuge (Eppendorf, model 5804 R) and spun at 10,000 rpm ($8,500 \times g$) for 30-45 minutes, depending on the degree of saturation of each core. Immediately following centrifugation, the extracted pore water was pooled together for each specific core, and analysis was conducted following previously-described methods (§ 3.2.2). For ease of data analysis, the midpoint depth of each core was utilized to represent the sampling depth. Remaining centrifuged sample was stored at -20°C until solid-phase analysis.

3.2.4 Solid-Phase Geochemical Characterization

Bulk mineralogy was examined by X-Ray Diffraction (XRD) on initial CFT samples obtained during lysimeter construction ($n = 2$) and on CFT samples collected in 2016

approximately 13 months after the experiment was initiated ($n = 18$). This approach facilitated comparison of changes in CFT mineralogy over time. Samples were prepared for XRD using two methods to mount solid samples on the slides, as a means of comparison for the purpose of maximizing spectra quality. Frozen solids were first thawed in an anoxic atmosphere ($<5\%$ H_2 gas, balance N_2 gas) and then placed within a vacuum desiccator. The vacuum desiccator was sealed using vacuum grease to ensure that pressure was maintained for over 24 hours. Using a vacuum pump, a tight vacuum seal was applied to desiccators in the anoxic chamber, and samples were left to dry for 24 hours. Once dried, samples were crushed to $<100 \mu\text{m}$ using an agate mortar and pestle, mounted on a glass slide, and mixed with methanol to create randomly oriented sample slides. Preferentially oriented sample mounts were prepared from thawed solids by creating a slurry with deionized water in order to suspend the solids. Samples were shaken for 10 seconds on a benchtop vortex and allowed to settle for 10 minutes to ensure heavier sands and quartz grains settled out and fine particles – including clays – to remain suspended. Approximately 1 mL of this suspension was pipetted onto a glass slide and allowed to air dry overnight. This approach permits clay platelets to settle in a well-oriented arrangement and leaves out heavier quartz grains that would otherwise dominate XRD spectra. Dried sample slides were then placed in an ethylene glycol atmosphere and left to glycolate at 65°C for 1 hour. Glycolation is done to treat swelling clays (i.e. smectites) and improve XRD data quality in clay-rich mounts (USGS, 2001). A Panalytical Empyrean diffractometer was used to perform XRD with a $\text{Co K}\alpha$ source ($\lambda = 1.79$) operated at 40 kV and 45 mA, with a $\text{Fe K}\beta$ filter and an incident beam slit size of 1° . One dimensional diffraction spectra were collected from $5\text{-}80^\circ 2\theta$ with a resolution and time per step of 0.0167° and 50 s, respectively. Baseline determination, phase identification, and peak labeling was completed using the X'Pert HighScore Plus software (version 3, Panalytical).

Cation exchange capacity was estimated on lysimeter CFT from core subsamples ($n = 13$) and Syncrude petroleum coke samples ($n = 2$) using the methylene blue method as described by Holden et al. (2012). Specific surface area of both CFT and petroleum coke samples was determined using values obtained through the methylene blue titration method, based on the methods outlined by Yukselen and Kaya (2008).

3.3 Geochemical Modeling and Statistical Analysis

Thermodynamic modeling using PHREEQCi (Version 3.3.5; Parkhurst and Appelo, 1999) with the WATEQ4F database (Ball and Nordstrom, 1991) was used to assess data quality and

controls on water chemistry. Saturation indices (SI) were determined from the modeling output to give an indication of the mineral phases most likely present in or out of solution, at equilibrium, and to assess changes in solid-phase geochemistry throughout waste layers. The charge balance error (CBE) provided by the PHREEQC model is a robust indication of data quality, and is given by the following equation:

$$CBE (\%) = \frac{(\Sigma cations + \Sigma anions)}{(\Sigma cations - \Sigma anions)} \times 100 \quad (3.1)$$

where a CBE of less than 5% is generally acceptable.

Pearson's correlation analysis was also conducted on all pore water samples obtained from lysimeter wells and core subsamples to assess relationships between dissolved constituents. Data was first normalized using a centered log-ratio transformation so that values would exhibit a normal distribution, reducing the amount of skew. To transform the dataset, the geometric mean of all analytes in the sample was tabulated, and the resulting mean was divided from the value of each analyte. This facilitates a change in the dataset such that the sum of all the values is 0. The mean and standard error of bulk pore water samples were also tabulated.

3.4 Laboratory Column Experiments

3.4.1 Column Setup

Laboratory column experiments were set up in order to investigate the mechanisms controlling salt transport across multi-layer waste systems, mimicking potential closure scenarios discussed by oil sand operators. Two columns measuring 1.52 m in height and having a 0.184 m inner diameter were acquired for use in this experiment. Sampling ports were installed at an interval of 0.1 m across the entire length of the columns – beginning at 0.2 m from the base (bottom most port) and ending at 1.4 m from the base (top most port) – and measure 0.0381 cm in diameter. Each sampling port was threaded and equipped with PVC caps at the time of column construction. A hole was drilled through each PVC cap, instrumented with a Rhizon soil moisture sampler (Eijkelkamp Soil and Water, model E365-192122), and sealed with marine silicon to prevent potential leaks throughout the experiment.

The specific layered waste arrangement used for this investigation was a thin, 0.05 m layer of tailings sand, overlain by 0.90 m of CFT, and capped by 0.5 m of petroleum coke. The CFT

used for these experiments was not amended with gypsum before being sent to the University of Saskatchewan. To maintain consistency with the field experiments, which contain gypsum amended CFT, all CFT samples received from the mine site were amended with gypsum ($\text{CaSO}_4 \cdot 2\text{H}_2\text{O}$; Sigma Aldrich) at the University of Saskatchewan. Analysis of CFT collected from the field lysimeters in October 2015 was utilized to estimate the gypsum amendment rate employed by SCL. It was assumed that the average CFT sulfate pore water concentration is indicative of the quantity of gypsum added, and that no appreciable amounts of sulfate precipitated into solid-phase minerals. The average concentration of sulfate in field CFT pore water was determined to be $1173 \pm 154 \text{ mg L}^{-1}$, which translates to 2.10 g of gypsum per liter of CFT pore water. Using this concentration, and the gravimetric water content of the CFT, the gypsum amendment rate was calculated to be 1.7 kg/tonne dry CFT. This value is in good agreement with the amendment rate used by SCL on full scale CFT deposits at the mine site, as reported by Heaton (2015). Gypsum was added to unamended CFT as a slurry, utilizing a 1:10 ratio of gypsum to ultrapure water ($18.2 \text{ } \Omega\text{m cm}^{-1}$, Mili-Q, Millipore), and homogenized thoroughly for 5 minutes.

A $\frac{3}{4}$ inch diameter PVC pipe was placed throughout the length of each column, serving as a support for the samplers. Waste materials were carefully placed into the columns using a chute made out of plastic sheeting, to allow for better control. PVC caps with samplers were not screwed into their respective ports until columns were filled to the height of the port. Samplers were secured to the PVC pipe using plastic zip ties, in order to prevent the samplers from being dragged during settlement of waste materials. Once the samplers were secured onto the columns, column filling was continued slowly as to not damage the samplers. After the columns were completely filled, one of the columns was fully saturated using deionized water and the other was left unsaturated for the first 6 months of the experiment. After 6 months, the unsaturated column was fully saturated with deionized water and monitored identically to the other column. The rationale for this was to begin taking measurements after initial settlement had slowed down extensively, allowing for a comparison between a system with a large initial advective release of pore water and that with minimal pore water release (Figure 3-3). Data from the unsaturated column after the 6 month timepoint will not be discussed in this thesis.

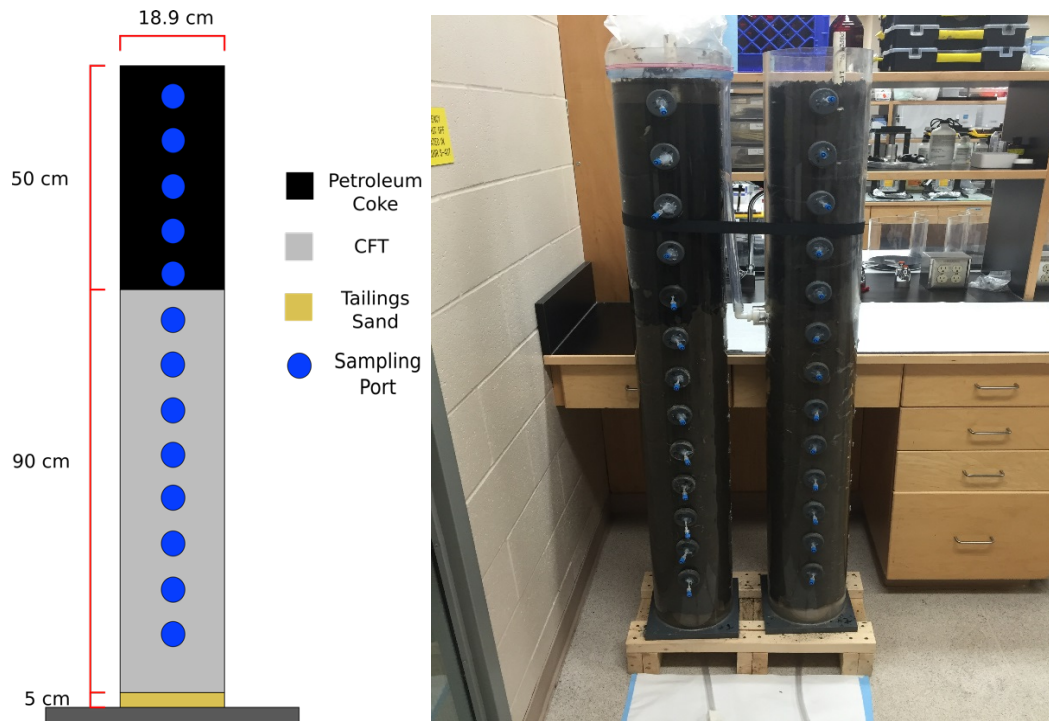


Figure 3-3: Left: schematic representation of layered column experiments; Right: photograph of the fully constructed columns. The left column is fully saturated and the right column unsaturated (September, 2016).

3.4.2 Pore-Water Sampling

Columns were left for 4 days prior to initial sampling so that the systems could settle. The first sampling period occurred in late September 2016, and was repeated twice in October 2016. Sampling was then carried out on a monthly basis beginning December 2016 onward to April 2017, allowing for 8 discrete sampling periods over a 202-day period (8 months). During the initial 6-month period, the unsaturated column did not yield water within the coke and, therefore, only sampling of CFT pore water could be successfully completed. Therefore, the unsaturated column was sampled over 146 days (February 2017), after which it was fully saturated in March 2017 permitting the collection of a full sampling profile. Monitoring of the newly saturated system continued until May 2017, and was sampled biweekly. Column pore water was collected by attaching a 30 mL syringe to each sampling port and applying a continuous vacuum to each of them. Draw in of water through the Rhizon soil samplers occurred slowly throughout the CFT layers, so syringes were left on the sampling ports for a period of 2 days under vacuum so that sufficient pore water could be collected for analysis. Geochemical analysis of column pore water

was completed using previously-described methods (see §3.2.2). Due to the limitation on the quantity of water extracted at each depth, water samples for analysis of major cations, anions, trace elements, and water isotopes were stored in 4 mL HDPE sample bottles.

3.4.3 Estimating Settlement Rates

Changes in the thickness and relative heights of each waste layer within the saturated and unsaturated columns were measured and recorded throughout the entirety of the experimental time frame, as a means of tracking CFT settlement. It was assumed that any apparent change in the total height of the waste material in either column associated with a decrease in the CFT volume. Although the petroleum coke layer may have settled slightly during the first few weeks of the experiment being run, the change in the layer thickness was minimal compared to the changes observed in the CFT layer. The decrease in CFT volume over the total experiment time was used to estimate the settling rate of the CFT. Using this information, it was possible to estimate the volume of water released from the CFT, assuming that the volume decrease corresponded to a release of an equal volume of water.

3.4.4 One-Dimensional Solute Transport Modeling

Pore-water movement and solute transport in the saturated experimental column was modeled using commercial finite element software (CTRAN/W, GEO-SLOPE International Ltd., 2012; SEEP/W, GEO-SLOPE International Ltd., 2015). Conservative, one-dimensional chloride transport models were developed to elucidate the major controls on mass distribution of a conservative tracer within the experimental system, simulating both diffusive and advective-hydrodynamic dispersive mass transport scenarios. A 1.4 m column was set as the model domain and divided into 2 layers: a 0.77 m CFT layer and 0.50 m petroleum coke layer. Setting the CFT layer at 0.77 m aimed to mimic total settlement of the CFT over 202 days and prevent over complication associated with modeling settlement over time. Advection rates were instead varied throughout the model to capture changing settlement. In the saturated column models, a 0.23 m water cap was placed to mimic the conditions of the saturated laboratory column, giving it an overall model domain of 1.5 m.

Model parameters for each layer material were selected based on values established in the literature and their appropriateness to the conceptual model (Table 3-3). For the purposes of this model, selection of specific material hydraulic conductivities was not necessary to satisfy the conceptual model. In order to maintain the applied darcy flux, the model simply altered the

hydraulic gradient regardless of the hydraulic conductivity used. The saturated hydraulic conductivity of petroleum coke was estimated using its effective grain size (D_{10}), which is reported as 0.08 mm by Kessler and Hendry (2006), yielding a value of $7.68 \times 10^{-3} \text{ cm s}^{-1}$. As the structure of petroleum coke resembles that of a coarse, well-sorted sand, comparison to the literature reveals that this estimate is in excellent agreement with the range of 10^{-4} to $10^{-1} \text{ cm s}^{-1}$ reported for sand (Freeze and Cherry, 1979). The value of saturated hydraulic conductivity used for the CFT was estimated from the void ratio based on a relationship described by Proskin et al. (2010) for MFT. The void ratio was determined using gravimetric data and an estimated value for CFT particle density, converting the information into a volumetric relationship. The K_{sat} value was determined to be $1.44 \times 10^{-7} \text{ cm s}^{-1}$, however for implementation in the model a value of $1.44 \times 10^{-3} \text{ cm s}^{-1}$ was chosen, being four orders of magnitude greater. Since the saturated hydraulic conductivity is not an important parameter to satisfy the conceptual model, the value was reduced to avoid over complicating the model simulation.

Porosity values were chosen under the assumption that a singular value could represent the pore structure of bulk CFT and coke deposits. However, it is important to recognize that the porosity of CFT changes throughout deposits as the pore structure collapses due to self-weight consolidation. Furthermore, the heterogeneous nature of petroleum coke would result in varying porosity values throughout the deposit. However, this assumption was made in order to prevent over complication of the model and to create a simple solution that would enhance understanding of salt distribution through layered systems. A porosity value of $0.6 \text{ m}^3 \text{ m}^{-3}$ was chosen for the CFT, which is reasonable for a material similar to a silty-clay. Studies have determined the volumetric water content of FFT and MFT to be around 0.86 (Owolagba and Azam, 2013; Dompierre and Barbour, 2016), with a decrease to a volumetric water content of 0.6 after centrifugation (Owolagba and Azam, 2013). Considering fine tailings remain tension saturated, the volumetric water content is a fairly reasonable estimate of the porosity of the material. The porosity of petroleum coke implemented in the model was $0.4 \text{ m}^3 \text{ m}^{-3}$ which is within the range of 0.26 to 0.43 reported for coarse sand (Das, 2008) and is close to the reported porosity of 0.38 for a sandy aquifer system (Dance and Reardon, 1983). The porosity of Syncrude petroleum coke was previously reported by Northwest Corporation (2003) as 0.3; however, this value seemed to provide a poor fit for the model. Petroleum coke contains a heterogeneous structure; therefore it is likely that the porosity varies through bulk deposits. The effective diffusion coefficient (D^*) for

each material was determined based on a value for the free ion diffusion coefficient of chloride (Li and Gregory, 1974; Cussler, 2009), the porosity and the tortuosity. A study by Boudreau (1996) defines a relationship between porosity and the tortuosity for fine grained materials. As CTRAN/W defines the D^* as the tortuosity multiplied by the coefficient of molecular diffusion, the porosity was used to calculate the tortuosity and thus determine the value of D^* . The relationship outlined by Boudreau (1996) worked well for estimating D^* of CFT, while an equation developed by Weissberg (1963) and later modified to create the Modified-Weissberg equation was used to estimate the tortuosity of petroleum coke:

$$\tau = \frac{1}{1-b*\ln(\theta)} \quad (3.2)$$

where τ is the tortuosity factor, θ is the porosity, and b is a fitting parameter.

The α_L and α_T were estimated to be 5×10^{-4} m and 10^{-10} m respectively, which are both low. Initially, the relationship described by Fetter (1999) was employed, estimating the dispersivity by multiplying the flow length by 0.1. For the columns, this yields a longitudinal dispersivity value of 0.05 m. However, when applied to the model, the results demonstrated that the level of dispersion was overestimated, resulting in a model that did not explain the data well. As the migrating plume within the experimental columns was observed to be small, the longitudinal dispersivity was estimated to be 0.0005 m, two orders of magnitude less than the initial value of 0.05 m. This value provided a better fit to the model. For the purposes of this model, it was assumed that flow and distribution of salts occurred principally parallel to the direction of groundwater flow (in the vertical direction), and therefore transverse dispersivity was assigned a low value of 10^{-10} m. The dry density values were taken from the Safety Data Sheets provided by Syncrude for both their fluid petroleum coke and centrifuged MFT.

To model the diffusion only scenario, a hydrostatic flow condition was established with a constant head (Dirichlet) condition of 1.5 m imposed at the top of the column. A transient flow condition was implemented for the advective-dispersive problem, imposing a constant head boundary at the top of the column with a constant head value of 1.5 m, and a specified flux (Neumann) condition at the bottom of the column. To address the specified flux boundary, a

Darcy flux (q) versus time function was estimated using the root time settlement method, based on consolidation theory, to simulate column settlement and associated advective pore water flux:

$$\text{Settlement} = \sqrt{t} \times a \quad (3.3)$$

where t is elapsed time and a is a constant representing the rate of settlement that can be adjusted to best suit the conceptual model. Settlement rates generated from the root time method were compared to measured column values to produce a best-estimate function for use in the numerical model. Using estimated advection rates from the measured column data was also used to determine how the value of Peclet's number changed over time. The Peclet number can be used to support the transport modeling results and reveal the dominating transport processes within these layered systems.

Table 3-3: Model input parameters.

Parameters	Materials		
	CFT	Petroleum Coke	Water Cap
K_{sat} (m/day)	1	6.64	100
Porosity (m^3/m^3)	0.60	0.40	1.0
D^* (m^2/day)	0.000080	0.00012	0.00016
α_L (m)	0.00050	0.00050	0.00050
α_T (m)	1×10^{-10}	1×10^{-10}	1×10^{-10}
Dry density (g/cm^3)	1.45	1.09	0
Activation Concentration (Normalized)	1	0	0

Sensitivity analyses were completed to assess the responsiveness of the model to variations in specific parameters. This allows for an understanding of which parameters exhibit a greater control on the model outcome and where the greatest amount of variability and uncertainty exists in a given numerical model. Moreover, sensitivity analysis provides a check on the optimization of parameters selected for the model by quantifying the amount of error between measured values and the predicted model. For the purposes of the one-dimensional conservative transport model, the root mean square error (RMSE) was computed to assess the

sensitivity of changes in the rate of settlement and the porosity of the coke. RMSE is computed by finding the average of the square of the residuals and taking the square root of that value.

CHAPTER 4: RESULTS

4.1 Field Experiments

4.1.1 Settlement

Measured settlement data in field systems revealed that after 13 months, total settlement ranged from 0.33 m (L1) to 0.57 m (L3) (Table 4-1). Additional data, 2 years from initial construction, was measured on saturated lysimeters, and the maximum settlement was 0.65 m. In general, lysimeters that contained a thicker CFT layer experienced less settlement than those with a thinner layer (i.e., L1, L4). Measurements were not performed on unsaturated lysimeters after two years, and settlement data was only recorded during major field campaigns to site. Consistent settlement data was not collected due to limited access to the field site.

Table 4-1: Measured settlement data in field systems.

Lysimeter	Initial depth to material surface, from top of lysimeter (m)	Total Settlement (m)		
		October, 2015	July, 2016	November, 2016
L1	0.085	0.31	0.33	-
L2	0.127	0.46	0.47	-
L3	0.088	0.51	0.57	-
L4	0.062	0.34	0.39	0.48
L5	0.076	0.37	0.46	0.61
L6	0.148	0.49	0.54	0.65

4.1.2 Pore-Water Geochemistry

4.1.2.1 Temperature, EC, and Volumetric Water Content

Data loggers provided both temporal and spatial understanding of water movement and salt migration in experimental lysimeters. Continuous temperature and bulk EC (EC_{bulk}) – a

combination of solution EC and soil EC – data was collected for 551 days since the initial construction of field lysimeters (October 28, 2015 – May 1, 2017), including information at 6 discrete depth locations in each system. Plots of temperature and EC_{bulk} over this 551-day period, at each depth, highlight the seasonal variations experienced within each reclamation prescription (Figure 4-1 and Figure 4-2). All lysimeters exhibited similar temperature trends over 551 days, characterized by seasonal highs in the summer months (June – August) and seasonal lows throughout the winter months (December – February). Spatially, shallower depths in all systems experience a greater extent of both daily and seasonal temperature fluctuations than deeper locations, highlighted by enhanced variability in the curves and greater extent of seasonal temperature change, near surface. The difference in variability with depth is attributed to differences in thermal material properties between the different material layers. Generally, CFT at lower depths contains more water as it is tension saturated and fine grained. As a result, tension saturated CFT loses heat slowly during the winter months and is less susceptible to temperature fluctuations, due to the high specific heat capacity of water. Furthermore, tension saturated CFT has a fairly low thermal conductivity relative to saturated petroleum coke, due to its finer grain size. This makes CFT more resistant to heat loss overall.

Near surface EC_{bulk} follows an almost identical trend to seasonal temperature variations, with highs and lows occurring over the same span of months, suggesting that temperature and EC_{bulk} fluctuations are closely related. However, differences are apparent in the winter months as EC_{bulk} plummets to values of near 0, beginning mid-December to January and remaining low until late spring. This immense drop in EC_{bulk} near the surface is most likely explained by freezing during the winter months. Time-domain reflectometry methods utilize the dielectric permittivity of the material to determine EC_{bulk} values (Noborio, 2001; Campbell Scientific, 2012). The dielectric constant of ice is much less than water (Noborio, 2001) making it much more difficult to measure EC_{bulk} when frozen, as ice cannot store as much electrical energy as water. At greater depth, EC_{bulk} remains between 0.5 to 2 mS cm^{-1} year-round, with the exception of L3 and L6 where values are consistently less than 1 mS cm^{-1} . Lysimeter 3 and 6 were constructed with tailings sand as the base layer, explaining the low salinity compared to the other systems which have highly saline CFT at the base.

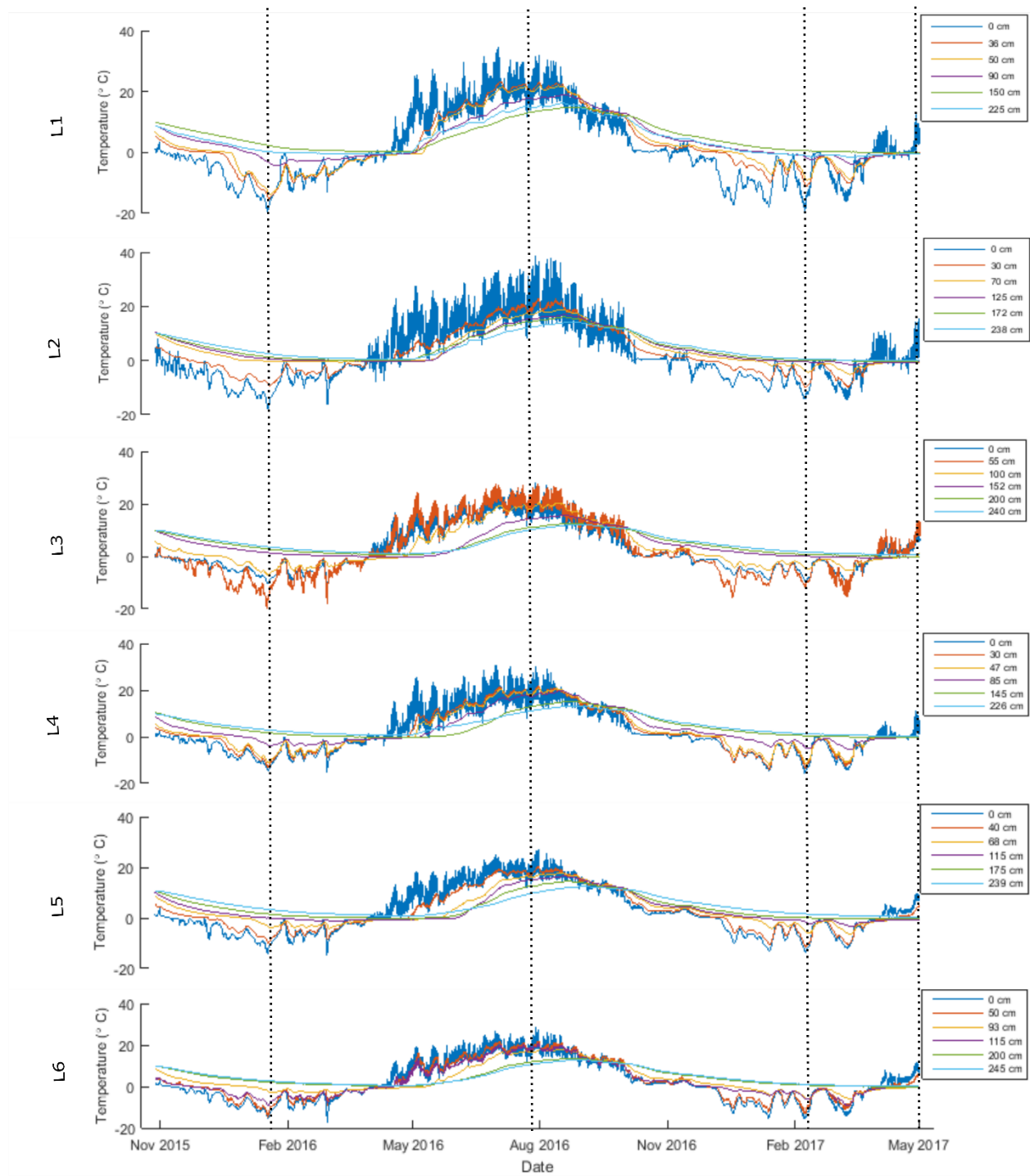


Figure 4-1: Temporal and spatial temperature profiles over a 551 day span, at 6 discrete depths in field lysimeters. Vertical dotted lines represent dates of interest, specifically seasonal maxima and minima and spring.

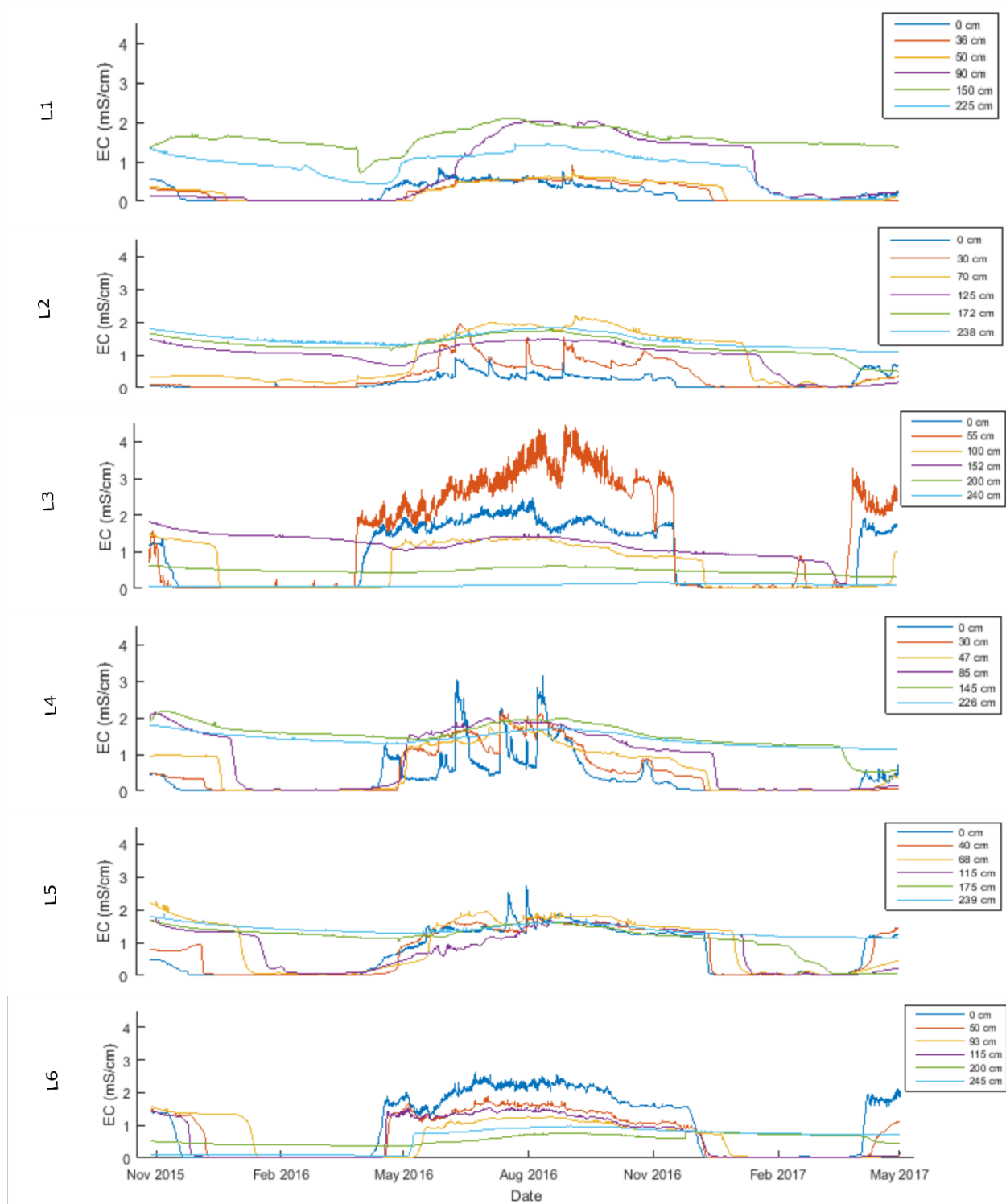


Figure 4-2: Temporal and spatial bulk EC profiles over a 551-day span, at 6 discrete depths in field lysimeters.

Crossplots comparing the mean daily temperature and mean daily EC_{bulk} of CFT layers, in the field lysimeters, were created to assess freezing temperatures in CFT layers (Figure 4-3). These crossplots provide visual confirmation of the temperature when the CFT freezes, as WCR probes are unable to record appropriate EC_{bulk} information in frozen media, due to the lower dielectric permittivity of ice relative to liquid water. This response translates to a drastic decrease in the apparent EC_{bulk} values in frozen media. Minimum mean daily temperatures over 551 days in CFT layers were observed to be $-1.7\text{ }^{\circ}\text{C}$ (L1), $-1.7\text{ }^{\circ}\text{C}$ (L2), $-18\text{ }^{\circ}\text{C}$ (L3), $0.26\text{ }^{\circ}\text{C}$ (L4), $-3.5\text{ }^{\circ}\text{C}$ (L5), and $-15\text{ }^{\circ}\text{C}$ (L6), while maximum mean daily temperatures were measured to be $16\text{ }^{\circ}\text{C}$ (L1), $17\text{ }^{\circ}\text{C}$ (L2), $25\text{ }^{\circ}\text{C}$ (L3), $13\text{ }^{\circ}\text{C}$ (L4), $17\text{ }^{\circ}\text{C}$ (L5), and $22\text{ }^{\circ}\text{C}$ (L6). In comparison, minimum mean daily EC_{bulk} data in CFT layers were observed as 0.035 mS cm^{-1} (L1), 0.034 mS cm^{-1} (L2), 0.0073 mS cm^{-1} (L3), 1.1 mS cm^{-1} (L4), 0.018 mS cm^{-1} (L5), and 0.0034 mS cm^{-1} (L6), with maximum mean daily EC_{bulk} measured at 1.4 mS cm^{-1} (L1), 1.8 mS cm^{-1} (L2), 4.1 mS cm^{-1} (L3), 1.8 mS cm^{-1} (L4), 1.8 mS cm^{-1} (L5), and 2.4 mS cm^{-1} (L6). Consistent across all field systems, as the mean daily temperature approaches $0\text{ }^{\circ}\text{C}$ the mean daily EC_{bulk} begins to decrease toward a value of 0 mS cm^{-1} . However, EC_{bulk} does not necessarily reach a value of 0 mS cm^{-1} at $0\text{ }^{\circ}\text{C}$, demonstrated by a wide spread of EC_{bulk} values at this temperature. Instead, the EC_{bulk} in CFT waste begins to flat line at low temperatures, reaching consistent values close to 0 mS cm^{-1} past this point. Based on these results, the freezing point of CFT can be narrowed down between -1 and $-2\text{ }^{\circ}\text{C}$. The magnitude of the decrease in EC_{bulk} between -1 and $-2\text{ }^{\circ}\text{C}$ provides substantial evidence that CFT begins freezing at this temperature. L1, L2, and L5 temperatures in the CFT do not extend below $-5\text{ }^{\circ}\text{C}$, while L3 and L6 demonstrate temperatures in the near surface CFT deposits close to $-20\text{ }^{\circ}\text{C}$. Lysimeter 4 is the only systems where the mean daily temperature of CFT does not decrease below $0\text{ }^{\circ}\text{C}$, illustrated by the lack of a sudden decrease in mean daily EC_{bulk} within the CFT.

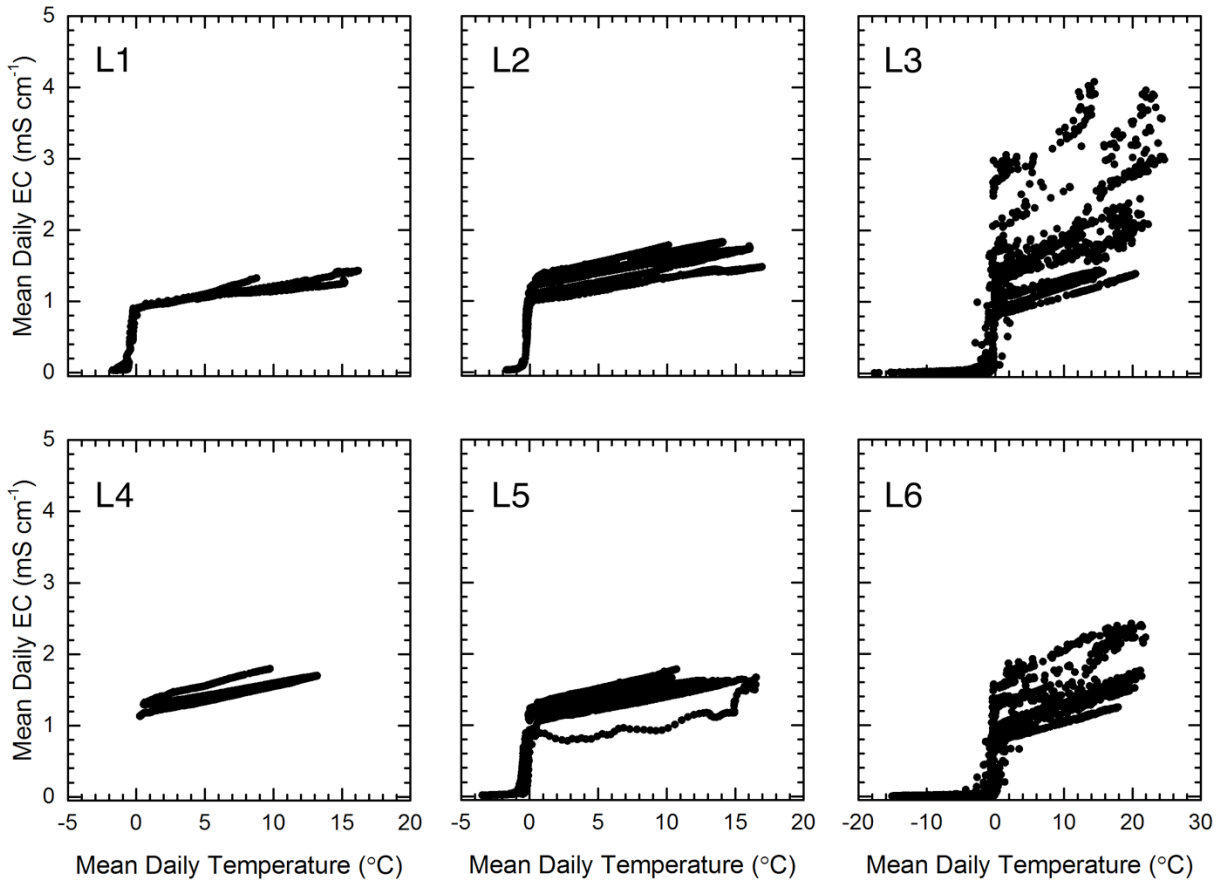


Figure 4-3: Crossplots of average daily bulk EC and average daily temperature within the CFT layer of field lysimeters.

To examine the extent of freeze-thaw on each of the field lysimeters, mean daily temperature profiles were plotted over depth in all systems (Figure 4-4). Four discrete time points were chosen for evaluation, and are marked by a vertical dashed line on the temperature profiles in Figure 4-1. These time points were selected based on periods near seasonal maxima (July 28, 2016) and minima (January 17, 2016; February 7, 2017), including one time point in the spring (May 1, 2017). For each day, hourly data was averaged to create a mean temperature profile. Amongst saturated and unsaturated complements, through all lysimeters, mean daily temperature exhibits identical trends of increasing temperature with depth during winter months, and decreasing temperature with depth in the summer and spring. In all lysimeters except L3 and L6, freezing occurs to a depth of about 1.5 m during winter minima, with material at depth >1.5 m ranging in temperature from -1.4 to 3.4°C. Material freezing in lysimeter 3 and 6 extends a greater depth to approximately 1.8 m, transitioning to positive temperatures at depth >1.8 m. Contrastingly,

throughout periods of high temperatures in the summer, it is apparent that temperatures comfortably higher than the freezing point are achieved over the entire depth of these systems, spanning from 10.0 to 24.9°C. The spring profiles were shown because they exemplify that temperatures in the lower depths of field lysimeters do fall below 0 °C for a part of the year. Each cell experiences spring-time temperatures at base depths departing lower than what was experienced during the peak of winter. Temperature in the CFT get as low as -0.6°C in cells with CFT as the base. Lysimeters 3 and 6 do not experience the same extent of freezing during spring, with positive temperatures to a depth around 1.6 m; however, the WCRs positioned deeper within the lysimeters did record temperatures at or below 0 °C. This is supported by the temperature profiles in Figure 4-1, illustrating the lowest base temperatures in the spring for L1 through L6. This delayed freezing with depth can be explained by the contrast in thermal conductivity of each material, as well as the shielding experienced in lower layers by cover materials.

Bulk EC and volumetric water content (VWC) depth profiles were created for unsaturated lysimeters (Figure 4-5) and their saturated complements (Figure 4-6). Profiles were drawn at specific times throughout the year – 18, 247, and 384 days after experiment setup – to highlight changes in EC_{bulk} and VWC seasonally and as the field experiments progressed. Identical dates in November (18 and 384 days) were chosen a year apart as a point of comparison alongside one date in July (247 days). Amongst the unsaturated lysimeters, L1 and L2 exhibited very similar decreasing upward trends in both VWC and EC_{bulk} near surface. The opposite trend was observed in L3, where increasing upward trends in EC_{bulk} and VWC were observed immediately below surface. Temporal comparisons among unsaturated systems illustrate that EC_{bulk} was consistently higher near the surface at 384 days compared to 18 days; however, both were lower than values observed after 247 days. A different progression is observed for the VWC, as water content increases over time from 18 days to 384 days, except in L3 which follows the same temporal pattern as EC_{bulk} .

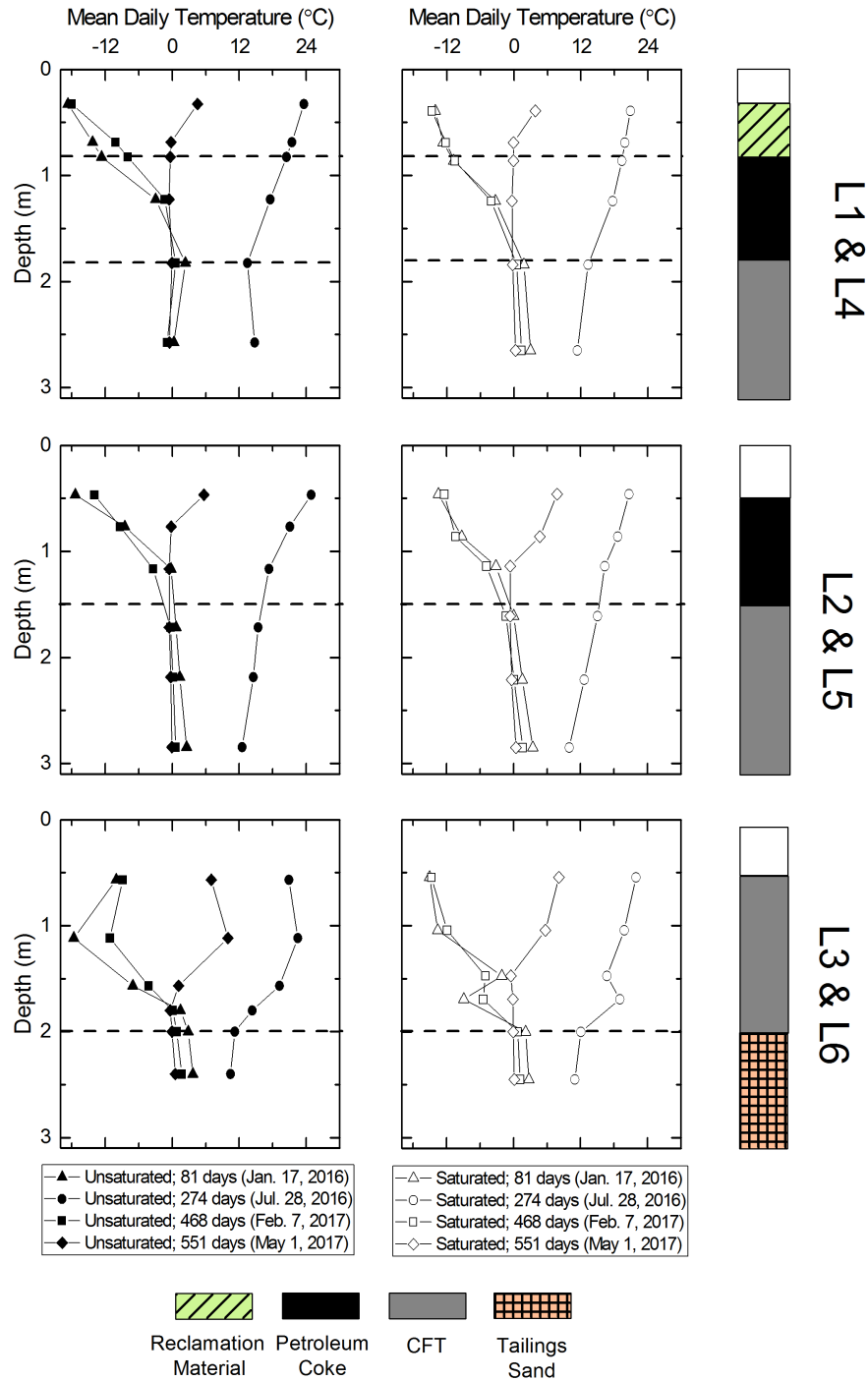


Figure 4-4: Depth profiles of mean daily temperature through field lysimeters after (i) 81 days, (ii) 274 days, (iii) 468 days, and (iv) 551 days. Horizontal dashed lines represent interfaces between waste layers.

For comparison, saturated lysimeters exhibited similar spatial trends for both EC_{bulk} and WVC as compared to the equivalent unsaturated lysimeter. The saturated lysimeters exhibited identical temporal patterns as the unsaturated systems for EC_{bulk} , but differ slightly for WVC.

Generally, VWC in L4 to L6 exhibits the same pattern over time as the EC_{bulk} data, with 247 days having the highest values and 18 days the lowest. Missing VWC data is due to a limitation with the WCR probes, where VWC values exceeding 0.55 could not be measured. Many data gaps exist in CFT layers, as the VWC may exceed this threshold.

Both EC_{bulk} and pore-water EC were measured during the August 2016 field campaign, 10 months following lysimeter construction and instrumentation (Figure 4-7). The pore water EC through all lysimeters varied from 0.851 to 11.61 mS cm^{-1} , a greater range than EC_{bulk} that showed conductivity values from 0.101 to 2.59 mS cm^{-1} . Bulk EC values are determined in part by the electrical conductivity of the solids fraction. Although the solution EC also contributes to EC_{bulk} determination, the presence of minerals in both tailings and petroleum coke with a weak electrical conductivity, such as quartz, would reduce the bulk electrical conductivity of the material. This is especially true in unsaturated systems, as the presence of water with dissolved ions, present in the pore space, enhances electrical conductivity. In most lysimeters, pore water EC demonstrates a sharp net increase toward shallower depth, particularly within the petroleum coke layer. The pore water EC profile for L4 does not follow the same trend as the others, illustrating a slight increase moving up into the coke until about 1.25 m is reached. At this point, a slight decrease is observed, with a sudden increase near surface. The increase in pore water EC at the base of L3 and L6 can be explained by the ingress of saline CFT pore water into the tailings sand over time. Comparison with EC_{bulk} values reveal that L3 to L6 follow similar patterns of net increase with shallower depth. Decreases in EC_{bulk} toward the surface are observed in L1 and L2, contrary to what was observed in lysimeter pore water. A lack of available pore water in the unsaturated lysimeters prevents full depth profiles from being observed, making it unclear whether near surface pore water EC profiles follow similar trends to EC_{bulk} in L1 and L2. The presence of porous, coarse petroleum coke in these arrangements facilitates rapid infiltration and drainage of water due to its structure (Nakata et al., 2011; Lahmira et al., 2013), which has the potential to facilitate geochemical mixing in unsaturated arrangements (Nesbitt, 2016). This would explain the decrease in EC_{bulk} at shallower depths in L1 and L2.

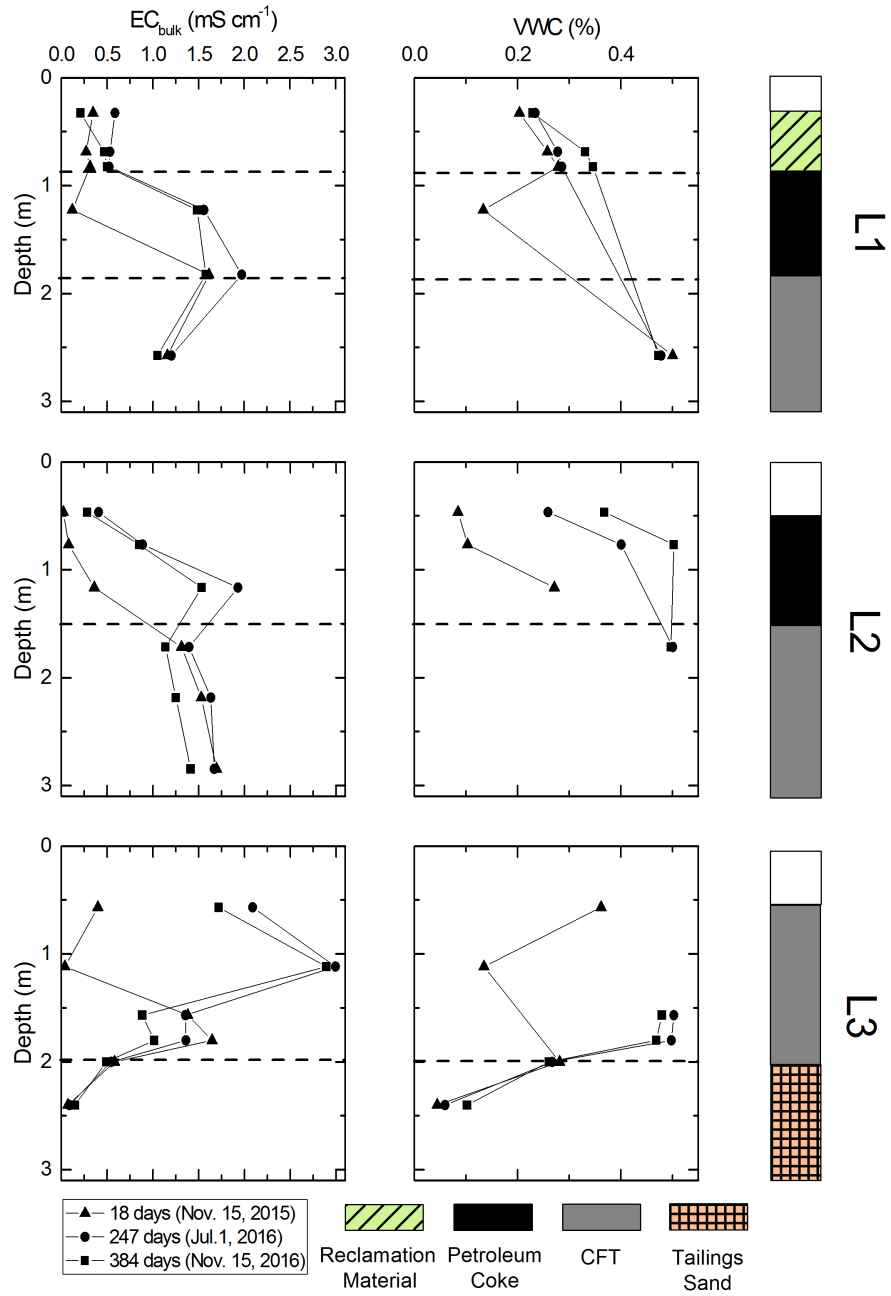


Figure 4-5: Depth profiles of bulk EC and VWC in unsaturated lysimeters at (i) 18 days, (ii) 247 days, and (iii) 384 days. Dashed horizontal lines indicate interfaces between waste layers.

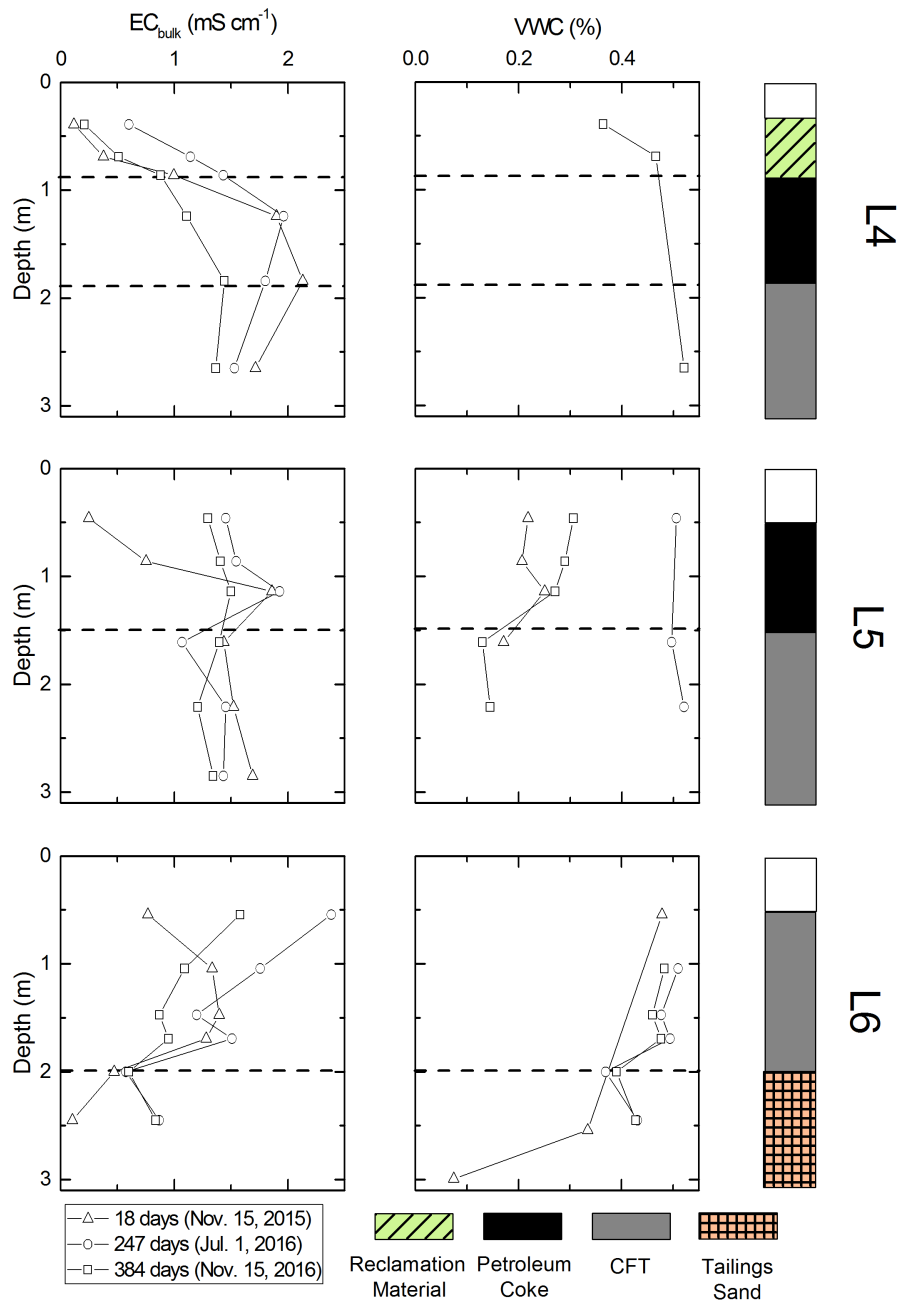


Figure 4-6: Depth profiles of bulk EC and VWC for saturated lysimeters at (i) 18 days, (ii) 247 days, and (iii) 384 days. Horizontal dashed lines delineate interfaces between waste layers.

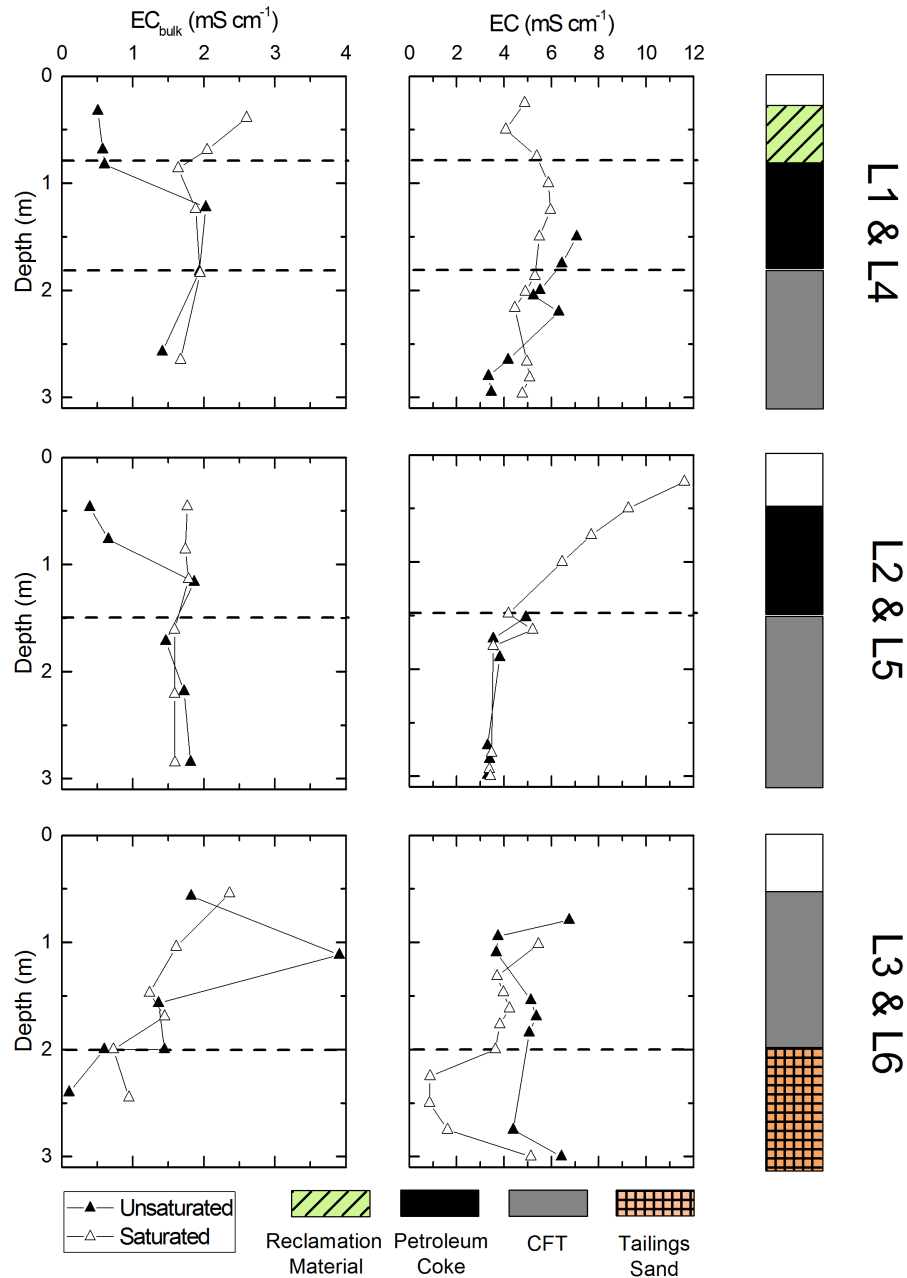


Figure 4-7: Comparison of depth profiles for EC_{bulk} and pore water EC during the August 2016 field campaign. EC_{bulk} values shown were measured on August 10, 2016.

4.1.2.2 Chloride, δ^2H , and $\delta^{18}O$

The isotopic signature of pore water within the lysimeters was plotted on a local meteoric water line (LMWL) developed by Baer et al. (2016) for the Mildred Lake mine (Figure 4-8). Using rainfall and precipitation data, a weighted least squares regression was employed to create a weighted LMWL with the equation $\delta^2H = 7.2 \delta^{18}O - 10.3\text{‰}$ (Baer et al., 2016). A local evaporation

line (LEL) was included in this plot as a reference to signatures observed for natural systems ($\delta^2\text{H} = 5.2\delta^{18}\text{O} - 50.6\text{‰}$; Gibson et al., 2015), and a regression line created from OSPW isotopic values in tailings was also plotted (Baer, 2014). Deuterium and $\delta^{18}\text{O}$ in well and core pore water samples varied from -122.5 to -108.6‰ and -13.98 to -11.26‰ , respectively. All lysimeter samples plotted against the LMWL demonstrate signatures that are not representative of meteoric origin, illustrated by clustering along the LEL and departure away from the LMWL. Varying degrees of enrichment and depletion are observed among pore-water samples; however, all samples remain fairly clustered within the same area between the line delineating an OSPW signature and the LEL. The signature of fresh water used to saturate lysimeters (i.e. fill water) was included as an end-member to highlight potential mixing within field cells. The fill water exhibits a composition that is depleted in both $\delta^2\text{H}$ and $\delta^{18}\text{O}$ relative to what is typically observed for rainfall at the Mildred Lake Site (Baer et al., 2016). This is most likely explained by a contribution from both rainfall and snowfall to the Mildred Lake reservoir, being the source of the fill water. Further influence by evaporation explains why the fill water signature tends toward the LEL. None of the pore-water samples collected from the lysimeters had compositions consistent with the fill water, however samples containing more depleted signatures are indicative of mixing with the fill water.

A strong, positive correlation existed between Cl and ^{18}O in lysimeter pore water samples (Figure 4-8). Due to the conservative nature of Cl and $\delta^{18}\text{O}$, both will behave similarly and are commonly used to track the fate of water within a variety of hydrologic settings. The spatial distribution of Cl and $\delta^{18}\text{O}$ in saturated and unsaturated lysimeters was assessed to better constrain the processes controlling the migration and fate of dissolved salts and pore water (Figure 4-9). Chloride concentrations vary between 311 to 2090 mg L^{-1} across the field experiments, with an average concentration of $719 \pm 41.8 \text{ mg L}^{-1}$. An upward decreasing trend in Cl concentration was observed in L1 and L4, which contrasts the increasing concentration of Cl toward the surface in L2 and L5. Lysimeter 3 and 6 demonstrated consistent values of Cl in the tailings sand, with an increase in Cl concentration occurring toward the surface of the CFT deposit. However, L3 exhibited a large decrease in the amount of Cl between 0 to 1 m depth. In comparison, $\delta^{18}\text{O}$ follows similar trends to Cl in these systems. A slight depletion in $\delta^{18}\text{O}$ toward the surface is observed in L1 and L4, however values remain relatively consistent through depth. Contrastingly, enrichment of $\delta^{18}\text{O}$ in pore water was observed toward the surface of the coke cap layer in L5, with more consistent, depleted values in the CFT layer at lower depths. No pore water data was available in

the coke layer of L2, however values of $\delta^{18}\text{O}$ do not vary greatly in the CFT. Both saturated and unsaturated complements in the system with CFT and tailings sand demonstrate similar trends. The base of the tailings sand in L3 and L6 are depleted in $\delta^{18}\text{O}$, but become more enriched as the interface with the CFT is approached. Within the CFT deposit, both cells demonstrate consistent signatures of slightly enriched pore water that begins to deplete slightly near the surface of the deposit. In L1 and L2, profiles are limited by the lack of pore water and therefore data does not extend far above the interface between the coke and CFT.

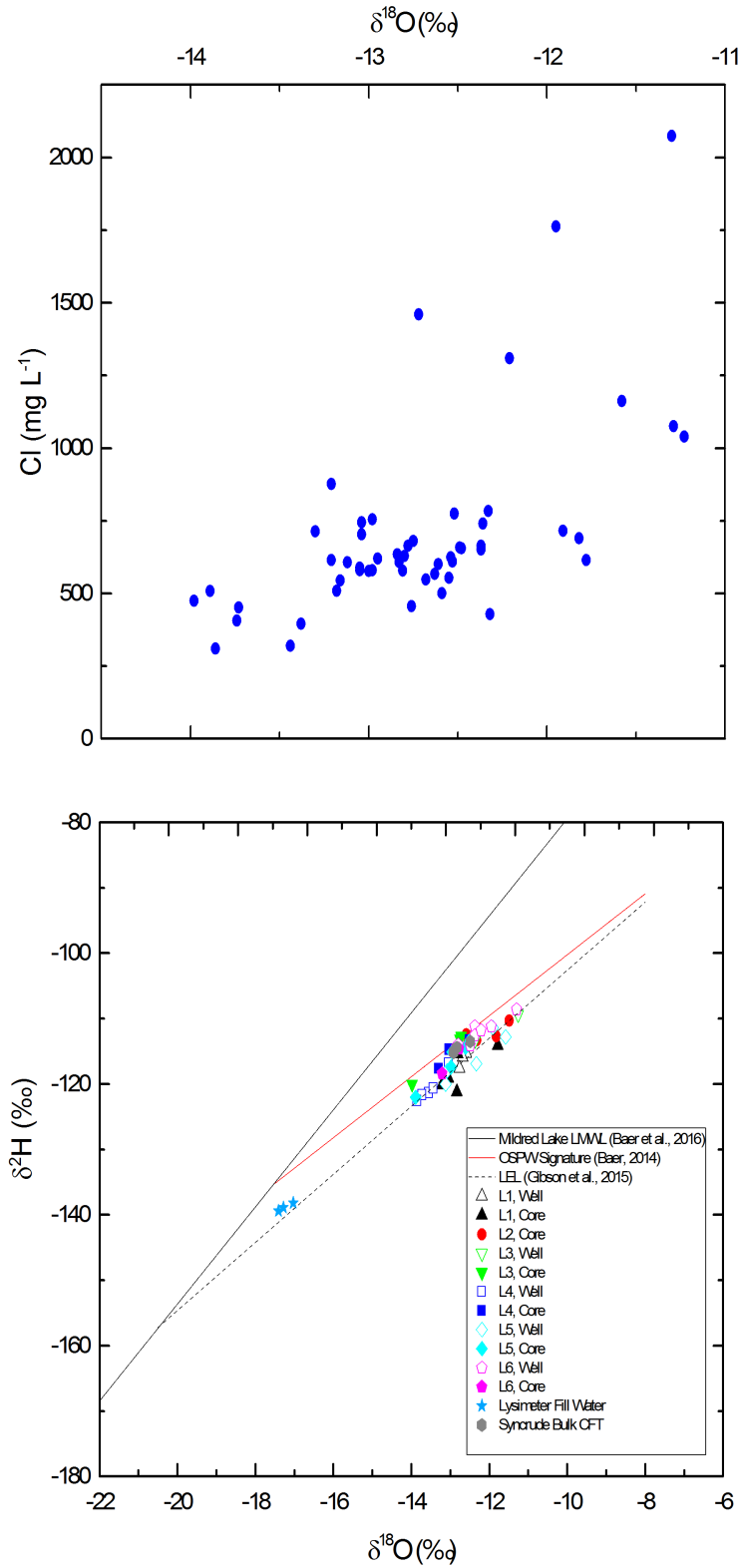


Figure 4-8: Correlation between field chloride and $\delta^{18}\text{O}$ (top) and plot of the Mildred Lake LMWL (Baer et al., 2016) with overlay of lysimeter pore water isotopic signatures.

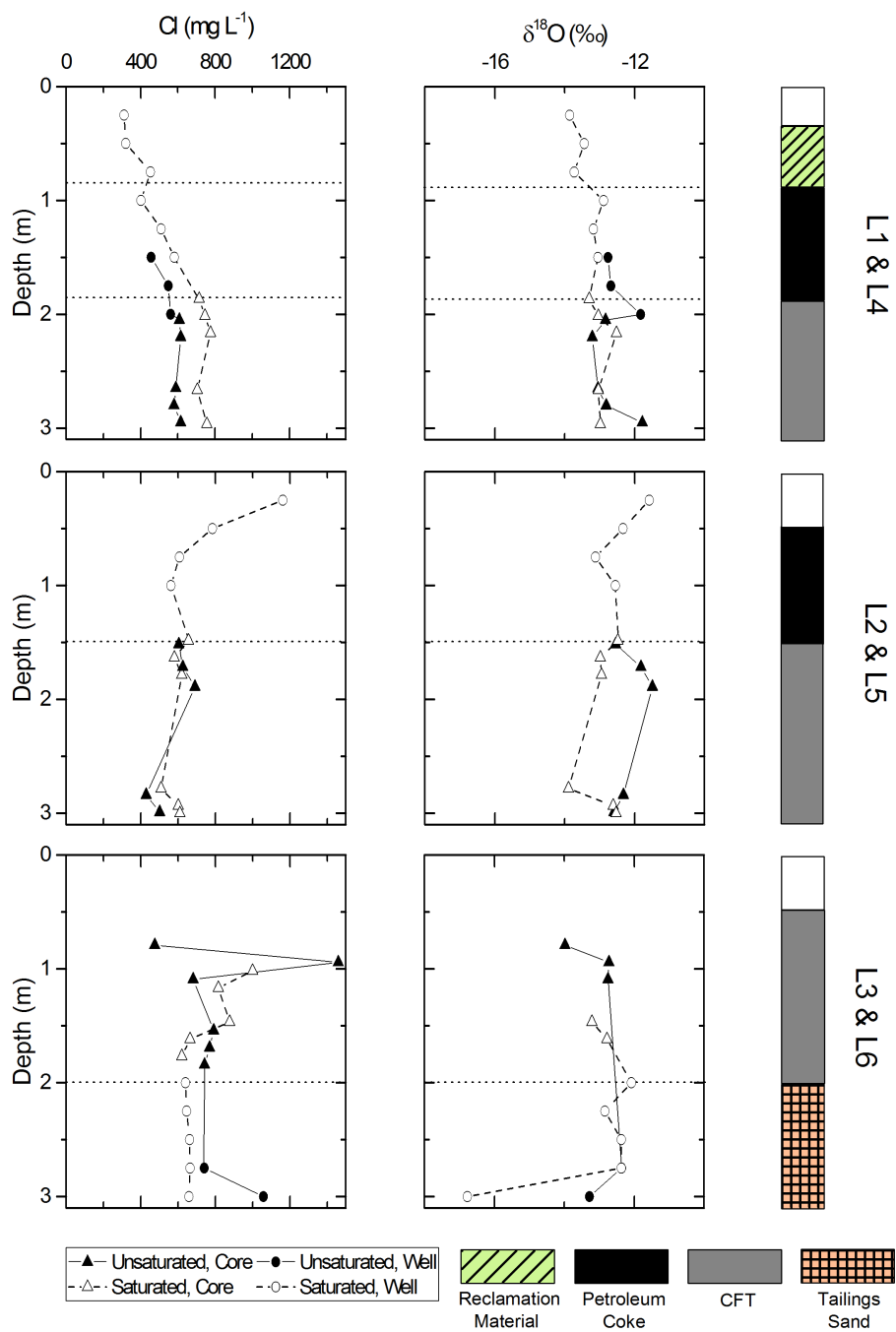


Figure 4-9: Depth profiles of Cl and $\delta^{18}\text{O}$ in unsaturated and saturated lysimeters. Horizontal dashed lines represent interfaces between waste.

4.1.2.3 *pH, Eh, and Alkalinity*

Field lysimeters exhibited near neutral pH measurements ranging from 6.8 to 8.4, with a mean value of 7.7 ± 0.04 ($n = 59$). Scenarios containing reclamation or petroleum coke cover exhibited an upward decreasing trend consistent amongst both saturated and unsaturated complements, indicative of an increase in abiotic CO_2 dissolution near the surface. The magnitude of the pH decrease through L4 and L5 was as high as 1.06 and 0.65 units, respectively. Conversely, a downward decreasing trend in pH was apparent in scenarios capped with CFT, with the lowest values occurring in the tailings sand layer. The pH in the CFT layer within L3 and L6 demonstrate a net decrease of 0.14 and 0.04 units, respectively. Generally, the pH observed in all CFT layers is consistent with previously reported values in FFT and MFT pore water (Penner and Foght, 2010; Chen et al., 2013; Dompierre et al., 2016).

The average oxidation-reduction potential (Eh) of lysimeter pore water from well and core samples was reported as 179 ± 22 mV ($n = 58$), with values ranging from -165 to 387 mV (Figure 4-10). An upward increasing trend was observed in systems containing reclamation substrate or petroleum coke as a cover layer – regardless of the degree of saturation – highlighting the presence of more reducing conditions in deeper CFT pore water and an oxic environment near surface. This trend does not translate to L3 and L6, where Eh remains highly positive and relatively unchanged through depth. In both saturated and unsaturated systems with CFT as a cap layer, seasonal freeze-thaw facilitated the formation of fissures and cracks that permit oxygen ingress into CFT deposits. This would explain the oxic environment observed in these arrangements.

Similar to the trends observed for pH, alkalinity demonstrates an upward decreasing trend in all lysimeters, exhibiting a range of values from 260 to 1560 mg L^{-1} and mean concentration of $824 \pm 40 \text{ mg L}^{-1}$ ($n = 57$). High alkalinity within tailings sand reflects the downward migration of CFT pore water over time. Based on the depth profiles of the aforementioned chemical parameters, the greatest magnitude of change in pH, Eh, and alkalinity spatially occurs across layer interfaces (Figure 4-10).

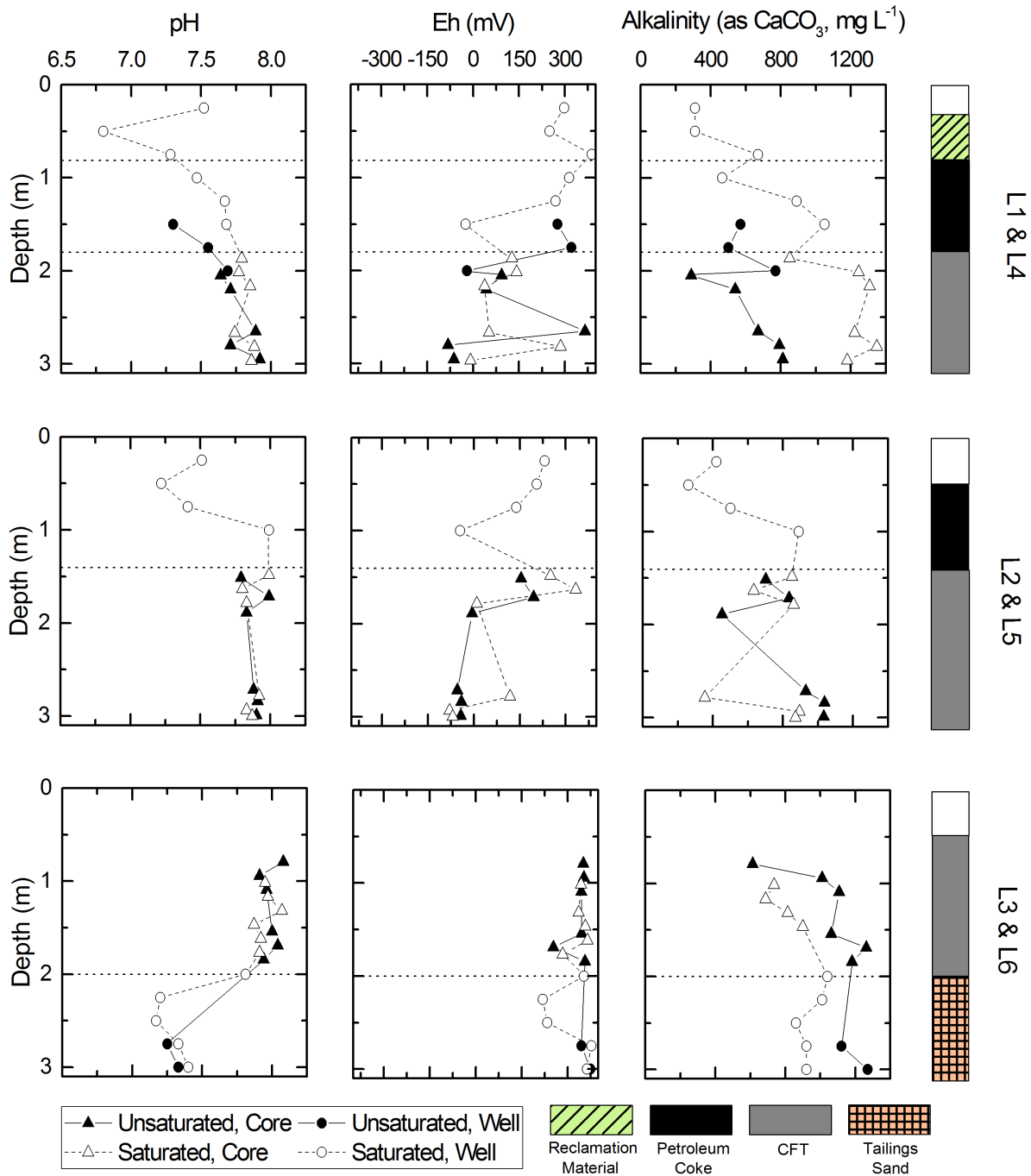


Figure 4-10: Depth profiles of pore water pH, oxidation-reduction potential, and alkalinity in field lysimeters. The horizontal dotted lines represent interfaces between materials within each system.

4.1.2.4 Major Cations

Dominant cation species in lysimeter pore water include Na, Ca, K, and Mg, exhibiting average concentrations ($n = 59$) of $1130 \pm 62 \text{ mg L}^{-1}$, $109 \pm 17 \text{ mg L}^{-1}$, $21.7 \pm 2.19 \text{ mg L}^{-1}$, and $62.6 \pm 11.3 \text{ mg L}^{-1}$, respectively. Concentrations of dissolved cations demonstrate large spatial variability through field systems, with Na ranging from 530 to 3381 mg L^{-1} , Ca from 11.7 to 534 mg L^{-1} , K from 7.7 to 95.1 mg L^{-1} , and Mg from 5.6 to 462.2 mg L^{-1} . These element concentrations are substantially higher than what has been reported previously for OSPW in fine tailings environments (Siwik et al., 2000; Leung et al., 2003; Allen, 2008; Abolfazlzadehdoshanbehbazari et al., 2013), natural freshwater fens in Alberta (Vitt and Chee, 1990), and reclaimed oil sands environments in the AOSR (Purdy et al., 2005). In lysimeters containing a cap of reclamation material (L1 and L4), the concentration of Ca and Mg follows an upward increasing trend toward the surface. Potassium concentrations exhibited a net increase toward the surface; however, there was greater variability among CFT, petroleum coke, and reclamation material layers. In contrast, Na concentrations in L1 increase until the interface with petroleum coke is reached, where it then begins to decrease. Lysimeter 4 experiences a decrease in the concentration of Na toward the surface layer, whereupon a slight increase is experienced directly at the surface. All major cations exhibit an upward increasing trend toward the surface in L2 and L5, with concentrations in the CFT remaining relatively consistent until the interface with petroleum coke is approached. Limited pore water in the unsaturated systems (L1 and L2) prevents a full understanding of the distribution of major cations in the surface petroleum coke and reclamation material layers.

Lysimeters that contained 1.0 m of tailings sand capped with 2.0 m of CFT (L3 and L6) exhibited increasing concentrations of major cations toward the surface, similar to the other lysimeters. Tailings sand in the lower 1 m of these cells show slight fluctuations in cation concentration that reflect migration of connate pore water from overlying CFT downward. No apparent spatial pattern exists until CFT layer is reached, where concentrations begin to increase. Generally, a net increase in the concentration of dissolved cations is observed toward the surface in all the field lysimeters (Figure 4-11).

Comparisons drawn between the different reclamation prescriptions reveals that the saturated lysimeter arrangement with a petroleum coke cap layer experienced the greatest magnitude of dissolved cation concentrations near surface. Due to restrictions on the amount of available pore water, unsaturated systems cannot be compared to the same extent as saturated ones

as there is limited information for near surface concentrations. Furthermore, the quantity of dissolved constituents through each prescription changes on the basis of the degree of saturation. Visually, it appears that unsaturated reclamation scenarios generally demonstrate a greater increase in concentration with decreasing depth in systems that contain a cap layer of reclamation material or coke. This is especially evident when the interface between CFT and coke is reached, through inspection of same-depth concentrations. Concentrations of major cations remain relatively similar in CFT layers, which explains why this trend is not present in L3 and L6.

To assess whether exchange process might be influencing the concentration of major cations within the petroleum coke, depth profiles of Na and Ca concentrations were normalized to Cl in L4 and L5 (Figure 4-12). Results show that there is a net increase toward the surface in normalized Na and Ca concentrations in L4 and L5. In L4, normalized Na concentrations demonstrate an observable decrease within the top of the petroleum coke into the reclamation material, from a depth of 1 m to 0.5 m. This is complemented by an increase in normalized Ca concentrations within the same depth range. Similarly, normalized data in L5 reveals a decrease in Na in the petroleum coke from a depth of 1.0 m to 0.75 m, with a simultaneous increase in Ca.

4.1.2.5 Sulfate and Ammonia

An increase in dissolved SO_4 concentrations toward shallow depths are observed across all lysimeter systems, regardless of the degree of saturation (Figure 4-13). Across all lysimeters, the average dissolved SO_4 concentration ($n = 57$) is $1260 \pm 195 \text{ mg L}^{-1}$ with value spanning a range from 2.18 to 6760 mg L^{-1} . Analogous to major cation data, the interface between CFT and coke layers corresponds to a substantial change in pore-water SO_4 concentrations in L1, L2, L4, and L5. Again, a lack of available pore water in L1 and L2 inhibits a clear understanding of the full spatial distribution of dissolved ions. Sulfate in lysimeters constructed with tailings sand and CFT behaves similarly to major cations. Increasing concentration in the tailings sand is apparent due to downward release of saline CFT pore water. Within the CFT layer, above the interface, concentrations do not fluctuate greatly within each system and between L3 and L6, demonstrating an increasing trend toward the surface at depths shallower than about 1 m.

Data from both saturated and unsaturated lysimeters reveal that the concentration of SO_4 at each depth in L1 is higher than L4 after 10 months, suggesting that salt accumulation near the water table is occurring faster in unsaturated systems. However, unsaturated systems hinder

complete surface migration of SO_4 in surface layers. This pattern cannot be discerned between L2 and L5, as there is no data within the coke layer of L2. CFT properties and pore water chemistry are identical between L3 and L6, explaining the lack of this trend in these arrangements. Sulfate concentrations are generally the same throughout the CFT layer. Net ammonia (NH_3) concentrations decrease toward the surface in lysimeters that included a petroleum coke layer. The opposite trend was observed in systems with tailings sand and CFT, illustrating an increasing upward trend in $\text{NH}_3\text{-N}$ concentrations. Large variability in $\text{NH}_3\text{-N}$ concentrations was apparent through all reclamation prescriptions, spanning values from 0.3 to 34.8 mg L^{-1} , with an average concentration ($n = 59$) of $8.5 \pm 0.90 \text{ mg L}^{-1}$ (Figure 4-13). The highest $\text{NH}_3\text{-N}$ concentration was observed near the CFT-coke interface in L1 (34.8 mg L^{-1}), with elevated concentrations also occurring at discrete points within the coke layers for both L4 (25.8 mg L^{-1}) and L5 (32.6 mg L^{-1}). These zones of elevated $\text{NH}_3\text{-N}$ concentrations do not correspond with patterns observed for other constituents.

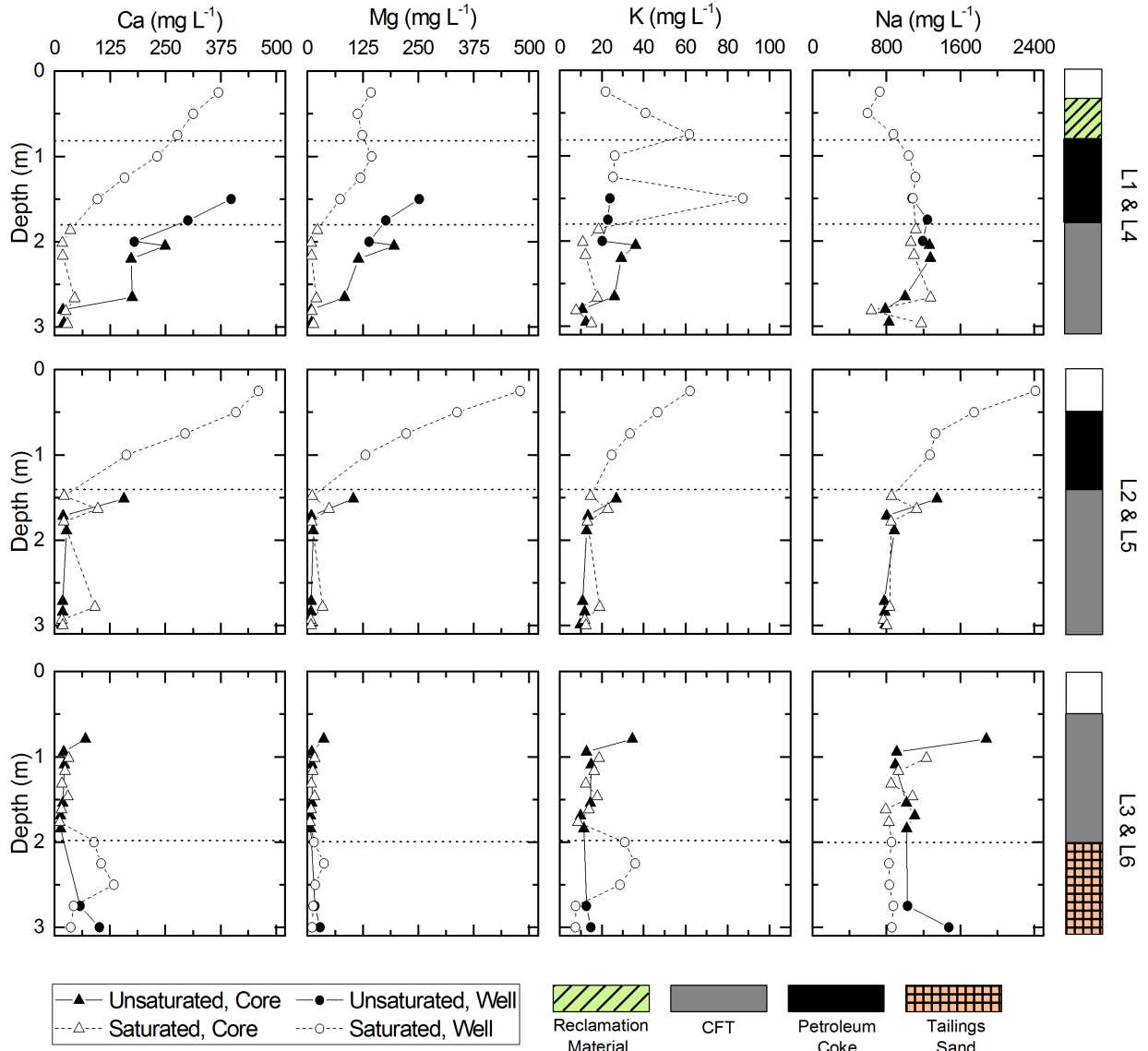


Figure 4-11: Depth profiles highlighting the concentration of major cations in different reclamation prescriptions. The dotted horizontal lines represent location of material interfaces.

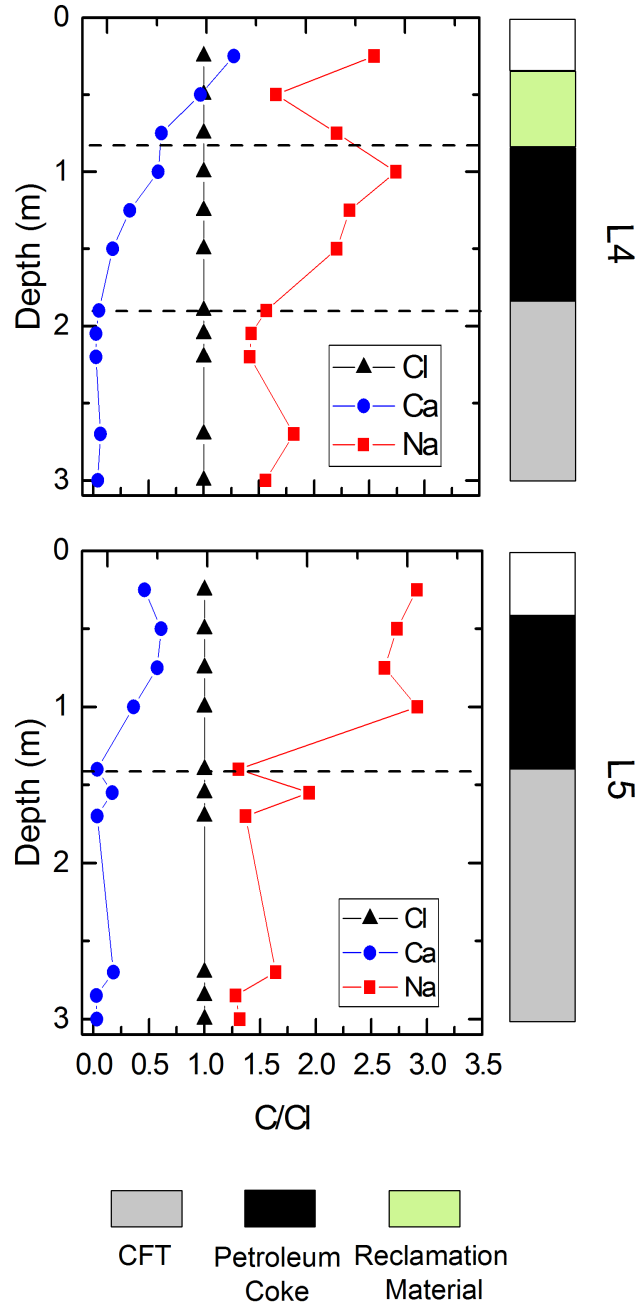


Figure 4-12: Depth profiles of Na and Ca concentrations that are normalized to Cl through L4 and L5. The dashed, horizontal line represents the interface between waste layers.

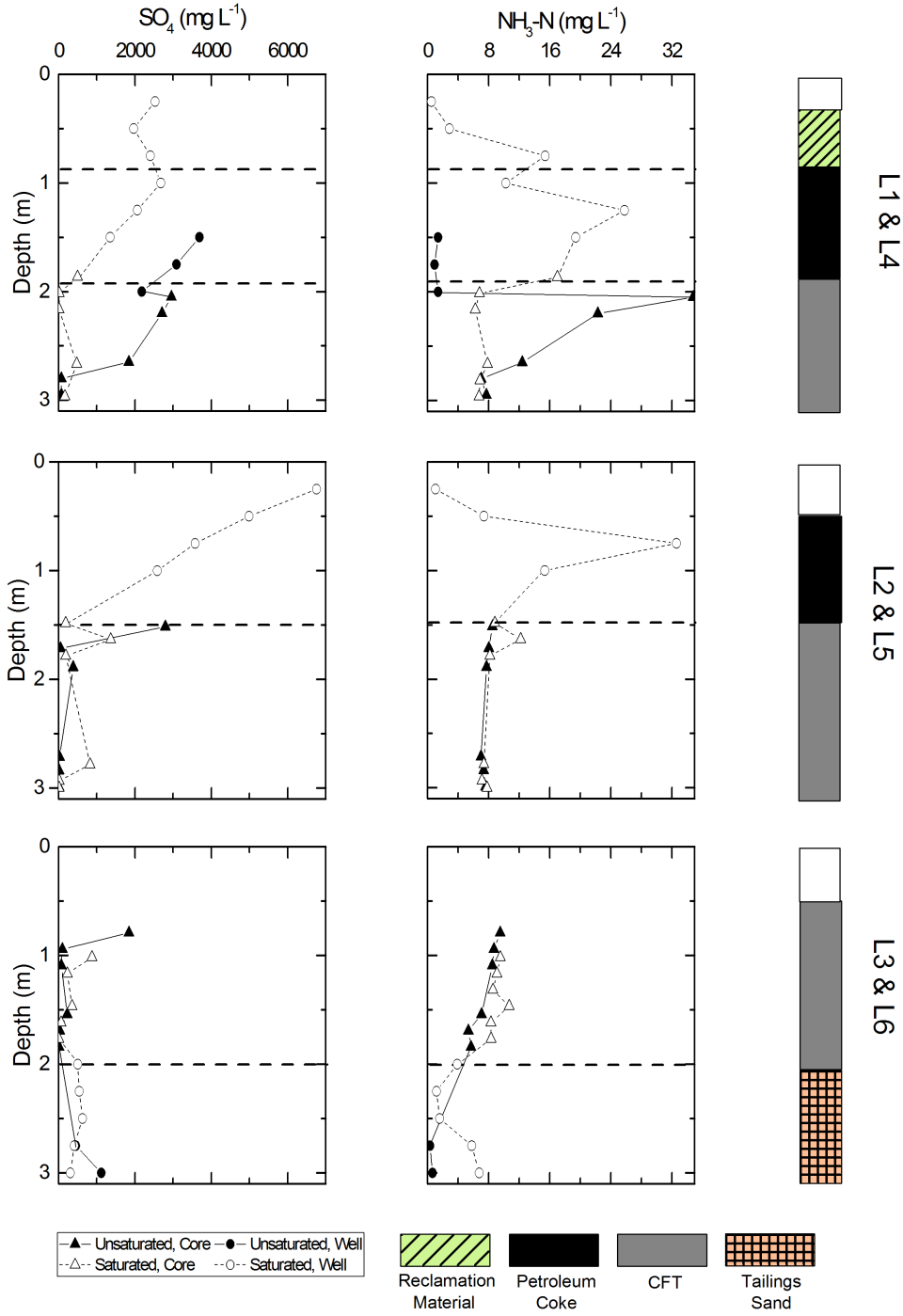


Figure 4-13: $\text{NH}_3\text{-N}$ and SO_4 depth profiles through field lysimeters. Horizontal lines represent locations of material interfaces.

4.1.3 Solid-phase analyses

4.1.3.1 Mineralogy

Diffraction patterns were generally consistent amongst all samples ($n = 19$), highlighting a clay dominated mineralogy with the presence of a few additional crystalline phases. Three CFT samples were analyzed from each of L1, L3, L4, L5 and L6, plus two CFT samples from L2 (Figure 4-14 and Figure 4-15). Coke mineralogy was not examined as it has previously been reported in the literature (González et al., 2010; Nesbitt et al., 2017). Clay peaks identified in XRD patterns corresponded to kaolinite, illite, chlorite, and in some samples, montmorillonite. Other identified peaks included quartz, calcite, and dolomite. These results are consistent with bulk mineralogy reported for other CFT deposits (Heaton, 2015) and fine tailings (Omotoso and Mikula, 2004; Kaminsky et al., 2009; Kasperski and Mikula, 2011). No major differences were observed between bulk CFT and lysimeter samples after a 10-month period.

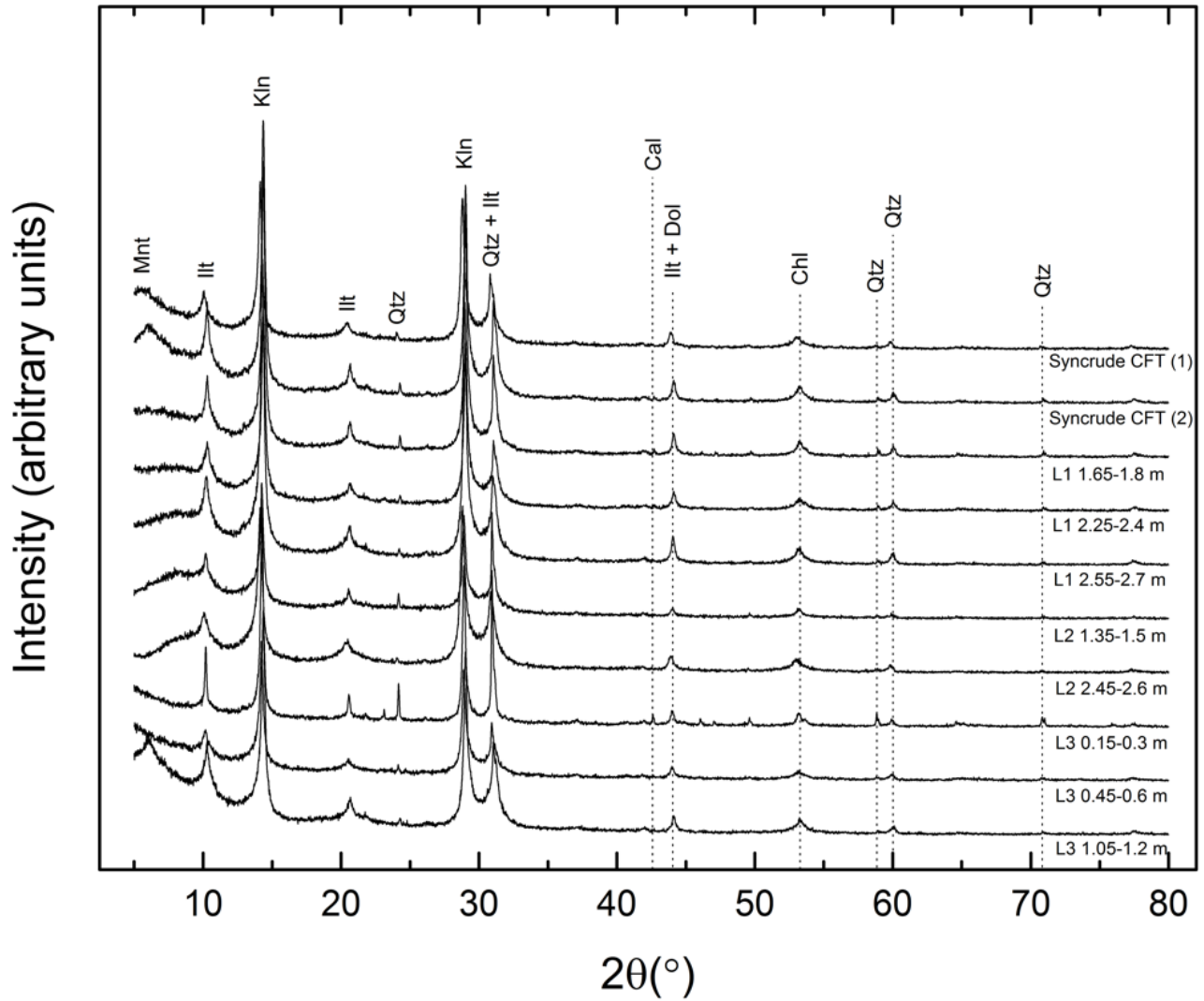


Figure 4-14: X-Ray Diffraction (XRD) patterns for CFT samples from unsaturated lysimeters. Bulk Syncrude CFT spectra are included for comparison; Mnt = montmorillonite, Illt = illite, Klin = kaolinite, Qtz = quartz, Chl = chlorite, Dol = dolomite, Cal = calcite.

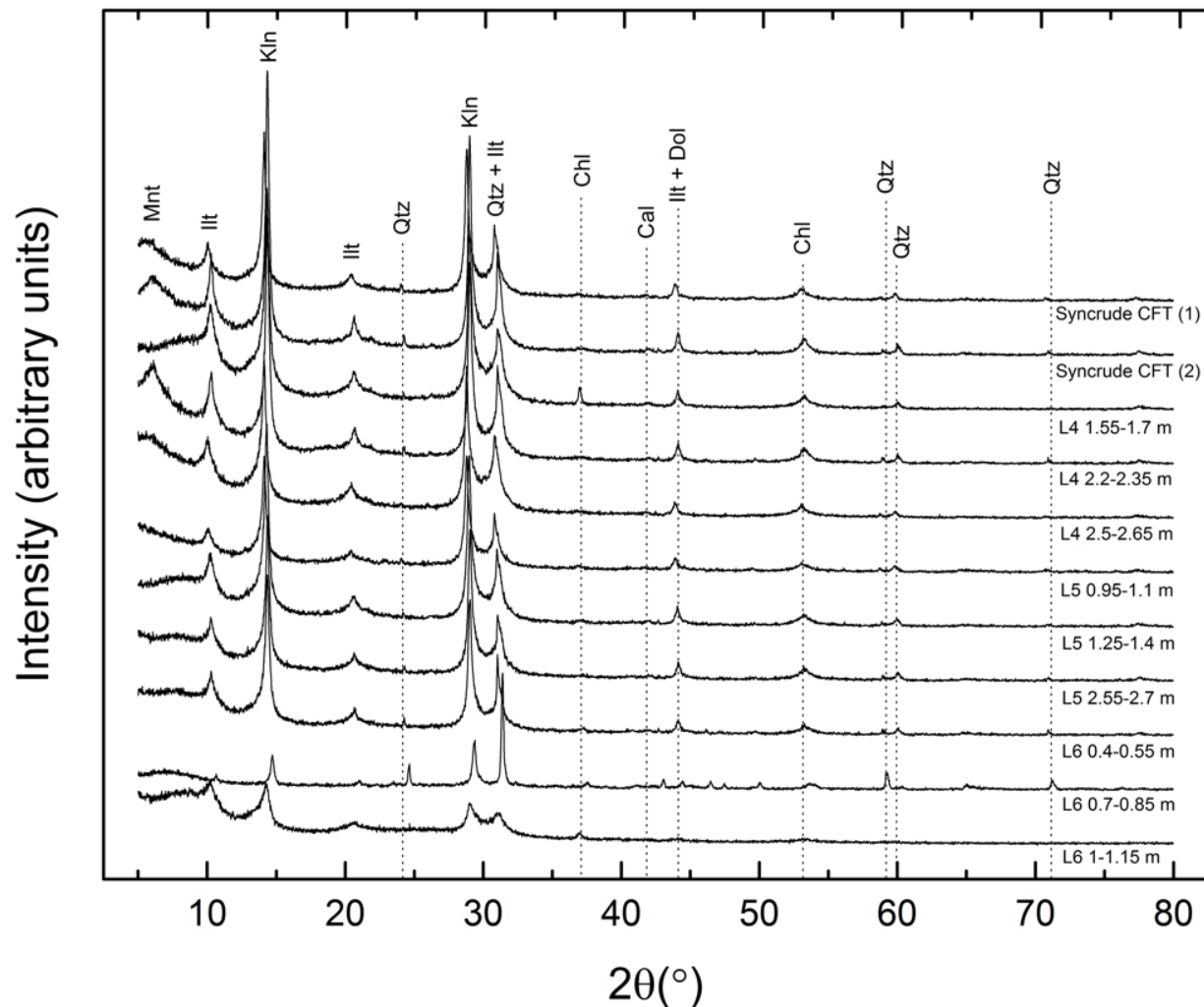


Figure 4-15: X-Ray Diffraction (XRD) patterns for CFT samples from saturated lysimeters. Bulk Syncrude CFT spectra are included for comparison; Mnt = montmorillonite, Illt = illite, Kln = kaolinite, Qtz = quartz, Chl = chlorite, Dol = dolomite, Cal = calcite.

4.1.3.2 Cation Exchange Capacity and Specific Surface Area

Measurements of CEC and SSA were performed on petroleum coke and CFT samples ($n = 15$) including two initial fluid petroleum coke samples, 11 CFT core samples, and two interface core samples that contained a mixture of coke and CFT (Appendix C). The CEC of CFT ranged from 6.4 to 21 meq 100 g⁻¹, being generally consistent with the range of 11 to 37 meq 100 g⁻¹ reported for fine tailings by Kaminsky et al. (2009). Samples containing both coke and CFT from the interface exhibited CEC values between 1.96 to 4.83 meq 100 g⁻¹, which was lower than that observed for CFT. This difference is most likely attributed to the presence of petroleum coke,

which was characterized by low CEC values spanning 0.38 to 0.43 meq 100 g⁻¹. These CEC values are the first for fluid petroleum coke to appear in the peer-reviewed literature. Specific surface area for the CFT samples fell within the range of 141 to 394 m² g⁻¹, which is consistent with values previously reported for MFT (Omotoso et al., 2002; Omotoso and Mikula, 2004; Kaminsky et al., 2009). The SSA of coke samples ranged from 19.3 to 21.9 m² g⁻¹, which was considerably lower than CFT. These SSA values were higher than the range of 4.5 to 11 m² g⁻¹ reported for Syncrude petroleum coke in several past studies (Fedorak and Coy, 2006; Alessi et al., 2014; Nesbitt et al., 2017). However, the measured SSA values are similar to one value of 27.3 m² g⁻¹ reported for raw fluid coke (Small et al., 2012), which demonstrates the variability of coke SSA. One explanation for this could be the heterogeneous nature of petroleum coke samples. Fluid coke produced by Syncrude consists of variable grain size fractions which may contribute to fluctuating SSA. The methylene blue method is commonly employed for the analysis of clay-rich materials (Yukselen & Kaya, 2008; Holden et al., 2012), but has been modified to include assessment of CEC for samples with a sand-like composition (Holden et al., 2012). Interface layer samples exhibit SSA values intermediate to both coke and CFT, observed as 37.9 to 93.0 m² g⁻¹.

4.1.4 PHREEQCi Modeling and Statistical Analysis

Correlation analysis results reveal there is a strong negative correlation between Ca and alkalinity ($R = -0.676$, $p \ll 0.05$), Mg and alkalinity ($R = -0.773$, $p \ll 0.05$), Ba and SO₄ ($R = -0.607$, $p \ll 0.05$), F and Ca ($R = -0.675$, $p \ll 0.05$), Ba and Ca ($R = -0.802$, $p \ll 0.05$), Mg and F ($R = -0.695$, $p \ll 0.05$), and Ba and Mg ($R = -0.783$, $p \ll 0.05$) within lysimeter pore water. Additionally, Ca and Mg ($R = 0.931$, $p \ll 0.05$), F and alkalinity ($R = 0.714$, $p \ll 0.05$), Ba and alkalinity ($R = 0.647$, $p \ll 0.05$), and Ba and F ($R = 0.706$, $p \ll 0.05$) demonstrate a strong positive correlation in these systems. All other analytes exhibit weak correlations ($R < \pm 0.6$) that may or may not be statistically significant (Table E-1, Appendix E).

Data quality determined from PHREEQCi demonstrates that the CBE obtained from pore water chemistry data ($n = 44$) are within an acceptable range of variability, with majority of samples ($n = 36$) having $< \pm 10\%$, and more than half the samples ($n = 25$) exhibiting $< \pm 5\%$. Values with $>5\%$ error exhibited both positive and negative bias, which may be attributed to overestimation or underestimation of SO₄ pore water concentrations. Saturation indices reveal that

the pore water in lysimeter systems, throughout depth, are consistently at or above saturation with respect to calcite and dolomite, and at or below saturation with respect to gypsum (Figure 4-16).

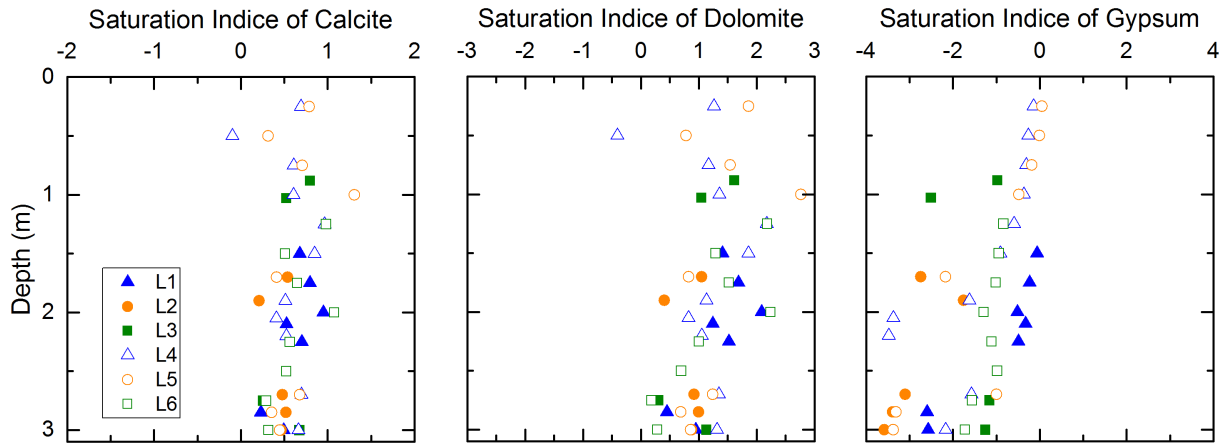


Figure 4-16: Saturation indices (SI) of calcite, dolomite, and gypsum for each lysimeter.

4.2 Column Experiments

4.2.1 Settlement Measurements

After 223 days, the saturated column (Saturated Column 1) experienced a total of 0.15 m of settlement, while the unsaturated column underwent 0.093 m over 146 days (Table 4-2). Once the unsaturated column was fully saturated (Saturated Column 2), the system underwent a total of 0.011 m of settlement over 48 days. In both the saturated and unsaturated columns, the greatest extent of this settlement occurred within the first 40 days. Past this point, the rate of settlement decreased substantially. Settlement measurements were best estimates given that smearing of waste materials along the side of the column made it difficult to take proper readings.

Table 4-2: Experimental column settlement data over time (days). All values are recorded in centimeters (cm). Thickness of petroleum coke and CFT layers are recorded, and BI represents the height from the base of the column to the PC-CFT interface. All hyphens (-) represent missing measurement at that time. Any italicized data represents values that may not be completely accurate due to smearing of CFT on the sides of the column during settlement, making it difficult to record a value.

Time	Saturated Column 1			Unsaturated Column			Saturated Column 2		
	PC	CFT	BI	PC	CFT	BI	PC	CFT	BI
1	49.9	87.5	92.1	53.5	86.6	91.6	-	-	-
40	48	81.7	86.7	50.3	78.5	83.5	-	-	-
112	48	<i>80.8</i>	<i>85.8</i>	50.1	77.8	82.7	-	-	-
126	-	<i>80.1</i>	<i>85.5</i>	49.9	77.1	82.3	-	-	-
146	-	<i>73.5</i>	<i>78.5</i>	49.0	77.0	82.3	-	-	-
175	-	73.5	78.5	-	-	-	51.4	75.1	80.1
180	-	73.5	78.5	-	-	-	51.1	75.1	80.1
190	-	73.5	78.5	-	-	-	50.5	74.8	79.8
223	-	<i>72.3</i>	<i>77.3</i>	-	-	-	50.7	74.0	79.0

4.2.2 Column Water Chemistry

Pore-water chemistry (i.e., pH, alkalinity, EC, Cl, Na, Ca, K, Mg, and NH₃-N) was examined at three discrete time points within the saturated (24, 114, and 202 days) and unsaturated (24, 114, and 146 days) column experiments (Figures 4-17, 4-18, and 4-19). Insufficient volumes of pore water within the coke layer of the unsaturated column prevented complete chemical profiles from being obtained. Across both columns, pH remained consistently circumneutral over time within CFT layers below the interface, with measured values ranging from 7.74 to 8.03. This trend is consistent with pH values observed for CFT pore water in the field lysimeters. However, above the interface, pH demonstrated a decreasing trend toward shallower depths in the coke and water cap at all time points. The pH ranged from 6.65 to 8.03 in the saturated column and exhibited an average value of 7.56 ± 0.07 ($n=38$), across the three time points. Temporally, an increase in pore water pH is observed above the interface, illustrated by an increase from 6.93 to 7.51 between 24 and 202 days at the top of the column. Pore-water alkalinity follows a pattern consistent with that observed for pH through both columns at all time points, showing slight variation in the CFT between 1220 to 1840 mg L⁻¹. In the saturated complement, a substantial decrease in alkalinity is observed through the coke layer to shallower depths at all time points. Alkalinity ranged from 9 to 1740 mg L⁻¹, with a mean concentration reported as 934 ± 114 mg L⁻¹ ($n = 37$) for the 24, 114, and 202 day time points. Within the saturated coke layer, alkalinity increased over time between

depths of 0.2 to 0.45 m above the interface. A decrease in surface alkalinity over time is attributed to additions of DI water to maintain saturation. Electrical conductivity exhibits generally consistent values in the CFT layer of the unsaturated column after 114 and 146 days, fluctuating from 3.01 to 3.74 mS cm⁻¹. However, an increase in EC toward the surface of the CFT deposit in the unsaturated column is observed after 24 days, increasing from 3.87 to 4.73 mS cm⁻¹ from the bottom to the interface. The saturated column exhibits a steady decrease in the EC from the CFT into the petroleum coke layer, toward the surface. This upward decreasing trend is consistent amongst all time points. Collectively across the time points of interest, saturated column EC ranged from 0.03 to 5.7 mS cm⁻¹, with mean EC reported as 3.05 ± 0.26 mS cm⁻¹ (n=38). Temporally, a decrease in EC at the top of the column, in the water cap, is observed, most likely due to the additions of DI to maintain saturation.

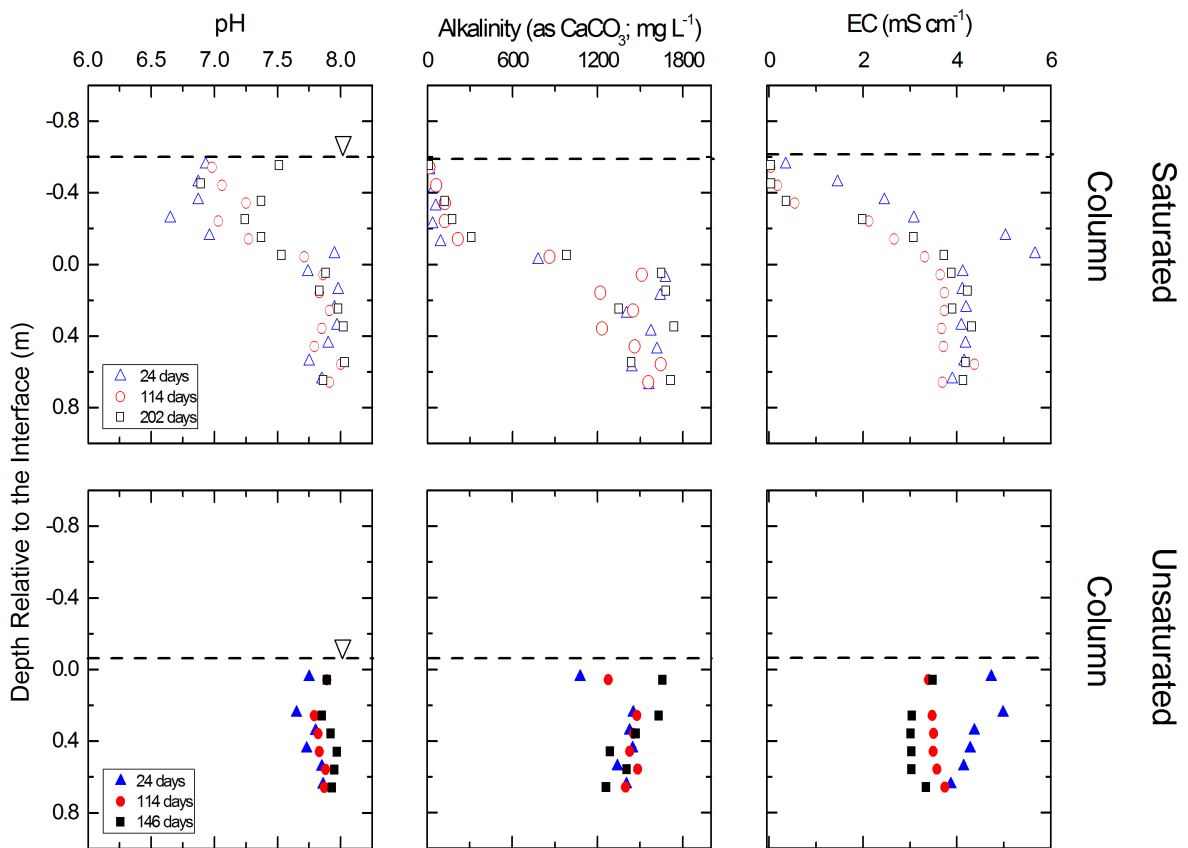


Figure 4-17: pH, alkalinity (as CaCO₃), and electrical conductivity (EC) depth profiles within laboratory column experiments. The dashed line represents the location of the water table. All depths have been normalized relative to the interface.

Within the unsaturated column, the concentration of Cl, Na, and NH₃-N did not vary greatly within the CFT layer, ranging in value from 445 to 492 mg L⁻¹, 899 to 971 mg L⁻¹, and 14.2 to 16.6 mg L⁻¹ across the reported time points, respectively. However, a clear transition to an upward decreasing trend is apparent for the aforementioned constituents across the interface into the coke layer and water cap of the saturated column. Concentrations of Cl, Na, and NH₃-N in the saturated column ranged from 0.45 to 508 mg L⁻¹, 3 to 1038 mg L⁻¹, and 0.0 to 15.5 mg L⁻¹, respectively, at the 24, 114, and 202-day time points collectively. Mean concentrations (n=38) of Cl, Na, and NH₃-N over the time points of interest were reported as 271 ± 33.5 mg L⁻¹, 614 ± 65.3 mg L⁻¹, and 8.65 ± 1.17 mg L⁻¹, respectively. Comparison of column concentrations at the different time points reveals that Cl, Na, and NH₃-N maintain similar quantities of these analytes in the unsaturated system, within the CFT. Pore-water Cl concentrations increased over time above the interface in the saturated column, while Na exhibits a decrease in concentration within the coke and water cap over the course of the experiment. Ammonia concentrations decrease rapidly above the interface in the saturated column, remaining consistently near a concentration of 0 toward the surface throughout the experiment.

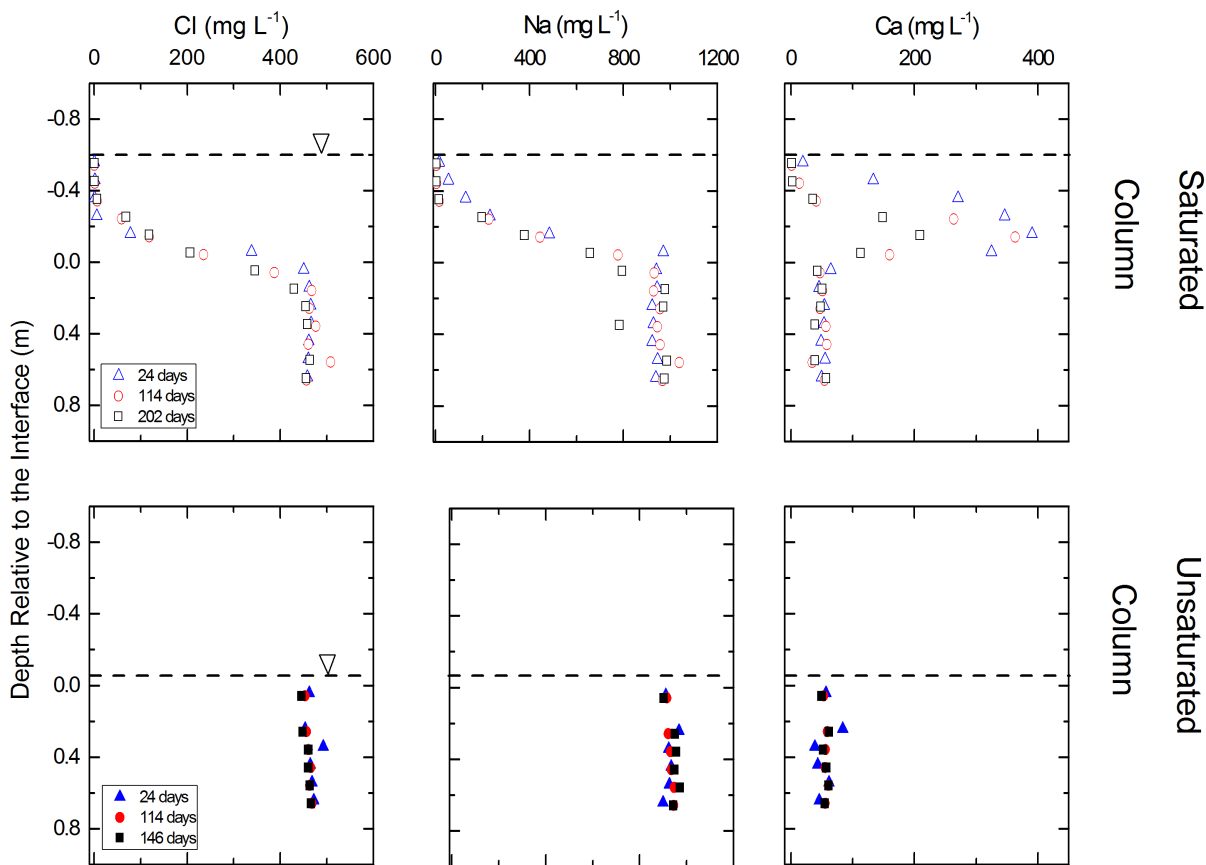


Figure 4-18: Depth profiles of Cl, Na, and Ca within laboratory column experiments. The dashed line represents the location of the water table in each column.

Profiles for Ca and Mg follow a similar trend to that of other dissolved constituents in the unsaturated column, with concentrations remaining relatively consistent between 38.8 to 84.0 mg L⁻¹ and 18.3 to 32.1 mg L⁻¹, respectively, across the specified time points. Alternatively, the saturated equivalent reveals a stark difference in the spatial distribution of these cations over the span of the column experiment. Within the CFT layer, concentrations of both cations in the saturated column remain consistent both temporally and spatially. However, a zone of elevated Ca and Mg concentration is observed at about 0.2 m above the interface in the saturated coke layer, consistent for both analytes. Concentrations then decrease rapidly toward the surface of the column. Throughout the saturated column, Ca and Mg concentrations range from 1.10 to 391 mg L⁻¹ and 0.470 to 259 mg L⁻¹, with mean concentrations (n=38) calculated as 101 ± 17.7 mg L⁻¹ and 57.9 ± 10.7 mg L⁻¹, respectively, at the 24, 114, and 202-day time points. Potassium concentrations exhibit a greater extent of variation to that of all dissolved constituents in the unsaturated column after 24 days, with reported concentrations varying from 14.1 to 43.5 mg L⁻¹.

This contrasts concentrations of K in the unsaturated column at the 114 and 202-day time points which are consistent through the CFT, between 18.1 to 20.3 mg L⁻¹. However, noticeable variation existed throughout the CFT layer in the saturated column at the 24-day time point and at the 202-day time point, illustrated by a larger spread of values. The concentration of K throughout the entire saturated column ranged from 0.22 to 61 mg L⁻¹, with an average concentration (n=38) of 18.8 ± 2.41 mg L⁻¹, across all time points of interest. At the CFT-coke interface in the saturated system, K decreases toward the surface at all time points. Temporally, a decrease in Ca, Mg, and K concentration in the coke and water cap layer is observed throughout the experiment. Through all analyte profiles, a decrease in surface concentration over time may be attributed to dilution caused by the addition of fresh water to the saturated column, as a means of maintaining an appropriate level of saturation.

To assess the potential for cation exchange within the petroleum coke layer of the saturated column, Na data were plotted against a conservative tracer (Cl) to compare relative concentrations over time (Figure 4-20). The data reveals that a distinctive offset is consistently present between Cl and Na, with Na exhibiting higher relative concentrations at each discrete time point than the conservative tracer.

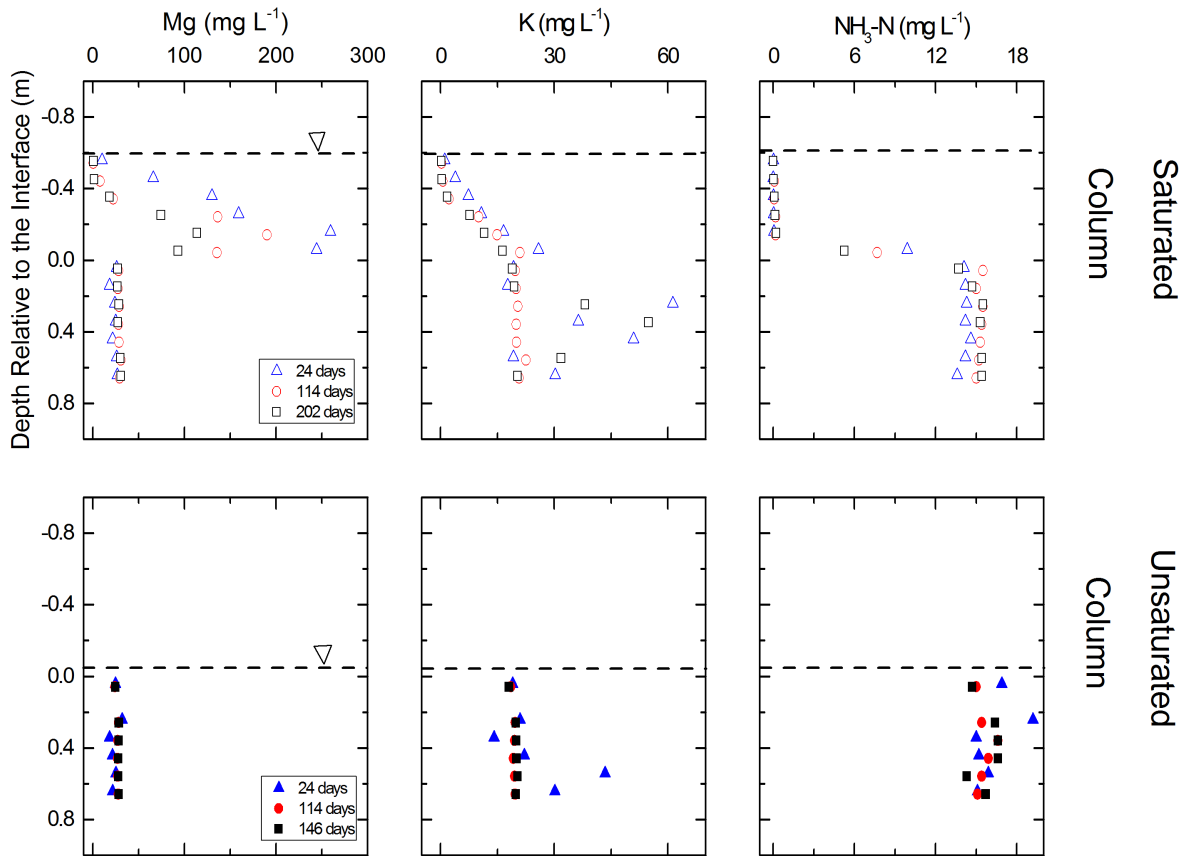


Figure 4-19: Depth profiles of Mg, K, and $\text{NH}_3\text{-N}$ within column experiments. Location of the water table is indicated by the dashed line.

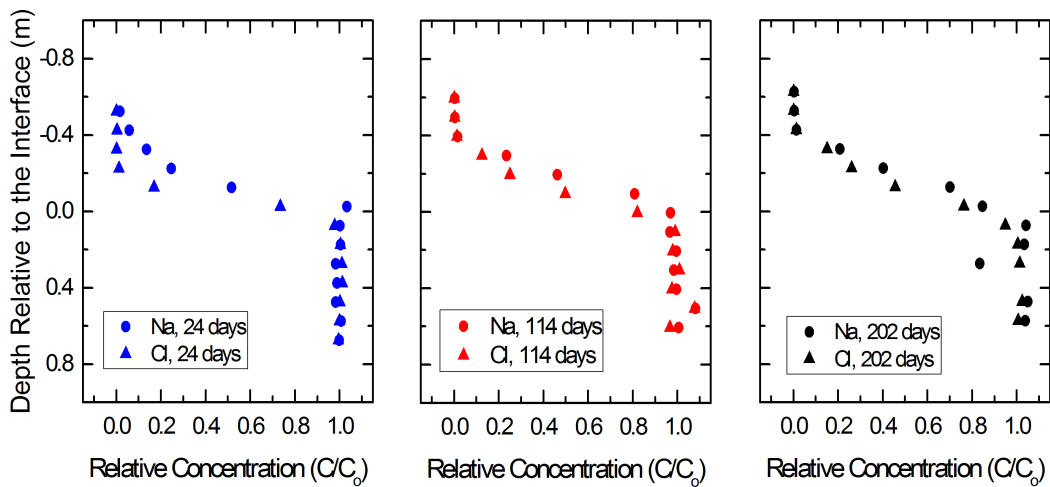


Figure 4-20: Comparison of the relative concentrations of Na and Cl in saturated column data at 24, 114, and 202 days.

4.2.3 *Transport Modeling*

Using the settlement data collected during the span of the column experiments, a root-time settlement function was compared against the data to come up with a best estimate of an advective flux versus time ($q(t)$) function. Although the root-time settlement function could be adjusted to fit the measured settlement data, it was observed that both the settlement data and root-time estimate heavily overestimated the amount of advection experienced by the system, providing a poor fit to the measured chloride values. To remedy this, the assumption was made that settlement and advection dominated the transport regime within the first 40 days of the experiment, based on settlement measurements within the column. After 40 days, both settlement and advection were considered almost negligible. Thus, root-time advection estimates were implemented for the first 40 days and then dropped to values of $1 \times 10^{-10} \text{ m d}^{-1}$. Once this approach was implemented, the root-time estimates gave a noticeably better fit to the measured Cl values after 202 days.

Once an appropriate $q(t)$ function was determined, a series of 1D transport models were created, using the parameters outlined in Table 3-3, and compared to measured chloride data at discrete time points. Two scenarios were considered for the conservative transport models: a diffusion only scenario (Figure 4-21A) and an advective-hydrodynamic dispersive scenario (Figure 4-21B) that implemented the estimated advection rates. These models were evaluated at 24, 114, and 202 days to constrain whether or not the developed model could appropriately capture the transport processes governing Cl migration at early, middle, and late stages of the experiment. In the diffusion only scheme, results indicate that the conservative models provide a relatively good fit to the measured chloride data across all time points. However, the diffusion models slightly underestimated Cl migration both below and above the interface and therefore are not an exhaustive description of the processes at work. Moreover, the conservative transport models that implement advective-hydrodynamic dispersive transport exemplify a superb fit to the experimental column data at all time points. The Cl data is well described within the petroleum coke layer and is fit much closer within the CFT below the interface as well, exemplifying the good fit of the advection-hydrodynamic dispersion model outputs to the experimental column data. At the 24 and 114-day time points, the advective-hydrodynamic dispersive model describes the measured data very well. After 202 days, the transport model still slightly underestimated measured Cl concentrations below the interface. Nevertheless, the overall fit remained strong. Overall, the advective-hydrodynamic dispersive models provide a more comprehensive explanation of the

measured chloride data, allowing for a better understanding of the processes governing chloride movement in the experimental system.

To validate that the modeling results provided an appropriate explanation of chemical mass transport in these layered systems, a plot of the Peclet number over time (Figure 4-22) was created for the saturated column system, using measured settlement data and the root-time settlement function to provide a best estimate of the advective flux over time. Results indicate that the Peclet number decreases rapidly to below a value of 10 within a year. After approximately 3 years has passed, the Peclet number approaches a value of 1 and continues to decrease below 1 over the span of a decade.

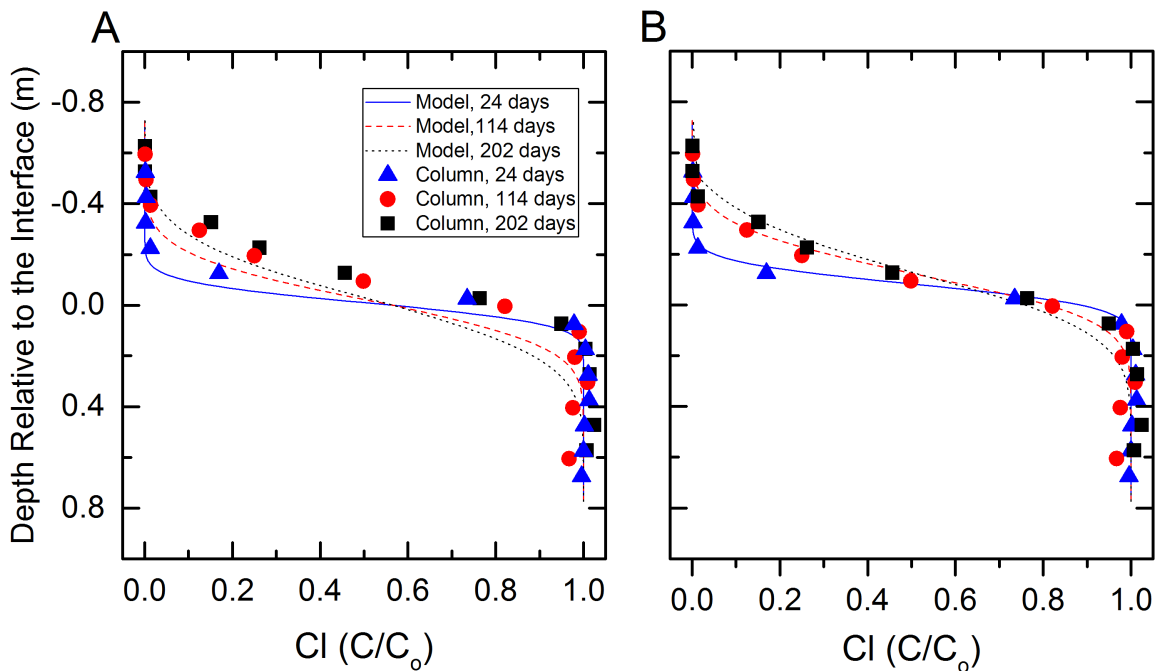


Figure 4-21: One-dimensional conservative transport models plotted against experimental chloride data from the saturated column. A diffusion only scenario (A) and advective-hydrodynamic dispersive scenario (B) were compared at 24, 114, and 202 days.

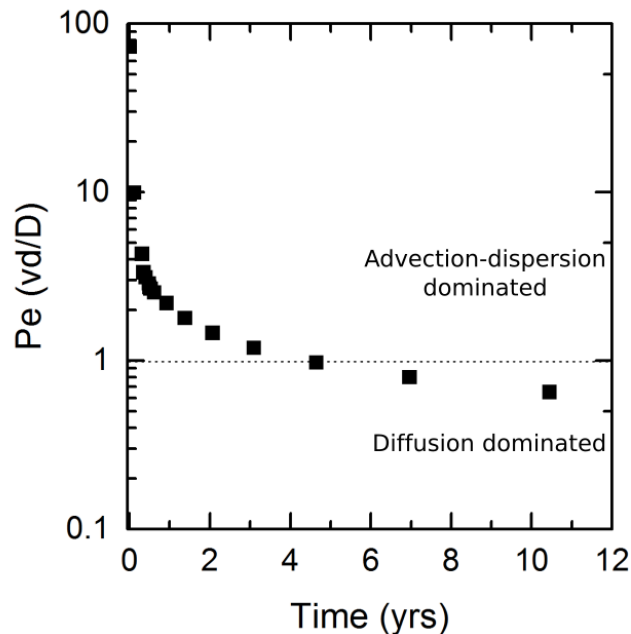


Figure 4-22: Peclet number over time (in years) for the saturated column system. The horizontal dotted line delineates a Peclet value of 1.

4.2.4 Sensitivity Analyses

A sensitivity analysis of models generated with different rates of advection were plotted with the measured chloride data after 202 days to understand the rate of settlement that best represented the data (Figure 4-23). Based on this, it was observed that a rate of settlement of 0.7 provided the best explanation of the column chloride data. Although all data points below the interface were underestimated by the transport models, above the interface chloride data demonstrated a good fit with the model generated using a rate of settlement of 0.7. The total amount of settlement estimated after 40 days by a rate of settlement of 0.7 is in good agreement with the measured amount of settlement in the column after 40 days.

Values for CFT settlement rate and petroleum coke porosity were varied at 24, 114, and 202 days, and the RMSE computed, to get an understanding of model responsiveness to these parameters (Table 4-3 and Table 4-4). Results of the sensitivity analysis reveal that RMSE is minimized for a rate of settlement of 0.9 at 24 days, and 0.7 after 114 and 202 days. The RMSE varies from 0.105 to 0.237, 0.0394 to 0.121, and 0.0445 to 0.0979 for the 24, 114, and 202 day time point, respectively. For petroleum coke porosity, the RMSE was minimized with a porosity

of 0.2 at 24 days, and at 0.4 for the 114 and 202-day time points. The range of RMSE was 0.105 to 0.237, 0.0394 to 0.121, and 0.0445 to 0.0979 for the 24, 114, and 202 day time points, respectively. Overall, there is a greater level of error and uncertainty associated with changes in both parameters after 24 days than 114 and 202 days.

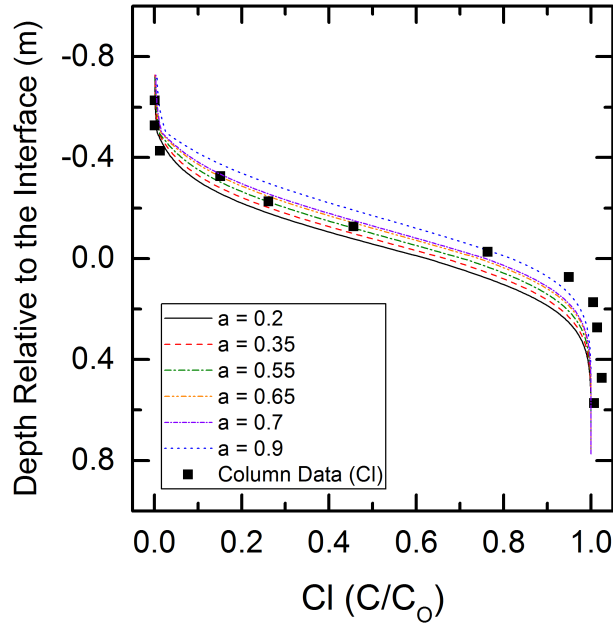


Figure 4-23: Sensitivity test of various rates of settlement against measured chloride data, after 202 days.

Table 4-3: RMSE calculated for changes in the rate of settlement parameter at 24, 114, and 202 days. Bolded values represent lowest calculated RMSE at each time point.

Parameter	Root Mean Square Error		
	24 days	114 days	202 days
Rate of Settlement (a)			
0.2	0.237	0.121	0.0979
0.35	0.212	0.094	0.0760
0.55	0.180	0.0622	0.0537
0.7	0.152	0.0394	0.0445
0.9	0.105	0.0527	0.0640

Table 4-4: RMSE determined for varying values of coke porosity after 24, 114, and 202 days. Bolded values represent lowest calculated RMSE at each time point.

Parameter	Root Mean Square Error		
Coke Porosity (n)	24 days	114 days	202 days
0.2	0.0157	0.134	0.133
0.3	0.106	0.0485	0.0623
0.4	0.152	0.0394	0.0445
0.5	0.180	0.0646	0.0607

CHAPTER 5: DISCUSSION

5.1 Water and Salt Transport

All reclamation scenarios simulated in the lysimeter experiments experienced seasonal near-surface freeze-thaw cycles. However, the lower portion of CFT layers underlying coke layers did not fully freeze (Figure 4-3 and Figure 4-4), suggesting that in these systems, freeze-thaw cycling was not a dominant driver of pore-water release from these CFT layers. Comparison of mean daily EC_{bulk} and mean daily temperature data over a 551-day period demonstrated that seasonal freezing was likely limited to the top of CFT layers in lysimeters where an overlying coke layer was located. This interpretation is corroborated by temporal profiles of temperature and EC_{bulk} (Figure 4-1 and 4-2) illustrate that positive temperatures and higher conductivity values were detected near the base of covered CFT layers compared to layers closer to the surface. Furthermore, depth profiles of temperature in each lysimeter (Figure 4-4) demonstrate that systems with covered CFT layers do not experience temperatures that fall below $-1\text{ }^{\circ}\text{C}$ near the base of CFT deposits during winter minima or spring. Despite the lack of full freezing of covered CFT layers, settlement data provides evidence that self-weight consolidation is the dominant process driving CFT settlement and concomitant release of process water in systems with a reclamation cover. In contrast, lysimeters with uncovered CFT layers experienced a greater degree of freezing, highlighted by mean daily temperatures that decreased well below 0°C in the CFT and causing the WCR probes to become non-responsive. As a result of this, EC_{bulk} values plummet to near 0 and consistently decrease once temperatures fall between -1 to $-2\text{ }^{\circ}\text{C}$, and lower. The larger measured settlement observed in Lysimeters 3 and 6 demonstrates that combined freeze-thaw cycling and self-weight consolidation enhanced CFT settlement in non-covered CFT layers. The depth at which freezing occurs will vary based on the field conditions, materials utilized, and reclamation (i.e., layering) scenarios. Seasonal temperature profiles (Figure 4-1) revealed that freezing began in late fall (i.e. November) and thawing was complete by late spring (i.e. June). Since freezing and thawing occur from a top-down direction, the deeper layers would be the last to fully freeze and thaw. A study of oil sands fine tailings subjected to natural freeze-thaw carried out by Dawson et al. (1999) discusses that

Fort McMurray experiences a 5-month freeze period from November to March, followed by a 5 month thaw period. These dates are consistent with what was observed in field lysimeters over nineteen months.

Volumetric water content and EC_{bulk} data suggests that natural self-weight consolidation, in addition to freeze-thaw cycles in Lysimeters 3 and 6, promoted advective transport of CFT pore water and associated solutes into adjacent layers. This interpretation was illustrated by a consistent increase in the VWC in the overlying coke layers or underlying tailings sand layers over time (Figure 4-5 and 4-6). The highest VWC was recorded in the summer months once the pore water was released following spring thawing. The release of process water from the CFT layers facilitated salt redistribution throughout the upper layers of the field lysimeters. The EC_{bulk} data exhibited noticeable increases at the surface of cover materials after 384 days, particularly saturated lysimeters. Similar to VWC, the largest EC_{bulk} increase within all systems occurred after the thaw period is complete during the summer months. The large increase in both VWC and EC_{bulk} is attributed to the pore-water release from CFT layers.

During the August 2016 field campaign, reclamation material and petroleum coke layers in L4 and L5 exhibited higher EC_{bulk} values than the unsaturated counterparts (Figure 4-7), with values that were approximately eight times and four times higher, respectively. Water-saturated conditions within the coke and reclamation material layers of L4 and L5 facilitated dissolved salt transport within pore water. Elevated EC values extended to the surface layers of L4 (reclamation material) and L5 (coke), with L5 exhibiting an EC that is approximately twice that of L4. Differences between these two systems was attributed to the cover material, which reduced the effect of evaporation thereby lessening upward vertical salt migration to surface. It is well established in the literature that evaporative accumulation of salts within reclaimed landscapes remains a challenge to successful growth of vegetation (Carey, 2008; Li et al., 2014; Simhayov et al., 2017). However, multiple studies have shown that proper implementation of cap or vegetation layers for waste management and reclamation design can act as an evaporative barrier (Yanful et al., 1994; Naeth et al., 2011; Ketcheson et al., 2016), supporting what is observed in the field lysimeters with the use of coke and reclamation material to cap underlying CFT deposits. Furthermore, the peat and clay-till that makeup the reclamation material have the potential to further mitigate salt transport via competitive ion exchange reactions and sorption processes. Although the extent of this has not been investigated in this study, an investigation conducted by

Holden et al. (2011) and Rezanezhad et al. (2012) demonstrate that both clay-till and peat, respectively, are capable of retarding the transport of salts through exchange reactions. In L3 and L6, pore water EC data indicated that CFT pore water also migrated downward into the underlying 1 m tailing sand layer. However, these layers can accommodate only a limited quantity of process water – approximately 2500 L, assuming tailings sand has a porosity of 35% – and upward vertical salt transport would likely dominate once this pore space is occupied. Both L3 and L6 exhibited similar EC profiles in both the CFT and tailings sand layers, with both downward and upward salt transport observed. Despite downward salt transport into tailings layers, upward migration of process water is apparent, with EC increases near the surface of CFT deposits most likely amplified by evaporation.

Chloride and $\delta^{18}\text{O}$ data (Figure 4-8) provided further evidence to support the pore water and bulk EC data, suggesting that the advective release and concomitant migration of process water occurs from CFT layers through to adjacent layers in these systems. Similar to the pore water EC data, the surface Cl concentration in L5 is about three times greater than what is observed in L4, attributed to the presence of the reclamation material cap in L4. The decrease in Cl toward the surface observed in L4 is indicative of a diffusive transport process, as Cl rich pore water within the CFT slowly moves toward surface layers. Chloride concentrations in CFT pore waters can range from 80 to 2200 mg L⁻¹ (Heaton, 2015), whereas FFT exhibits a smaller range from 100 to 700 mg L⁻¹ (Holowenko et al., 2000; Salloum et al., 2002; Allen, 2008; Siddique et al., 2014; Dompierre et al., 2016). These values are generally consistent with concentrations observed for pore water throughout all layers of the field lysimeters. Dissolved Cl concentrations in the field lysimeters were greater than these FFT pore-water concentrations, which is indicative of evaporative concentration. Heaton (2015) reported that evaporation from the surface of CFT deposits increases dissolved concentrations of chloride and other solutes, which is consistent with results from the lysimeter experiments. Chloride data in arrangements containing tailings sand and CFT further support the EC data, demonstrating that although tailings sand accommodates downward ingress of process water, there is an observable increase in Cl concentration near the surface.

Similarly, the $\delta^{18}\text{O}$ signature in L4 remained relatively consistent through the coke and reclamation cover, with slightly depleted values likely due to mixing of pore water with fresh water used to fill the lysimeters. Pore water was less depleted with $\delta^{18}\text{O}$ in L5 than in L4, supporting the

interpretation that evaporation has a large influence on salt distribution in systems without a reclamation cover. Baer et al. (2016) reported $\delta^{18}\text{O}$ values ranging from -13.6‰ to -10.4‰ in FFT, which is consistent with data for L4 and L5 and suggests this water has been mixed with pore water from the CFT layer. Depletion of $\delta^{18}\text{O}$ within the tailings sand of L3 and L6 is most likely caused by infiltration of precipitation within the open end of the monitoring well at the surface. Upward depletion of $\delta^{18}\text{O}$ within L3 and L6 is due to the presence of desiccation fractures which permit infiltration of more depleted fresh water used to fill the lysimeters.

Varying the waste and cover layer thicknesses has the potential to limit the impact of evaporative processes on the release and transport of process water. Decreasing the thickness of CFT deposits in reclamation design places a restriction on the volume of pore water that can be released upward and therefore on the extent of salt distribution toward the surface. Placement of a vegetative cover layer demonstrates promise in mitigating the influence of evaporation. A study by Kessler et al. (2010) concluded that thicker covers experience decreased salinity and are capable of maintaining appropriate water storage to promote plant growth, facilitating better overall reclamation performance. Thus, assessing changes in cap material thickness above CFT holds promising implications for mitigating evaporation, however care must be taken to ensure that the layer thickness is not increased to an extent that would jeopardize water storage and access to moisture by vegetation (Huang et al., 2015).

5.2 Ion Exchange Reactions

The water-saturated lysimeters exhibited elevated dissolved salt concentrations through CFT, coke and reclamation material layers, whereas salt migration did not extend through coke layers within the water-unsaturated systems. Pore-water volumes released from CFT within L1 and L2 was volumetrically accommodated within the pore space of the overlying coke layers. Sodium migration did not, therefore, extend into the reclamation material layer (L1) or to surface (L2). Evaporation in lysimeters with a reclamation cover is diminished, permitting a diffusive distribution effect, illustrated by the shape of the Na profile in L4. However, the net increase in Ca, Mg and K complement the decrease in Na toward the surface of L4, suggesting that cation exchange may be occurring within the coke layer. Ion exchange reactions, similar to what was outlined in Equation 1.1, occur in the petroleum coke as Na-rich process water travels from CFT into overlying layers. Elevated levels of Na entering the coke promotes a shift toward exchange with Ca, Mg, and K on mineral surfaces, facilitating their release and concomitant sorption of Na.

The same process is observed in L5, however near surface concentrations are significantly larger. The reason for this is that the influence of evaporation is greater in L5 due to the lack of an additional cover layer. Therefore, although we would expect a retardation in the amount of Na migrating toward the surface due to exchange on mineral sites, coke exhibits a low CEC and small SSA (Table C-1, Appendix C). As a result, exchange sites on individual coke grains cannot accommodate the amount of Na that is being concentrated by evaporation, thereby facilitating a large increase in the Na concentration at the surface of L5. Dissolved Ca, Mg, and K concentrations increase within the coke of L5 due to exchange and evaporative concentrations. At the surface, L5 contained approximately two, four, three, and four times greater concentrations of Ca, K, Mg, and Na, respectively, than L4 after a 10-month period, demonstrating that salt accumulation is amplified in the absence of reclamation soil covers and, therefore, increased evaporation. Increases in Ca and Mg pore water concentrations near the surface of L4 and L5 are also indicative of calcite and dolomite dissolution, which is supported by pH data that indicates a decrease to circumneutral pH in the coke and reclamation material. Additionally, the high CEC of peat and till in reclamation material demonstrates promise to facilitate exchange and attenuation of dissolved salts (Vessey and Lindsay, 2017), potentially contributing to the lower concentration of major cations observed within the reclamation material cap of L4. Both unsaturated and saturated scenarios containing a bulk CFT layer and tailings sand base have near identical profiles after 10 months, exhibiting consistent concentrations throughout CFT until near surface evaporation facilitates an increase. Similar to what was observed with Cl, the concentration of dissolved ions in the tailings sand increases initially as pore water migrates downward, diminishing the advective flux of water upward toward the surface. However, the tailings sand was unable to volumetrically accommodate significant quantities of released water, resulting in the eventual release of pore water to the top of the deposit once the sand pores are filled.

Comparisons of normalized Na and Ca data in systems with a reclamation cover reveal that there is a net release of Na and Ca toward the surface compared to Cl (Figure 4-11). As a baseline in these systems, the effects of evaporation and chemical mass transport processes facilitate the distribution of dissolved salts within L4 and L5. As Cl is a conservative tracer, any observed differences in the concentration of Na and Ca would suggest that some other process is contributing to observed deviations from the Cl profile. The net increase of normalized Na through the petroleum coke and reclamation material indicate that exchange reactions may be contributing to

the release of Na from the petroleum coke. This is substantiated by Cl and Na data from the saturated column experiment. In the saturated column, Cl migrates into the petroleum coke from underlying CFT, exhibiting mass accumulation near the surface over time. Comparison to Na profiles in the saturated column reveal that a similar trend is apparent, however the extent of mass transport is slightly different (Figure 4-20). Over time, the concentration of Na that is present throughout the coke layer is slightly more than Cl, creating an offset in the graphs. The concentration of Na does not change substantially over time, suggesting that the greater ratio of Na to Cl at each time point is not a product of transport processes. In the absence of significant evaporation, the offset in the graphs reflects geochemical exchange reactions that initially release Na from the petroleum coke, which further supports the presence of exchange reactions in the field data. As petroleum coke is initially slurried with Na-rich OSPW, ingressing process water from underlying CFT layers that is rich in Ca, Mg, K, and Na would facilitate exchange that removed Na from the petroleum coke.

Increased Ca and Mg concentrations within and below reclamation material layers may result from ion exchange or mineral dissolution reactions. This interpretation is supported by pore-water pH, which decreases to a circumneutral pH of less than 7.5 in the petroleum coke and reclamation material, potentially enhancing carbonate-mineral dissolution. In support of this, the saturated column experiments demonstrate inputs of Ca and Mg into the pore water 0.2 m above the interface, which is most likely contributed by exchange reactions within the coke. Petroleum coke is not rich in carbonate minerals, however the pore water pH of the coke in the saturated column would support dissolution of calcite and dolomite. Within the field systems, dolomite dissolution is most likely occurring within the peat-till layer, and contributing Ca and Mg in underlying layers via downward transport. Furthermore, Na in the process water can actively engage in exchange with Ca and Mg, which are released from the coke, contributing more Ca and Mg into the pore water. Thus, the petroleum coke can host limited exchange reactions, however field experiments reveal that the exchange capacity and SSA are not enough to offset the massive increases induced by evaporation.

Contribution of dissolved cation species from petroleum coke that has been slurried with OSPW is probable, as Nesbitt (2016) reports concentrations of Ca (0.19 to 176 mg L⁻¹), K (4.18 to 20.10 mg L⁻¹), Mg (0.21 to 122 mg L⁻¹), and Na (36.7 to 1300 mg L⁻¹) in the pore water of bulk petroleum coke deposits, which are all smaller than that observed in the field lysimeters. The

concentrations of major cations in CFT pore water have been described for Mg (10 to 150 mg L⁻¹), Ca (10 to 470 mg L⁻¹), K (10 to 60 mg L⁻¹), and Na (260 to 3700 mg L⁻¹), with the highest values of these cations being observed near surface as a result of evaporation (Heaton, 2015). These concentrations were generally consistent with values observed in the field experiments; however, evaporation amplified concentrations of all solutes at the surface of lysimeters, which produced higher concentrations than previously reported. As process water was released from CFT into overlying petroleum coke, a combination of ion exchange reactions and evaporative solute concentration influenced pore-water chemistry.

5.3 Biogeochemical Processes

Accumulation of dissolved SO₄ is apparent in the L4 coke layer and reclamation cover, which is supported by PHREEQC modeling results that reveals pore water in L4 is consistently under saturated with respect to gypsum. In the upper 0.5 m of L5, pore water is at or near saturation with respect to gypsum, suggesting that precipitation of gypsum may occur near the surface due to enhanced evaporation. However, the remainder of the pore water in L5 exhibit negative saturation indices for gypsum, supporting dissolution of gypsum. The concentration of SO₄ in the CFT layers were generally low, likely due to potential anaerobic sulfate reduction by sulfate-reducing microbes. The addition of gypsum to CFT increases the amount of available SO₄ in the pore water and can stimulate reduction (Ramos-Padrón et al., 2011). This interpretation is supported by large HS⁻ concentrations observed in CFT layers, which are indicative of sulfate consuming metabolisms (Table B-1, Appendix B). Additionally, the ingress of sulfidic water from the CFT into petroleum coke, under anoxic conditions, may inhibit the release and mobility of trace metals from petroleum coke. Studies focused on V and Ni mobility in petroleum coke demonstrated that saturated, anoxic, and alkaline pore water conditions favour reduced mobility of these trace metals (Nesbitt, 2016; Nesbitt and Lindsay, 2017). Increases in concentration in the upper layers of L4 and L5 is most likely due to evaporation, exhibiting concentrations 2.68 times greater at the top of L5 than in L4, consistent with what was observed for most dissolved ions in these systems. Observed SO₄ concentrations in field lysimeters depart well above concentrations reported in tailings ponds (Stasik et al., 2014) and in gypsum-amended composite tailings underlying an experimental reclamation fen (Reid and Warren, 2016). Lysimeter 3 and 6 also exhibit accumulation of dissolved SO₄ near the surface that is driven by evaporation, with limited

variability in concentration that extends downward into the tailings sand. Sulfate accumulation at the top of the surface indicates that petroleum coke and reclamation substrate have minimal impact on the attenuation of dissolved salts. Moreover, the concentration of NH_3 in lysimeters is generally consistent with values that have been measured within tailings and coke dominated systems (Siwik et al., 2000; Mackinnon et al., 2001; Nesbitt, 2016), but exhibits noticeably higher concentrations in specific arrangements most likely due to the effect of evaporation. Furthermore, Dompierre et al. (2016) reports average $\text{NH}_3\text{-N}$ values in an FFT filled End-Pit lake of $9.9 \pm 4.7 \text{ mg L}^{-1}$, which is in close agreement with what is observed in the field lysimeters. Allen (2008) also reports that $\text{NH}_3\text{-N}$ concentrations exceeding 10 mg L^{-1} is common for OSPW. Elevated NH_3 concentrations occur above the coke-CFT interface, which could be indicative of cation exchange processes or the presence of endemic microbial metabolisms within the petroleum coke that are capable of producing NH_3 from available nitrogen sources (Dompierre et al., 2016). Studies conducted by Kay-Shoemake et al. (1998a,b) have demonstrated that polyacrylamide, a nitrogen bearing flocculating agent added to CFT, can be broken down by aerobic microorganisms into usable ammonium. Declining concentrations of NH_3 near the surface reflects a more aerobic environment, which may suggest nitrification involving biotic NH_3 oxidation into nitrate and nitrite via a variety of in-situ microbial metabolisms. Studies conducted in oil sands environments (Saidi-Mehrabad et al., 2013; Choi and Liu, 2014) and oil contaminated soils (Kurola et al., 2005) have identified nitrifying microbial genera.

5.4 Conceptual Model

The one-dimensional, chloride transport models support the Cl data from the saturated column over the experiment lifespan. Based on the models, transport of dissolved salts is initially driven by large advection rates and dispersion caused by initial settlement of CFT. As settlement attenuates over time, the transport regime shifts from predominantly advection-dispersion driven to a molecular diffusion dominated system. Despite a generally close fit, diffusion-only models underrepresent the Cl data at all time points, highlighting the important of advection in bridging the gap between the model and the experimental data. Within the context of layered waste systems and continuous CFT deposits, CFT undergoes self-weight consolidation over time that promotes water release; a process that is enhanced by freeze-thaw cycles of near surface CFT deposits. This results in settlement that is reflected by a decrease in the total volume of CFT in the system. To accommodate this decrease in waste volume, an equal volume of pore water is ejected upward and

released to the surface. As a result, overlying materials and vegetative covers must accommodate infiltrating process water. Initially, the rate of settlement is large such that the transport of highly saline process water is driven by an advective-dispersive dominated regime, with migration via molecular diffusion occurring in the background. However, the rate of consolidation attenuates rapidly, facilitating a transition to diffusion dominated salt transport with minimal advective-dispersive contribution (Figure 5-1). These findings are supported by the research of Dompierre and Barbour (2016), who discuss that the reclamation of FFT in an End-Pit lake is characterized by initial advection dominated mass transport, transitioning to a diffusion driven regime over the long-term. Additionally, calculated Peclet numbers for the modeled system provide evidence that these systems are transitional. Within one year, Peclet numbers decrease rapidly but remain well above 1, indicating that advection and dispersion are dominating processes early on. However, between approximately two to four years, layered systems begin to experience a stark transition to more diffusion controlled transport processes, corroborated by modeled Peclet numbers that decrease to a value of 1. After approximately 5 years, the value of the Peclet number continues to drop below 1 and supports a diffusion dominated system. Therefore, the developed transport models provide substantial evidence that significant mass accumulation of salts is possible near the surface of saturated layered systems, as contaminant transport processes work in combination to carry salts into cover layers over time. This is not the case for unsaturated prescriptions, as molecular diffusion cannot move dissolved constituents across a concentration gradient in the absence of water. As demonstrated by the unsaturated column experiments, advection from settlement is not enough to drive process water throughout the entire extent of the coke layer. These findings support what was observed in the field systems, demonstrating that saturated reclamation landscapes may pose more short-term problems to reclamation than unsaturated analogs. A study of salt transport in reclamation landscapes conducted by Kelln et al. (2008) is in agreement with this, discussing that diffusion of salts is reduced by maintaining unsaturated conditions, limiting the extent to which solutes traveled into cover layers.

Moreover, it is apparent that petroleum coke is unable to mitigate significant quantities of dissolved salts through ion exchange, demonstrated by the elevated levels of salts within reclamation substrate and throughout coke layers in saturated systems. Although surface concentrations are significantly decreased with the implementation of a 0.5 m vegetative cover, salt accumulation still occurs at levels that are unacceptable for long-term reclamation. The weak

SSA and exchange properties of coke do not permit it to act as a substantial cation sink, and are overshadowed by evapoaccumulative processes. Furthermore, chemically inert tailings sand does not appear to provide an appropriate diversion for released water during CFT settlement, as both L3 and L6 experience rising contaminant concentrations near the surface. Increasing the quantity of tailings sand below CFT would accommodate a larger volume of process water and, potentially, limit upward advective solute transport. Results from the field experiments would suggest that reclaimed landscapes should be kept unsaturated, as diffusive transport of contaminants is hindered by the absence of water within the pore space. Lysimeters with an unsaturated coke prescription consistently demonstrate that they are able to accommodate released process water without any major accumulation of dissolved salts within surface covers. However, a thin layer of petroleum coke overtop CFT may not contain a substantial volume of pores to accept all the incoming CFT process water, considering settlement and, in some instances freeze-thaw, enhances its advective release.

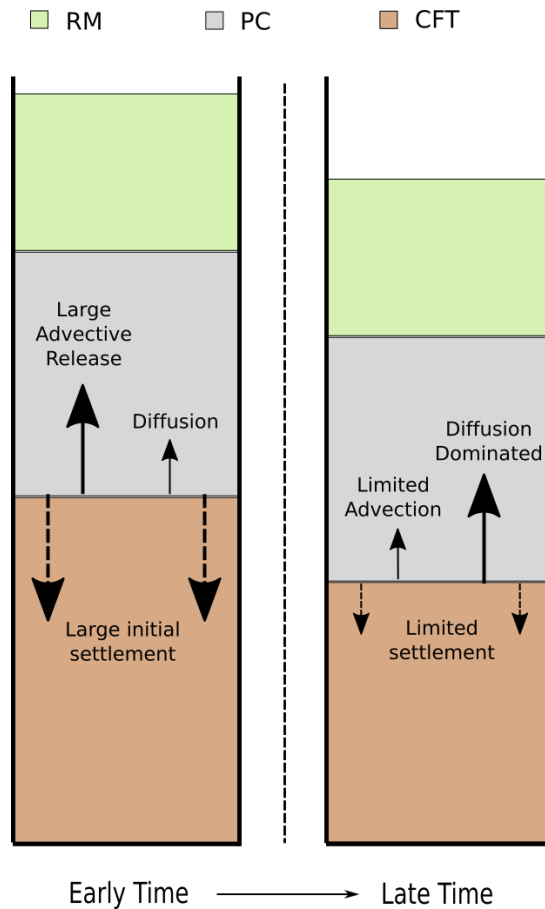


Figure 5-1: Conceptual diagram outlining the intrinsic processes controlling movement of process water within layered systems implementing CFT. Dashed arrows represent settlement and solid arrows contaminant transport processes. RM = Reclamation Material, PC = Petroleum Coke, CFT = Centrifuge Fine Tailings.

5.5 Model Limitations and Sensitivity

These models present a non-unique solution to the conceptual understanding of these layered systems, however parameters were chosen as best estimates in an attempt to simulate this scenario closely. Literature values were used to estimate porosity, hydraulic conductivity, diffusion coefficients, and dispersivity without overcomplicating the model. As previously mentioned, advection rates were estimated using the settlement data measured over time in the columns as a means of providing a fit that was representative of the system. Sensitivity analysis instills confidence that the selected rate of settlement (i.e. advection rates) and porosity of petroleum coke provide the best fit for the model to the experimental data. Root Mean Square Error was minimized

for the selected rate of settlement and coke porosity, however all values generated relatively low error values. Both the rate of settlement and coke porosity were identified as the most sensitive parameters to change, as the settlement rate dictates the advective flux and the coke porosity is important in determining the diffusion coefficient within the petroleum coke. Some of the major experiment and model limitations are that field conditions are not taken into consideration, such that the saturated column is not a true analog for the field experiments. Evaporation rates and freeze-thaw are not included in the numerical model, which therefore underestimates what is observed in the field. However, the contaminant transport processes simulated in the model still capture the essence of salt distribution in these systems, and can therefore provide appropriate insight into long-term reclamation considerations. Furthermore, there is a high degree of uncertainty surrounding the settlement data collected throughout the column experiments, as adhesive forces acting on the CFT during settlement facilitated unclear and uneven interface locations in the column. Additionally, measurements could have been made more consistently throughout the lifespan of the experiment to attain higher resolution in the settlement data. Despite all this, best estimates were used when determining advection rates from the settlement data, and the results are in good agreement with the experimental columns and the conceptual model of the system.

The numerical models are sensitive to increases and decreases in the rate of settlement, demonstrated by the changes in the RMSE during sensitivity analysis. Placing a thicker deposit of CFT within these layered systems as a means of reclaiming more tailings waste would result in a greater amount of settlement. The heavier surface loading by the thicker deposit would increase the stress to the system, facilitating greater self-weight consolidation that is augmented by freeze-thaw cycles. The advection rates that would result from this would be much larger than what the models predicted, facilitating greater release of process water and enhancing the accumulation of salt within vegetative cover material. Without a subsequent increase in the thickness of the coke layer, the volume of pores would be unable to keep up with the ingress of OSPW, jeopardizing successful reclamation in a shorter amount of time. In contrast with this scenario, decreasing the volume of CFT implemented into reclamation design, all other things remaining constant, would decrease the amount of settlement and lower advection rates. Although this has the potential to diminish transport of salts over a longer time span, molecular diffusion is still an active process in saturated systems, and may cause negative long-term impacts. Based on the column experiments

and the modeling results, implementation of an unsaturated layer of petroleum coke over CFT would hinder the migration of dissolved salts over a short time span, buying time for oil sands operators to develop a solution that could hydraulically divert released process water away from surface layers and establishing vegetation. This arrangement would limit diffusion driven transport into vegetation layers, while ensuring that there is available pore volume in the petroleum coke to accommodate a finite quantity of process water released by settlement. In addition, implementation of a suitable reclamation cover would help diminish the effect of evaporative accumulation of salts near the surface, providing the best chance at long-term reclamation come mine closure.

CHAPTER 6: CONCLUDING REMARKS

6.1 Conclusion

Six experimental lysimeters were constructed within an active oil sands mine to assess the feasibility of specific reclamation prescriptions in preparation for mine closure. The working objectives of this thesis were to understand the physical and chemical transport processes governing the movement of dissolved salts from CFT layers in these systems. Results demonstrated that lysimeter systems with reclamation covers experience partial freeze-thaw near the surface, with covered CFT layers remaining largely unfrozen throughout the year. Instead, uncovered surface CFT layers freeze almost entirely during the winter months, indicating that freeze-thaw cycles are an important mechanisms of pore-water release. However, settlement data revealed that self-weight consolidation is still a dominant control on the release of process water into adjacent layers, regardless of the freeze-thaw influence. Electrical conductivity data revealed that water-saturated systems experienced migration of process water from CFT into adjacent layers, with enhanced conductivity at the surface of layered systems. However, data also indicated that reclamation material covers can suppress evaporation and associated salt accumulation near surface. In CFT deposits underlain by tailings sand, the tailings sand can volumetrically accommodate a finite quantity of released pore water, however, migration of dissolved salts to the surface of CFT still occurs. These findings were further supported by Cl data and $\delta^{18}\text{O}$ signatures, which demonstrate that pore water of CFT origin migrates to the surface of cover layers in the water-saturated systems. Consistently, water-unsaturated systems containing petroleum coke and reclamation cover do not experience appreciable migration of process water past the CFT and coke interface.

Field and column experiments demonstrate that petroleum coke has a weak capacity to facilitate ion exchange reactions, preventing the retardation of dissolved salt migration. As a result, exchange reactions are overshadowed by evaporation and dissolved salts concentrate in large quantities at the surface of layered systems. Therefore, petroleum coke is not a reactive sink for dissolved Na within reclamation landscapes. The ingress of anoxic, sulfidic pore water from CFT also presents the opportunity for biogeochemical reactions to occur within adjacent waste layers,

however further study is required to elucidate the influence of these processes on pore water chemistry.

One-dimensional, conservative transport models enhance our conceptual understanding of dissolved salt migration in these layered systems, revealing that, initially, large settlement and advective release of OSPW facilitates an advection-hydrodynamic dispersion dominated regime. Over time, as the rate of settlement decreases, chemical mass transport of dissolved salts transition to a diffusion dominated regime as the advective flux diminishes. Sensitivity analyses done through calculation of the RMSE supports the good fit of the model to the experimental data.

Research conducted for this thesis has provided important insight into physical and chemical processes that influence salt transport and distribution within layered oil sands waste systems. Layered petroleum coke and centrifuged fine tailings have not previously been integrated into individual oil sands mine closure landscapes, making the results of this thesis crucial for tailings management and reclamation decisions in preparation for mine closure. Oil sands operators can use this information to inform decision making surrounding sustainable reclamation design that will promote establishment of vegetation and wildlife proliferation, while dealing with the excessive quantities of mine waste currently stored onsite.

6.2 Recommendations and Future Work

Implementation of unsaturated deposits would prevent molecular diffusion from facilitating mass loading of dissolved salts near the surface. The use of permeable material, such as petroleum coke or tailings sand, demonstrate promise to volumetrically accommodate ingressing pore water and limit the interaction between released process water and the vegetative cap. As a result, water quality in cover layers would experience a substantial improvement. A major caveat to the implementation of an unsaturated layer within reclamation design is the potential to limit the availability of water to cover vegetation. Moreover, saturated systems consistently resulted in increased Na concentrations within cover layers over time, as these materials hold a limited capacity to attenuate Na via ion exchange. However, the use of an additional reclamation cover (i.e. peat-mineral mix) demonstrates promise in decreasing the impact of evapoaccumulation of dissolved salts. Based on the information gathered from this investigation, implementation of a thin layer of petroleum coke or tailings sand above the CFT would allow for short-term volumetric accommodation of released process water. Additionally, placement of an additional cover would

help mitigate the full effect of evaporation, decreasing the quantity of dissolved salts concentrated at the surface. The permeable nature of the tailings sand and petroleum coke would permit appropriate infiltration of precipitation, providing ample water for establishing vegetation. This arrangement, although not a long-term solution, would give operators time to consider options that would help divert Na-rich process water away from cover layers. One solution may be to hydraulically connect these systems in a way that would permit horizontal water flow, permitting a flushing of ingressing Na away from cover layers, and diluting Na concentrations throughout the system. The feasibility of full scale layered systems in this way is the subject of future collaboration between researchers and oil sands operators.

To further the work carried forward by this thesis, additional monitoring of both field and laboratory experiments can be done to assess how observed trends evolve through time. To gain a more in depth understanding of advection rates within these systems, settlement must be measured consistently and accurately over time. Numerical modeling can be translated over to the field lysimeters to better understand the extent of geochemical exchange reactions, as well as physical chemical transport processes controlling dissolved salt distribution across waste layers. Additionally, to better understand the geochemical implications of layering multiple waste streams, a full characterization of the endemic microbial metabolisms in the CFT and petroleum coke is required. This would provide crucial information regarding the presence or absence of important redox processes that may contribute or remove contaminants from migrating process water. Any of this additional information would be valuable to oil sands operators throughout the reclamation design and implementation process, ensuring that decision making is informed and carried out sustainably.

REFERENCES

- Abolfazlzadehdoshanbehbazari, M., Birks, S.J., Moncur, M.C., and Ulrich, A.C., 2013. Fate and transport of oil sand process-affected water into the underlying clay till: A field study. *Journal of Contaminant Hydrology* 151, 83–92
- AER, 2009. Directive 074: Tailings Performance Criteria and Requirements for Oil Sands Mining Schemes. Calgary, AB
- AER, 2016. Directive 085: Fluid Tailings Management for Oil Sands Mining Projects. Calgary, AB
- Alessi, D.S., Alam, M.S., and Kohler, M.C., 2014. Designer biochar-coke mixtures to remove naphthenic acids from oil sands process-affected water (OSPW). Oil Sands Research and Information Network, University of Alberta, School of Energy and the Environment, Edmonton, Alberta. OSRIN Report No. TR-57. 38 pp
- Allen, E. W., 2008. Process water treatment in Canada's oil sands industry: I. Target pollutants and treatment objectives. *Journal of Environmental Engineering and Science* 7(2), 123–138
- Appelo, C. A. J. and Postma, D., 2005. *Geochemistry, groundwater and pollution*. Amsterdam, the Netherlands: CRC press
- Baer, T., Barbour, S.L., and Gibson, J.J., 2016. The stable isotopes of site wide waters at an oil sands mine in northern Alberta, Canada. *Journal of Hydrology* 541, 1155–1164
- Baer, T., 2014. An evaluation of the use of natural stable isotopes of water to track water movement through oil sands mine closure landforms. M.Sc. Thesis, Department of Civil and Geological Engineering, University of Saskatchewan. Saskatoon, SK
- Baker, L.F., Ciborowski, J.J.H., and MacKinnon, M.D., 2012. Petroleum coke and soft tailings sediment in constructed wetlands may contribute to the uptake of trace metals by algae and aquatic invertebrates. *Science of the Total Environment* 414, 177–186
- Ball, J. W. and Nordstrom, D. K., 1991. User's manual for WATEQ4F, with revised thermodynamic data base and test cases for calculating speciation of major, trace, and redox elements in natural waters. U.S. Geological Survey, Open-File Report 91-183

- Barbour, S.L., Hendry, M.J., and Wassenaar, L.I., 2012. In situ experiment to determine advective-diffusive controls on solute transport in a clay-rich aquitard. *Journal of Contaminant Hydrology* 131(1–4), 79–88
- Botha, L. and Soares, J.B.P., 2015. The Influence of Tailings Composition on Flocculation: Linda. *The Canadian Journal of Chemical Engineering* 93(9), 1514–1523
- Boudreau, B.P., 1996. The diffusive tortuosity of fine-grained unlithified sediment. *Geochimica et Cosmochimica Acta* 60(16), 3139–3142
- Brown, D., Ramos-Padrón, E., Gieg, L., and Voordouw, G., 2013. Effect of calcium ions and anaerobic microbial activity on sedimentation of oil sands tailings. *International Biodeterioration & Biodegradation* 81, 9–16
- Campbell Scientific, 2012. CS650 and CS655 Water Content Reflectometers: Instruction Manual. Campbell Scientific, Inc. Retrieved from: <https://s.campbellsci.com/documents/es/manuals/cs650.pdf>
- Canadian Association of Petroleum Producers (CAPP), 2017. Retrieved from: <http://www.capp.ca/>
- Carey, S. K., 2008. Growing season energy and water exchange from an oil sands overburden reclamation soil cover, Fort McMurray, Alberta, Canada. *Hydrological Processes* 22(15), 2847–2857
- Chalaturnyk, R.J., Don Scott, J., and Özüim, B., 2002). Management of Oil Sands Tailings. *Petroleum Science and Technology* 20(9–10), 1025–1046
- Chen, M., Walshe, G., Chi Fru, E., Ciborowski, J.J.H., and Weisener, C.G., 2013. Microcosm assessment of the biogeochemical development of sulfur and oxygen in oil sands fluid fine tailings. *Applied Geochemistry* 37, 1–11
- Choi, J. and Liu, Y., 2014. Biodegradation of oil sands process affected water in sequencing batch reactors and microbial community analysis by high-throughput pyrosequencing. *International Biodeterioration & Biodegradation* 92, 79–85
- Canadian Oil Sands Innovation Alliance (COSIA), 2017. COSIA’s Water Mining Performance Goal. Retrieved from: <http://www.cosia.ca/watermining>
- Cussler, E.L., 2009. *Diffusion: Mass Transfer in Fluid Systems*. New York, NY: Cambridge University Press
- Dance, J.T. and Reardon, E.J., 1983. Migration of contaminants in groundwater at a landfill: a case study: 5. Cation migration in the dispersion test. *Journal of Hydrology* 63(1–2), 109–130

- Das, B.M., 2008. *Advanced Soil Mechanics*. New York, NY: Taylor & Francis
- Dawson, R.F., Segó, D.C., and Pollock, G.W., 1999. Freeze-thaw dewatering of oil sands fine tails. *Canadian Geotechnical Journal* 36(4), 587–598
- Dobchuk, B.S., Shurniak, R.E., Barbour, S.L., O’Kane, M.A., and Song, Q., 2013. Long-term monitoring and modelling of a reclaimed watershed cover on oil sands tailings. *International Journal of Mining, Reclamation and Environment* 27(3), 180–201
- Dompierre, K.A. and Barbour, S.L., 2016. Characterization of physical mass transport through oil sands fluid fine tailings in an end pit lake: a multi-tracer study. *Journal of Contaminant Hydrology* 189, 12–26
- Dompierre, K.A., Lindsay, M.B.J., Cruz-Hernández, P., and Halferdahl, G.M., 2016. Initial geochemical characteristics of fluid fine tailings in an oil sands end pit lake. *Science of The Total Environment* 556, 196–206
- Environment Canada, 2016. Canadian Climate Data [online] Available at: <http://climate.weather.gc.ca/> (Accessed: September 2016)
- Fedorak, P. and Coy, D., 2006. Oil sands cokes affect microbial activities. *Fuel* 85(12–13), 1642–1651
- Fetter, C.W., 1999. *Contaminant Hydrogeology*. Long Grove, IL: Waveland Press, Inc.
- Fetter, C.W., 2001. *Applied Hydrogeology*. Upper Saddle River, NJ: Prentice Hall, Inc.
- Frank, R.A., Fischer, K., Kavanagh, R., Burnison, B.K., Arsenault, G., Headley, J.V., Peru, K.M., Van Der Kraak, G., and Solomon, K.R., 2009. Effect of Carboxylic Acid Content on the Acute Toxicity of Oil Sands Naphthenic Acids. *Environmental Science & Technology* 43(2), 266–271
- Freeze, R.A. and Cherry, J.A., 1979. *Groundwater*. Englewood Cliffs, NJ: Prentice-Hall Inc.
- Gibson, J.J., Birks, S.J., Yi, Y., and Vitt, D.H., 2015. Runoff to boreal lakes linked to land cover, watershed morphology and permafrost thaw: a 9-year isotope mass balance assessment: Boreal Lakes Isotope Mass Balance Assessment. *Hydrological Processes* 29(18), 3848–3861
- Gibson, J.J., Fennell, J., Birks, S.J., Yi, Y., Moncur, M.C., Hansen, B., and Jasechko, S., 2013. Evidence of discharging saline formation water to the Athabasca River in the oil sands mining region, northern Alberta. *Canadian Journal of Earth Sciences* 50(12), 1244–1257
- Giesy, J.P., Anderson, J.C., and Wiseman, S.B., 2010. Alberta oil sands development. *Proceedings of the National Academy of Sciences* 107(3), 951–952

- González, A., Moreno, N., Navia, R., and Querol, X., 2010. Study of a Chilean petroleum coke fluidized bed combustion fly ash and its potential application in copper, lead and hexavalent chromium removal. *Fuel* 89(10), 3012–3021
- Gosselin, P., Hruday, S.E., Naeth, M.A., Plourde, A., Therrien, R., Van Der Kraak, G., and Xu, Z., 2010. Environmental and Health Related Impacts of Canada's Oil Sands Industry. The Royal Society of Canada
- Government of Alberta, 2015. Lower Athabasca Region Tailings Management Framework for the Mineable Athabasca Oil Sands. AB
- Gray, M.R., 2015. *Upgrading oilsands bitumen and heavy oil*. University of Alberta, Edmonton, AB: Pica Pica Press
- Hach Company, 2007. Sulfide - USEPA Methylene Blue Method 8131. Hach Company, 1–6.
- Hach Company, 2007. Nitrogen , Ammonia - Salicylate TNT Method 10031. Hach Company, 1–6.
- Han, X., MacKinnon, M.D., & Martin, J.W., 2009. Estimating the in situ biodegradation of naphthenic acids in oil sands process waters by HPLC/HRMS. *Chemosphere* 76(1), 63–70
- Heaton, K.K., 2015. Biogeochemical Investigation of Centrifuged Fine Tailings Deposits at an Oil Sands Mine in Northern Alberta, Canada. M.Sc. Thesis, Department of Geological Sciences, University of Saskatchewan. Saskatoon, SK
- Hein, F.J. and Cotterill, D.K., 2006. The Athabasca Oil Sands — A Regional Geological Perspective, Fort McMurray Area, Alberta, Canada. *Natural Resources Research* 15(2), 85–102
- Hendry, M.J. and Wassenaar, L.I., 2000. Controls on the distribution of major ions in pore waters of a thick surficial aquitard. *Water Resources Research* 36(2), 503–513.
- Hendry, M. Jim and Wassenaar, L.I., 2011. Millennial-scale diffusive migration of solutes in thick clay-rich aquitards: evidence from multiple environmental tracers. *Hydrogeology Journal* 19(1), 259–270
- Ho, C.K. and Webb, S.W., 1998. Capillary barrier performance in heterogeneous porous media. *Water Resources Research* 34(4), 603-609

- Holden, A.A., Haque, S.E., Mayer, K.U., and Ulrich, A.C., 2013. Biogeochemical processes controlling the mobility of major ions and trace metals in aquitard sediments beneath an oil sand tailing pond: Laboratory studies and reactive transport modeling. *Journal of Contaminant Hydrology* 151, 55–67
- Holden, A.A., Mayer, K.U., and Ulrich, A.C., 2012. Evaluating methods for quantifying cation exchange in mildly calcareous sediments in Northern Alberta. *Applied Geochemistry* 27(12), 2511–2523
- Holden, A.A., Donahue, R.B., and Ulrich, A.C., 2011. Geochemical interactions between process-affected water from oil sands tailings ponds and North Alberta surficial sediments. *Journal of Contaminant Hydrology* 119, 55-68
- Holowenko, F.M., MacKinnon, M.D., and Fedorak, P.M., 2000. Methanogens and sulfate-reducing bacteria in oil sands fine tailings waste. *Canadian Journal of Microbiology* 46(10), 927–937
- Hooshiar, A., Uhlik, P., Ivey, D.G., Liu, Q., and Etsell, T.H., 2012. Clay minerals in nonaqueous extraction of bitumen from Alberta oil sands. *Fuel Processing Technology* 96, 183–194
- Huang, M., Barbour, S.L., and Carey, S.K., 2015. The impact of reclamation cover depth on the performance of reclaimed shale overburden at an oil sands mine in Northern Alberta, Canada. *Hydrological Processes* 29(12), 2840–2854
- Kaminsky, H.A.W., Etsell, T.H., Ivey, D.G., and Omotoso, O., 2009. Distribution of clay minerals in the process streams produced by the extraction of bitumen from Athabasca oil sands. *The Canadian Journal of Chemical Engineering* 87(1), 85–93
- Kasperski, K.L. and Mikula, R.J., 2011. Waste Streams of Mined Oil Sands: Characteristics and Remediation. *Elements* 7(6), 387–392
- Kay-Shoemake, J.L., Watwood, M.E., Lentz, R.D., and Sojka, R.E., 1998a. Polyacrylamide as an organic nitrogen source for soil microorganisms with potential effects on inorganic soil nitrogen in agricultural soil. *Soil Biology and Biochemistry* 30(8/9), 1045-1052
- Kay-Shoemake, J.L., Watwood, M.E., Sojka, R.E., and Lentz, R.D., 1998b. Polyacrylamide as a substrate for microbial amidase in culture and soil. *Soil Biology and Biochemistry* 30(13), 1647-1654
- Kelln, C., Barbour, L., and Qualizza, C., 2007. Preferential flow in a reclamation cover: hydrological and geochemical response. *Journal of Geotechnical and Geoenvironmental Engineering* 133(10), 1277–1289
- Kelln, C., Barbour, S.L., and Qualizza, C., 2008. Controls on the spatial distribution of soil moisture and solute transport in a sloping reclamation cover. *Canadian Geotechnical Journal* 45(3), 351–366

- Kessler, S., Barbour, S.L., van Rees, K.C.J., and Dobchuk, B.S., 2010. Salinization of soil over saline-sodic overburden from the oil sands in Alberta. *Canadian Journal of Soil Science* 90(4), 637–647
- Kessler, S. and Hendry, M.J., 2006. Geochemistry and Leaching of Coke from Syncrude and Suncor Sites. Department of Geological Sciences, University of Saskatchewan
- Ketcheson, S.J., Price, J.S., Carey, S.K., Petrone, R.M., Mendoza, C.A., and Devito, K.J., 2016. Constructing fen peatlands in post-mining oil sands landscapes: Challenges and opportunities from a hydrological perspective. *Earth-Science Reviews* 161, 130–139
- Kotylar, L.S., Sparks, B.D., and Schutte, R., 1996. Effect of salt on the flocculation behavior of nano particles in oil sands fine tailings. *Clays and Clay Minerals* 44(1), 121–131
- Kurola, J., Salkinoja-Salonen, M., Aarnio, T., Hultman, J., and Romantschuk, M., 2005. Activity, diversity and population size of ammonia-oxidising bacteria in oil-contaminated landfarming soil. *FEMS Microbiology Letters* 250(1), 33–38
- Lahmira, B., Barbour, L., and Huang, M., 2014. Numerical Modeling of Gas Flow in the Suncor Coke Stockpile Covers. *Vadose Zone Journal* 13(1), 1-12
- Leung, S.S., MacKinnon, M.D., and Smith, R.E., 2003. The ecological effects of naphthenic acids and salts on phytoplankton from the Athabasca oil sands region. *Aquatic Toxicology* 62(1), 11–26
- Li, Y. and Gregory, S., 1974. Diffusion of ions in sea water and in deep-sea sediments. *Geochimica et Cosmochimica Acta* 38, 703-714
- Li, X., Chang, S.X., and Salifu, K.F., 2014. Soil texture and layering effects on water and salt dynamics in the presence of a water table: a review. *Environmental Reviews* 22(1), 41–50
- Light, T.S., 1972. Standard solution for redox potential measurements. *Analytical Chemistry* 44(6), 1038–1039
- Liu, J., Xu, Z., and Masliyah, J., 2004. Role of fine clays in bitumen extraction from oil sands. *AIChE Journal* 50(8), 1917–1927
- Lottermoser, B.G., Munksgaard, N.C., and Daniell, M., 2009. Trace Element Uptake by Mitchell Grasses Grown on Mine Wastes, Cannington Ag–Pb–Zn Mine, Australia: Implications for Mined Land Reclamation. *Water, Air, and Soil Pollution* 203(1–4), 243–259
- Luna Wolter, G.L. and Naeth, M.A., 2014. Dry Mature Fine Tailings as Oil Sands Reclamation Substrates for Three Native Grasses. *Journal of Environment Quality* 43(4), 1510
- Malusis, M.A., Shackelford, C.D., and Olsen, H.W., 2003. Flow and transport through clay membrane barriers. *Engineering Geology* 70(3–4), 235–248

- Masliyah, J., Zhou, Z., Xu, Z., Czarnecki, J., and Hamza, H., 2004. Understanding Water-Based Bitumen Extraction from Athabasca Oil Sands. *The Canadian Journal of Chemical Engineering* 82, 628–654
- Matthews, J.G., Shaw, W.H., MacKinnon, M.D., and Cuddy, R.G., 2002. Development of Composite Tailings Technology at Syncrude. *International Journal of Surface Mining, Reclamation and Environment* 16(1), 24–39
- Mikula, R.J., Munoz, V.A., Omotoso, O., 2009. Centrifugation options for production of dry stackable tailings in surface-mined oil sands tailings management. *Journal of Canadian Petroleum Technology* 48(09), 19–23
- Naeth, M.A., Chanasyk, D.S., and Burgers, T.D., 2011. Vegetation and soil water interactions on a tailings sand storage facility in the Athabasca oil sands region of Alberta Canada. *Physics and Chemistry of the Earth, Parts A/B/C* 36(1–4), 19–30
- Nakata, C., Qualizza, C., MacKinnon, M., and Renault, S., 2011. Growth and Physiological Responses of *Triticum aestivum* and *Deschampsia caespitosa* Exposed to Petroleum Coke. *Water, Air, & Soil Pollution* 216(1–4), 59–72
- Nesbitt, J.A., 2016. Geochemical Investigation of Fluid Petroleum Coke Deposits at an Oil Sands Mine in Northern Alberta, Canada. M.Sc. Thesis, Department of Geological Sciences, University of Saskatchewan. Saskatoon, SK
- Nesbitt, J.A. and Lindsay, M.B.J., and Chen, N., 2017. Geochemical characteristics of oil sands fluid petroleum coke. *Applied Geochemistry* 76, 148–158
- Nesbitt, J.A. and Lindsay, M.B.J., 2017. Vanadium Geochemistry of Oil Sands Fluid Petroleum Coke. *Environmental Science and Technology* 51(5), 3102-3109
- Noborio, K., 2001. Measurement of soil water content and electrical conductivity by time domain reflectometry: a review. *Computers and Electronics in Agriculture* 31(3), 213–237
- Nordstrom, D.K., 1977. Thermochemical redox equilibria of ZoBell's solution. *Geochimica et Cosmochimica Acta* 41, 1835–1841
- Omotoso, O. and Mikula, R.J., 2004. High surface areas caused by smectitic interstratification of kaolinite and illite in Athabasca oil sands. *Applied Clay Science* 25(1–2), 37–47
- Omotoso, O., Mikula, R.J., and Stephens, P.W., 2002. Surface area of interstratified phyllosilicates in Athabasca oil sands from synchrotron XRD. *Advances in X-Ray Analysis* 45, 363–391

- Owolagba, J. and Azam, S., 2013. Unsaturated soil properties of centrifuged oil sand fine tailings. *In press Proceedings, 66th Canadian Geotechnical Conference*, GEOMontreal 2013
- Parkhurst, D.L. and Appelo, C.A.J., 2013. Description of input and examples for PHREEQC version 3—A computer program for speciation, batch-reaction, one-dimensional transport, and inverse geochemical calculations: U.S. Geological Survey Techniques and Methods, book 6, chap. A43, 497
- Penner, T.J. and Foght, J.M., 2010. Mature fine tailings from oil sands processing harbour diverse methanogenic communities. *Canadian Journal of Microbiology* 56(6), 459–470
- Proskin, S., Segó, D., and Alostaz, M., 2010. Freeze-thaw and consolidation tests on Suncor mature fine tailings (MFT). *Cold Regions Science and Technology* 63, 110-120
- Purdy, B.G., Macdonald, S. E., and Lieffers, V.J., 2005. Naturally saline boreal communities as models for reclamation of saline oil sand tailings. *Restoration Ecology* 13(4), 667–677
- Puttaswamy, N. and Liber, K., 2011. Identifying the causes of oil sands coke leachate toxicity to aquatic invertebrates. *Environmental Toxicology and Chemistry* 30(11), 2576–2585
- Puttaswamy, N. and Liber, K., 2012. Influence of inorganic anions on metals release from oil sands coke and on toxicity of nickel and vanadium to *Ceriodaphnia dubia*. *Chemosphere* 86(5), 521–529
- Puttaswamy, N., Turcotte, D., and Liber, K., 2010. Variation in toxicity response of *Ceriodaphnia dubia* to Athabasca oil sands coke leachates. *Chemosphere* 80(5), 489–497
- Ramos-Padrón, E., Bordenave, S., Lin, S., Bhaskar, I.M., Dong, X., Sensen, C.W., Fournier, J., Voordouw, G., and Gieg, L.M., 2011. Carbon and Sulfur Cycling by Microbial Communities in a Gypsum-Treated Oil Sands Tailings Pond. *Environmental Science and Technology* 45(2), 439-446
- Reid, M.L. and Warren, L.A., 2016. S reactivity of an oil sands composite tailings deposit undergoing reclamation wetland construction. *Journal of Environmental Management* 166, 321–329
- Rezanezhad, F., Price, J.S., and Craig, J.R., 2012. The effects of dual porosity on transport and retardation in peat: A laboratory experiment. *Canadian Journal of Soil Science* 92, 723-732
- Rima, U.S. and Azam, S., 2015. Centrifuge dewatering of polymer-amended oil sand tailings. *Environmental Geotechnics*, 2(3), 175–180

- Rooney, D.J., Brown, K.W., and Thomas, J.C., 1998. The effectiveness of capillary barriers to hydraulically isolate salt contaminated soils. *Water, Air, and Soil Pollution* 104(3–4), 403–411
- Saidi-Mehrabad, A., He, Z., Tamas, I., Sharp, C.E., Brady, A.L., Rochman, F.F., Bodrossy, L., Abell, G.C.J., Penner, T., Dong, X., Sensen, C.W., and Dunfield, P.F., 2013. Methanotrophic bacteria in oilsands tailings ponds of northern Alberta. *International Society for Microbial Ecology* 7, 908–921
- Salloum, M.J., Dudas, M.J., and Fedorak, P.M., 2002. Microbial reduction of amended sulfate in anaerobic mature fine tailings from oil sand. *Waste Management & Research* 20(2), 162–171
- Shah, A.A., Fishwick, R.P., Leeke, G.A., Wood, J., Rigby, S.P., and Greaves, M., 2011. Experimental optimization of catalytic process in situ for heavy-oil and bitumen upgrading. *Journal of Canadian Petroleum Technology* 50(11–12), 33–47
- Siddique, T., Kuznetsov, P., Kuznetsova, A., Arkell, N., Young, R., Li, C., Guigard, S., Underwood, E., and Foght, J.M., 2014. Microbially-accelerated consolidation of oil sands tailings. Pathway I: changes in porewater chemistry. *Frontiers in Microbiology* 5(106), 1–11
- Simhayov, R.B., Price, J.S., Smeaton, C.M., Parsons, C., Rezanezhad, F., and Van Cappellen, P., 2017. Solute pools in Nikanotee Fen watershed in the Athabasca oil sands region. *Environmental Pollution* 225, 150–162
- Singh, B.B., 1971. Effect of vanadium on the growth, yield and chemical composition of maize (*Zea Mays* L.). *Plant and Soil* 34(1), 209–213
- Siwik, P.L., Van Meer, T., MacKinnon, M.D., and Paszkowski, C.A., 2000. Growth of fathead minnows in oilsand-processed wastewater in laboratory and field. *Environmental Toxicology and Chemistry* 19(7), 1837–1845
- Small, C.C., Ulrich, A.C., and Hashisho, Z., 2012. Adsorption of Acid Extractable Oil Sands Tailings Organics onto Raw and Activated Oil Sands Coke. *Journal of Environmental Engineering* 138(8), 833–840
- Stasik, S., Loick, N., Knöller, K., Weisener, C., and Wendt-Potthoff, K., 2014. Understanding biogeochemical gradients of sulfur, iron and carbon in an oil sands tailings pond. *Chemical Geology* 382, 44–53
- Sworska, A., Laskowski, J.S., and Cymerman, G., 2000. Flocculation of the Syncrude fine tailings: Part I. Effect of pH, polymer dosage and Mg²⁺ and Ca²⁺ cations. *International Journal of Mineral Processing* 60(2), 143–152

- Tchounwou, P.B., Yedjou, C.G., Patlolla, A.K., and Sutton, D.J., 2012. Heavy Metal Toxicity and the Environment. In A. Luch (Ed.), *Molecular, Clinical and Environmental Toxicology* (Vol. 101, pp. 133–164). Basel: Springer Basel
- Tordoff, G.M., Baker, A.J.M., and Willis, A. J., 2000. Current approaches to the revegetation and reclamation of metalliferous mine wastes. *Chemosphere* 41(1), 219–228
- U.S. Geological Survey, 2001. A laboratory manual for X-Ray powder diffraction. Open-file report 01-041. Retrieved from: <https://pubs.usgs.gov/of/2001/of01-041/htmldocs/methods.htm#oamount>
- Vessey, C.J. and Lindsay, M.B.J., 2017. Transport and exchange of salt rich tailings water into a reclaimed peatland. Unpublished manuscript, Department of Geological Sciences, University of Saskatchewan, Saskatoon, Canada
- Vitt, D.H., & Chee, W.L., 1990. The relationships of vegetation to surface water chemistry and peat chemistry in fens of Alberta, Canada. *Plant Ecology* 89(2), 87–106
- Ward, G.M., 1978. Molybdenum toxicity and hypocuprosis in ruminants: a review. *Journal of Animal Science* 46(4), 1078–1085
- Wassenaar, L.I., Hendry, M.J., Chostner, V.L., and Lis, G.P., 2008. High Resolution Pore Water $\delta^2\text{H}$ and $\delta^{18}\text{O}$ Measurements y $\text{H}_2\text{O}_{(\text{liquid})} - \text{H}_2\text{O}_{(\text{vapor})}$ Equilibration Laser Spectroscopy. *Environmental Science and Technology* 42(24), 9262-9267
- Weissberg, H.L., 1963. Effective Diffusion Coefficient in Porous Media. *Journal of Applied Physics* 34(9), 2636–2639
- World Health Organization (Ed.), 2011. *Guidelines for drinking-water quality* (4th ed). Geneva: World Health Organization
- Yanful, E.K., Aubé, B.C., Woyshner, M., and St-Arnaud, L.C., 1994. Field and Laboratory Performance of Engineered Covers on the Waite Amulet Tailings. *International Land Reclamation and Mine Drainage Conference and the Third International Conference on the Abatement of Acidic Drainage*. Pittsburgh, PA
- Yuan, M., Tong, S., Zhao, S., and Jia, C.Q., 2010. Adsorption of polycyclic aromatic hydrocarbons from water using petroleum coke-derived porous carbon. *Journal of Hazardous Materials* 181(1–3), 1115–1120
- Yukselen, Y. and Kaya, A., 2008. Suitability of the methylene blue test for surface area, cation exchange capacity and swell potential determination of clayey soils. *Engineering Geology* 102(1–2), 38–45

Zubot, W., MacKinnon, M.D., Chelme-Ayala, P., Smith, D.W., and Gamal El-Din, M., 2012. Petroleum coke adsorption as a water management option for oil sands process-affected water. *Science of The Total Environment* 427–428, 364–372

APPENDIX A: LYSIMETER SAMPLE LIST AND SAMPLE TYPE

Table A-1: List of lysimeter field samples, sample types, and sample depths. Types of samples collected include pore water (PW) and core (C).


Sample ID	Lysimeter ID	Sample Type	Depth from Top of Lysimeter (m)
US-L1-P175	L1	PW	1.5
US-L1-P200	L1	PW	1.75
US-L1-P225	L1	PW	2
L1 1.5-1.65 m	L1	C	1.9
L1 1.65-1.8 m	L1	C	2.05
L1 1.8-1.95 m	L1	C	2.2
L1 2.25-2.4 m	L1	C	2.65
L1 2.4-2.55 m	L1	C	2.8
L1 2.55-2.7 m	L1	C	2.95
L2 0.95-1.15 m	L2	C	1.515
L2 1.15-1.35 m	L2	C	1.715
L2 1.35-1.5 m	L2	C	1.89
L2 2.15-2.3 m	L2	C	2.69
L2 2.3-2.45 m	L2	C	2.84
L2 2.45-2.6 m	L2	C	2.99
US-L3-P300	L3	PW	2.75
US-L3-P300C	L3	PW	3
L3 0.15-0.3 m	L3	C	0.792
L3 0.3-0.45 m	L3	C	0.942
L3 0.45-0.6 m	L3	C	1.092
L3 0.9-1.05 m	L3	C	1.542
L3 1.05-1.2 m	L3	C	1.692
L3 1.2-1.35 m	L3	C	1.842
US-L4-P050	L4	PW	0.25
US-L4-P075	L4	PW	0.5
US-L4-P100	L4	PW	0.75
US-L4-P125	L4	PW	1
US-L4-P150	L4	PW	1.25
US-L4-P175	L4	PW	1.5
L4 1.4-1.55 m	L4	C	1.865
L4 1.55-1.7 m	L4	C	2.015
L4 1.7-1.85 m	L4	C	2.165
L4 2.2-2.35 m	L4	C	2.665
L4 2.35-2.5 m	L4	C	2.815

L4 2.5-2.65 m	L4	C	2.965
US-L5-P050	L5	PW	0.25
US-L5-P075	L5	PW	0.5
US-L5-P100	L5	PW	0.75
US-L5-P125	L5	PW	1
US-L5-P300C	L5	PW	3
L5 0.95-1.1 m	L5	C	1.484
L5 1.1-1.25 m	L5	C	1.634
L5 1.25-1.4 m	L5	C	1.784
L5 2.25-2.4 m	L5	C	2.784
L5 2.4-2.55 m	L5	C	2.934
L5 2.55-2.7 m	L5	C	3
US-L6-P150	L6	PW	1.25
US-L6-P175	L6	PW	1.5
US-L6-P200	L6	PW	1.75
US-L6-P225	L6	PW	2
US-L6-P250	L6	PW	2.25
US-L6-P275	L6	PW	2.5
US-L6-P300	L6	PW	2.75
US-L6-P300C	L6	PW	3
L6 0.4-0.55 m	L6	C	1.017
L6 0.55-0.7 m	L6	C	1.167
L6 0.7-0.85 m	L6	C	1.317
L6 0.85 1.0 m	L6	C	1.467
L6 1.0-1.15 m	L6	C	1.617
L6 1.15-1.3 m	L6	C	1.767

Table A-2: Lysimeter core sub-sample list. Information regarding pushed core length (m), recovered core length (m), and scaling factor for linear compression are all recorded.

Lysimeter ID	Parent Core ID	Pushed Depth	Recovered Depth	Compression Factor	Core Sub-sample
L1	L1 0-0.6 m	0.6	0.35	0.583	L1 0-0.15 m
					L1 0.15-0.3 m
					L1 0.3-0.45 m
					L1 0.45-0.6 m
	L1 0.6-1.2 m	0.6	0.35	0.583	L1 0.9-1.05 m (a)
					L1 0.9-1.05 m (b)
	L1 1.2-1.8 m (a)	0.6	0.16	1	L1 1.05-1.2 m
					L1 1.2-1.35 m
	L1 1.2-1.8 m (b)	0.6	0.47	1	L1 1.35-1.5 m
					L1 1.5-1.65 m
	L1 1.8-2.4 m	0.6	0.37	0.617	L1 1.65-1.8 m
					L1 1.8-1.95 m
					L1 1.95-2.1 m
L1 2.15-2.7 m	0.55	0.35	0.636	L1 2.1-2.25 m	
				L1 2.25-2.4 m	
				L1 2.25-2.4 m	
				L1 2.4-2.55 m	
L2	L2 0.15-0.75 m	0.6	0.45	0.75	L1 2.55-2.7 m
					L2 0.15-0.3 m
					L2 0.3-0.45 m
					L2 0.45-0.6 m
	L2 0.75-1.35 m	0.6	0.35	0.583	L2 0.6-0.75 m
					L2 0.75-0.95 m
					L2 0.95-1.15 m
	L2 1.35-1.95 m	0.6	0.6	1	L2 1.15-1.35 m
					L2 1.35-1.5 m
					L2 1.5-1.65 m
	L2 1.95-2.6 m	0.65	0.65	1	L2 1.65-1.8 m
					L2 1.8-1.95 m
					L2 1.85-2.0 m
L2 2.0-2.15 m					
L2 2.15-2.3 m					
L3	L3 0.15-0.75 m	0.6	0.45	0.75	L2 2.3-2.45 m
					L2 2.45-2.6 m
					L3 0.15-0.3 m
					L3 0.3-0.45 m
	L3 0.75-1.35 m (a)	0.6	0.15	1	L3 0.45-0.6 m
					L3 0.6-0.75 m
	L3 0.75-1.35 m (b)	0.45	0.35	0.778	L3 0.75-0.9 m
					L3 0.90-1.05 m
					L3 1.05-1.2 m
					L3 1.2-1.35 m

	L3 1.35-1.65 m	0.3	0.28	0.933	L3 1.35-1.5 m
	L3 1.65-2.2 m	0.6	0.35	0.583	L3 1.5-1.65 m
					L3 1.65-1.75 m
					L3 1.75-1.9 m
					L3 1.9-2.05 m
					L3 2.05-2.2 m
L4	L4 0.2-0.8 m	0.6	0.55	0.917	L4 0.2-0.35 m
					L4 0.35-0.5 m
					L4 0.5-0.65 m
					L4 0.65-0.8 m
	L4 0.8-1.4 m	0.6	0.45	0.75	L4 0.8-0.95 m
					L4 0.95-1.1 m
					L4 1.1-1.25 m
					L4 1.25-1.4 m
	L4 1.4-2.0 m	0.6	0.58	0.967	L4 1.4-1.55 m
					L4 1.55-1.7 m
					L4 1.7-1.85 m
					L4 1.85-2.0 m
	L4 2-2.65 m	0.65	0.39	0.6	L4 2.05-2.2 m
					L4 2.2-2.35 m
					L4 2.35-2.5 m
					L4 2.5-2.65 m
L5	L5 0.5-1.1 m	0.6	0.58	0.967	L5 0.5-0.65 m
					L5 0.65-0.8 m
					L5 0.8-0.95 m
					L5 0.95-1.1 m
	L5 1.1-1.7 m	0.6	0.55	0.917	L5 1.1-1.25 m
					L5 1.25-1.4 m
					L5 1.4-1.55 m
					L5 1.55-1.7 m
	L5 1.7-2.3 m	0.6	0.55	0.917	L5 1.7-1.85 m
					L5 1.85-2.0 m
					L5 2.0-2.15 m
					L5 2.15-2.3 m
	L5 2.3-2.7 m	0.4	0.36	0.9	L5 2.25-2.4 m
					L5 2.4-2.55 m
					L5 2.55-2.7 m
L6	L6 0.4-1.0 m	0.6	0.3	0.5	L6 0.4-0.55 m
					L6 0.55-0.7 m
					L6 0.7-0.85 m
					L6 0.85-1.0 m
	L6 1.0-1.6 m	0.6	0.53	0.883	L6 1-1.15 m
					L6 1.15-1.3 m
					L6 1.3-1.45 m
					L6 1.45-1.6 m
	L6 1.6-2.2 m	0.6	0.6	1	L6 1.6-1.75 m



L6 1.75-1.9 m
L6 1.9-2.05 m
L6 2.05-2.2 m

APPENDIX B: FIELD LYSIMETER PORE WATER GEOCHEMISTRY

Table B-1: Pore water and core chemistry of field lysimeters. Parameters included are pH, E_{measured} (E; mV), electrical conductivity (EC; mS cm^{-1}), temperature (T; $^{\circ}\text{C}$), alkalinity as CaCO_3 (Alk.; mg L^{-1}), dissolved sulfide (S^{2-} ; $\mu\text{g L}^{-1}$), and dissolved nitrogen reported as ammonia ($\text{NH}_3\text{-N}$; mg L^{-1}). Samples with an asterisk (*) delineates averaged values from duplicate samples. Hyphens (-) present in the table indicate lack of sufficient pore water for that specific measurement.

Sample ID	pH	E	EC	T	Alk.	S^{2-}	$\text{NH}_3\text{-N}$
US-L1-P175	7.3	73	7.07	21.1	570	2	1.37
US-L1-P200	7.55	120.8	6.44	23.9	500	30	0.906
US-L1-P225	7.69	-220.8	5.52	23.3	770*	1590*	1.365*
L1 1.5-1.65 m	7	26	-	-	-	-	-
L1 1.65-1.8 m	7.64	-109.3	5.24	21.4	288	35	34.8
L1 1.8-1.95 m	7.71	-159.8	6.31	20.7	540	2650	22.3
L1 2.25-2.4 m	7.89	163.9	4.17	22.7	670	-	12.4
L1 2.4-2.55 m	7.71	-283.5	3.34	22	792	18550	7.01
L1 2.55-2.7 m	7.92	-264.9	3.46	21.8	811	12850	7.69
L2 0.95-1.15 m	7.79	-48.6	4.92	20.8	702	-	8.49
L2 1.15-1.35 m	7.99	-7.8	3.54	20.9	836	95	8.02
L2 1.35-1.5 m	7.83	-208.8	3.82	20.7	452	5140	7.71
L2 2.15-2.3 m	7.88	-257.2	3.3	20.5	930	13700	7
L2 2.3-2.45 m	7.91	-244	3.39	20.5	1037	13380	7.35
L2 2.45-2.6 m	7.9	-246.1	3.3	20.5	1033	15480	7.59
US-L3-P300	7.25	144.1	4.39	23.3	1120	2	0.304
US-L3-P300C	7.33	171.2	6.42	20.7	1270*	4*	0.6315*
L3 0.15-0.3 m	8.08	149.1	6.75	21.5	613	10	9.51
L3 0.3-0.45 m	7.91	150.9	3.74	21.8	1010	24	8.69
L3 0.45-0.6 m	7.96	144.4	3.67	23.6	1108	-	8.48
L3 0.9-1.05 m	8	143.1	5.13	20.9	1062	-	7.07
L3 1.05-1.2 m	8.04	50.8	5.36	21	1262	-	5.33
L3 1.2-1.35 m	7.94	153.9	5.06	21.3	1181	-	5.68
US-L4-P050	7.52	96	4.87	22.3	310	5	0.49
US-L4-P075	6.8	46.6	4.07	20.6	310	18	2.86
US-L4-P100	7.28	184.3	5.38	20.6	670	1	15.40
US-L4-P125	7.47	114.2	5.87	25.1	465*	2*	10.25*
US-L4-P150	7.67	69.7	5.96	25	890	377	25.80
US-L4-P175	7.68	-226.1	5.49	22.5	1050	15450	19.40
L4 1.4-1.55 m	7.79	-75.9	5.3	21	851	250	17
L4 1.55-1.7 m	7.77	-60.7	4.9	20.8	1245	170	6.79
L4 1.7-1.85 m	7.85	-165.7	4.45	20.7	1308	1310	6.24
L4 2.2-2.35 m	7.74	-150.9	4.96	20.7	1222	990	7.86
L4 2.35-2.5 m	7.88	82.4	5.08	20.4	1348	-	6.86
L4 2.5-2.65 m	7.86	-211.1	4.77	21.3	1179	2200	6.74
US-L5-P050	7.51	33.4	11.61	27	420	4	1.02
US-L5-P075	7.22	7.7	9.25	26.9	260	0	7.37

US-L5-P100	7.41	-59.9	7.68	26.6	500	360	32.6
US-L5-P125	7.99	-244.1	6.45	25.5	890*	11200*	15.35*
US-L5-P300C	8.09	-363	5.67	25.9	1560	28900	5.07
L5 0.95-1.1 m	7.99	47.5	4.18	21	852	-	8.81
L5 1.1-1.25 m	7.8	131	5.21	22.1	634	-	12.2
L5 1.25-1.4 m	7.83	-192.2	3.54	21.9	861	900	8.16
L5 2.25-2.4 m	7.92	-83.6	3.47	22.1	354	10	7.37
L5 2.4-2.55 m	7.83	-281.5	3.38	21.7	895	17800	7.11
L5 2.55-2.7 m	7.87	-271	3.42	22	871	11000	7.78
US-L6-P150	8.37	107.8	6.55	24.8	480	160	6.72
US-L6-P175	8	-138.9	10.39	29.2	400	880	5.78
US-L6-P200	7.78	-313.5	5.53	30.4	680	660	1.58
US-L6-P225	7.81	156.5	3.63	28	1040	144	1.17
US-L6-P250	7.2	20.2	0.871	26	1010	62	1.47
US-L6-P275	7.17	34.6	0.851	25.7	860	25	4.91
US-L6-P300	7.33	179.7	1.613	26.3	920	20	2.78
US-L6-P300C	7.4	164.5	5.13	25.8	920	42	3.20
L6 0.4-0.55 m	7.95	141.4	5.45	21.2	735	-	9.53
L6 0.55-0.7 m	7.97	150.7	-	-	687	-	9.08
L6 0.7-0.85 m	8.07	134	3.7	21.8	814	-	8.56
L6 0.85 1.0 m	7.87	155.7	3.97	21.9	900	-	10.7
L6 1.0-1.15 m	7.92	162.5	4.23	21.3	-	-	8.29
L6 1.15-1.3 m	7.91	81.3	3.82	21.1	-	-	8.32

Table B-2: Major cations analyzed by Inductively Coupled Plasma – Optical Emission Spectroscopy (ICP-OES). All samples reported in mg L⁻¹. A hyphen (-) indicates insufficient pore water for measurement. Any sample with reported replicates (Y) is an average value from duplicate samples. Samples with BDL were at concentrations below the detection limit.

Sample ID	Rep.	As	Ba	Fe	P	S	Mo
US-L1-P175		0.046	0.026	0.041	0.083	1260.3	1.94
US-L1-P200		0.067	0.039	0.008	0.122	1086.2	0.98
US-L1-P225	Y	0.109	0.074	0.052	0.187	763.9	0.46
L1 1.5-1.65 m		-	-	-	-	-	-
L1 1.65-1.8 m		0.043	0.053	BDL	0.115	1113.9	0.32
L1 1.8-1.95 m		0.052	0.157	BDL	0.154	937.2	0.10
L1 2.25-2.4 m		BDL	0.340	BDL	0.097	632.6	0.38
L1 2.4-2.55 m		0.057	0.378	BDL	0.269	693.6	BDL
L1 2.55-2.7 m		0.048	0.439	BDL	0.293	299.2	BDL
L2 0.95-1.15 m		BDL	0.111	BDL	0.175	934.2	0.58
L2 1.15-1.35 m	Y	0.079	0.439	BDL	0.264	30.6	0.02
L2 1.35-1.5 m	Y	0.061	0.314	BDL	0.235	275.6	0.02
L2 2.15-2.3 m		0.090	0.403	0.034	0.279	807.8	BDL
L2 2.3-2.45 m		0.076	0.398	BDL	0.317	484.9	BDL
L2 2.45-2.6 m	Y	0.070	0.351	BDL	0.257	410.1	BDL
US-L3-P300		0.165	0.047	0.003	0.265	161.0	BDL

US-L3-P300C	Y	0.179	0.034	0.013	0.298	400.9	0.02
L3 0.15-0.3 m		0.055	0.061	BDL	0.132	698.0	0.21
L3 0.3-0.45 m		0.058	0.124	BDL	0.196	45.6	0.02
L3 0.45-0.6 m		0.078	0.169	BDL	0.228	41.4	0.03
L3 0.9-1.05 m		0.083	0.320	BDL	0.203	81.7	0.05
L3 1.05-1.2 m		0.073	0.283	BDL	0.138	12.9	0.04
L3 1.2-1.35 m		0.032	0.322	BDL	0.121	9.9	BDL
US-L4-P050		0.037	0.126	1.467	0.090	968.4	0.01
US-L4-P075		0.054	0.109	4.425	0.113	762.0	0.07
US-L4-P100		0.051	0.053	0.168	0.101	877.4	0.84
US-L4-P125	Y	0.066	0.032	0.011	0.116	929.9	0.92
US-L4-P150		0.111	0.073	0.084	0.195	733.4	0.54
US-L4-P175		0.134	0.077	0.039	0.299	985.0	0.04
L4 1.4-1.55 m		0.016	0.386	BDL	0.181	194.3	0.14
L4 1.55-1.7 m		0.015	0.387	BDL	0.251	11.5	BDL
L4 1.7-1.85 m	Y	0.031	0.449	BDL	0.273	13.8	BDL
L4 2.2-2.35 m		BDL	0.069	BDL	0.238	209.9	BDL
L4 2.35-2.5 m		BDL	0.024	BDL	0.137	119.3	BDL
L4 2.5-2.65 m		0.025	0.156	BDL	0.254	84.9	BDL
US-L5-P050		0.020	0.016	0.034	0.039	2345.0	1.81
US-L5-P075		0.026	0.021	BDL	0.043	1736.0	1.27
US-L5-P100		0.068	0.055	0.284	0.133	1242.8	1.05
US-L5-P125	Y	0.092	0.093	0.040	0.227	951.3	0.11
US-L5-P300C		0.171	0.260	0.026	0.355	934.5	BDL
L5 0.95-1.1 m		0.030	0.337	BDL	0.214	82.4	BDL
L5 1.1-1.25 m		0.042	0.312	BDL	0.131	529.7	0.39
L5 1.25-1.4 m		0.031	0.378	BDL	0.258	85.8	BDL
L5 2.25-2.4 m		0.032	0.224	BDL	0.118	335.0	0.28
L5 2.4-2.55 m		0.036	0.367	BDL	0.278	81.6	BDL
L5 2.55-2.7 m		0.034	0.412	BDL	0.243	26.6	BDL
US-L6-P150		0.046	0.126	0.011	0.095	1061.9	0.16
US-L6-P175		0.045	0.303	0.010	0.088	910.0	0.16
US-L6-P200		0.090	0.160	0.055	0.174	683.8	0.10
US-L6-P225		0.141	0.205	0.031	0.228	179.2	BDL
US-L6-P250		0.149	0.138	0.885	0.240	201.1	BDL
US-L6-P275		0.122	0.077	1.598	0.195	236.2	BDL
US-L6-P300		0.125	0.048	0.310	0.207	138.1	BDL
US-L6-P300C		0.107	0.054	0.508	0.170	131.7	0.00
L6 0.4-0.55 m		0.032	0.076	BDL	0.224	227.6	0.10
L6 0.55-0.7 m		0.043	0.231	BDL	0.158	94.6	0.07
L6 0.7-0.85 m		0.033	0.273	BDL	0.183	46.3	0.03
L6 0.85-1.0 m		BDL	0.495	BDL	0.216	152.3	BDL
L6 1.0-1.15 m		0.030	0.366	BDL	0.189	36.2	0.04
L6 1.15-1.3 m		BDL	0.285	BDL	0.237	4.6	BDL

Table B-2. continued

Sample ID	Rep.	Al	Cd	Se	Na	K	Mg	Ca
US-L1-P175		BDL	BDL	0.028	1078.1	24.0	252.1	398.1
US-L1-P200		BDL	BDL	0.020	1244.3	22.9	177.0	300.6
US-L1-P225	Y	BDL	BDL	BDL	1194.0	20.2	139.2	179.7
L1 1.5-1.65 m		BDL	BDL	BDL	-	-	-	-
L1 1.65-1.8 m		BDL	BDL	BDL	1266.6	36.1	195.3	249.5
L1 1.8-1.95 m		BDL	BDL	BDL	1276.5	29.3	115.3	172.3
L1 2.25-2.4 m		BDL	BDL	BDL	1003.7	26.1	84.0	174.9
L1 2.4-2.55 m		BDL	BDL	BDL	788.3	10.7	8.6	18.4
L1 2.55-2.7 m		BDL	BDL	BDL	827.3	12.4	9.1	20.9
L2 0.95-1.15 m		BDL	BDL	BDL	1349.1	26.9	103.7	156.5
L2 1.15-1.35 m	Y	BDL	BDL	BDL	801.8	13.4	8.9	19.3
L2 1.35-1.5 m	Y	BDL	BDL	BDL	886.4	12.8	13.2	27.1
L2 2.15-2.3 m		BDL	BDL	BDL	777.9	10.9	8.5	18.4
L2 2.3-2.45 m		BDL	BDL	BDL	782.0	11.9	8.2	18.3
L2 2.45-2.6 m	Y	BDL	BDL	BDL	786.3	9.8	7.3	16.6
US-L3-P300		BDL	BDL	BDL	1029.4	12.7	16.9	57.4
US-L3-P300C	Y	BDL	BDL	0.012	1476.9	14.8	28.5	101.3
L3 0.15-0.3 m		BDL	BDL	BDL	1883.3	34.6	36.8	69.9
L3 0.3-0.45 m		BDL	BDL	BDL	911.7	12.7	9.8	20.6
L3 0.45-0.6 m		BDL	BDL	BDL	896.6	14.9	10.5	22.1
L3 0.9-1.05 m		BDL	BDL	BDL	1017.3	14.6	10.0	18.9
L3 1.05-1.2 m		BDL	BDL	BDL	1106.6	9.9	7.0	13.5
L3 1.2-1.35 m		BDL	BDL	BDL	1020.4	11.4	7.5	13.9
US-L4-P050		BDL	BDL	BDL	728.4	21.8	143.4	369.4
US-L4-P075		0.0041	BDL	BDL	595.5	40.9	113.1	312.5
US-L4-P100		BDL	BDL	BDL	877.3	61.8	123.9	277.0
US-L4-P125	Y	BDL	BDL	0.008	1040.3	26.2	144.8	231.2
US-L4-P150		BDL	BDL	BDL	1115.6	25.4	119.8	157.9
US-L4-P175		BDL	BDL	BDL	1087.2	87.3	73.8	96.6
L4 1.4-1.55 m		BDL	BDL	BDL	1120.2	18.5	22.6	35.6
L4 1.55-1.7 m		BDL	BDL	BDL	1064.3	11.0	8.7	17.5
L4 1.7-1.85 m	Y	BDL	BDL	BDL	1098.3	12.2	9.2	18.5
L4 2.2-2.35 m		BDL	BDL	BDL	1278.2	17.9	20.2	45.2
L4 2.35-2.5 m		BDL	BDL	BDL	636.3	7.7	10.1	24.9
L4 2.5-2.65 m		BDL	BDL	BDL	1177.3	15.1	13.6	28.8
US-L5-P050		BDL	BDL	0.074	2414.6	62.1	479.5	460.3
US-L5-P075		BDL	BDL	0.027	1750.5	46.6	337.7	409.4
US-L5-P100		BDL	BDL	BDL	1332.2	33.5	222.7	294.9
US-L5-P125	Y	BDL	BDL	BDL	1271.9	24.8	130.9	162.1
US-L5-P300C		BDL	BDL	BDL	1044.4	15.9	22.9	21.5
L5 0.95-1.1 m		BDL	BDL	BDL	855.4	14.6	10.8	21.6
L5 1.1-1.25 m		BDL	BDL	BDL	1126.5	22.9	49.0	97.8
L5 1.25-1.4 m		BDL	BDL	BDL	849.4	13.2	10.1	20.9
L5 2.25-2.4 m		BDL	BDL	BDL	835.2	19.0	34.4	91.3

L5 2.4-2.55 m	BDL	BDL	BDL	768.4	11.9	7.5	16.5
L5 2.55-2.7 m	BDL	BDL	BDL	803.3	12.4	8.2	18.8
US-L6-P150	BDL	BDL	BDL	2465.0	37.9	68.3	79.0
US-L6-P175	BDL	BDL	BDL	2142.7	32.3	55.5	56.8
US-L6-P200	BDL	BDL	BDL	1674.9	24.3	43.4	61.8
US-L6-P225	BDL	BDL	BDL	855.3	15.0	31.0	88.8
US-L6-P250	BDL	BDL	BDL	827.7	37.4	36.0	105.0
US-L6-P275	BDL	BDL	BDL	832.3	17.6	28.7	134.1
US-L6-P300	BDL	BDL	BDL	874.4	12.9	7.5	43.3
US-L6-P300C	BDL	BDL	BDL	857.7	10.3	7.5	36.5
L6 0.4-0.55 m	BDL	BDL	BDL	1234.0	18.7	16.4	31.6
L6 0.55-0.7 m	BDL	BDL	BDL	929.9	16.4	12.0	23.8
L6 0.7-0.85 m	BDL	BDL	BDL	851.1	12.4	8.6	16.7
L6 0.85 1.0 m	BDL	BDL	BDL	1083.2	17.9	16.3	30.2
L6 1.0-1.15 m	BDL	BDL	BDL	792.7	13.9	8.4	15.8
L6 1.15-1.3 m	0.1225	BDL	BDL	827.4	8.7	5.6	11.7

Table B-3: Stable isotopes of water (δD & $\delta^{18}\text{O}$) and inorganic anions measured by ion chromatography. All anion values are reported in mg L^{-1} . Any samples with replicates (Y) are average values from duplicate samples. Hyphens (-) represent missing data values. Samples below detection limit are labeled BDL.

Sample ID	Rep.	δD (‰)	$\delta^{18}\text{O}$ (‰)	Cl	SO_4	F	$\text{NO}_3\text{-N}$
US-L1-P175		-117.6	-12.76	456.3	3686.5	1.07	7.67
US-L1-P200		-115.9	-12.68	548.2	3087.2	1.27	11.48
US-L1-P225	Y	-115.3	-12.59	560.7	2174.7	1.41	7.22
L1 1.5-1.65 m		-	-	-	-	-	-
L1 1.65-1.8 m		-121.2	-12.83	608.0	83.4	1.38	1.58
L1 1.8-1.95 m		-120.1	-13.21	615.0	55.8	1.99	<0.4
L1 2.25-2.4 m		-119.1	-13.05	589.0	408.0	1.40	0.52
L1 2.4-2.55 m		-115.4	-12.81	579.0	402.0	1.38	0.82
L1 2.55-2.7 m		-114.1	-11.78	615.0	26.5	1.38	<0.4
L2 0.95-1.15 m		-	-	604.0	14.8	1.45	<0.4
L2 1.15-1.35 m	Y	-113.6	-12.54	625.0	12.1	1.42	0.52
L2 1.35-1.5 m	Y	-112.7	-11.82	690.5	71.3	1.60	<0.4
L2 2.15-2.3 m		-110.3	-11.49	<20	926.0	<10	<40
L2 2.3-2.45 m		-113.3	-12.32	429.0	3290.0	0.75	38.70
L2 2.45-2.6 m	Y	-112.4	-12.59	501.5	2045.0	1.23	29.30
US-L3-P300		-113.3	-12.36	740.6	449.0	1.01	1.43
US-L3-P300C	Y	-109.4	-11.26	1058.0	1114.5	1.13	1.24
L3 0.15-0.3 m		-120	-13.98	475.0	2760.0	0.77	0.50
L3 0.3-0.45 m		-112.7	-12.72	1460.0	1880.0	2.28	<0.4
L3 0.45-0.6 m		-113.1	-12.75	681.0	92.7	1.83	0.53
L3 0.9-1.05 m		-	-	791.0	264.0	1.77	0.90
L3 1.05-1.2 m		-	-	769.0	38.1	1.24	0.42
L3 1.2-1.35 m		-	-	742.0	15.9	1.62	<0.4

US-L4-P050		-122.5	-13.86	310.7	2524.5	BDL	BDL
US-L4-P075		-120.6	-13.44	320.1	1962.8	0.68	0.25
US-L4-P100		-121.6	-13.73	452.4	2401.3	BDL	1.27
US-L4-P125	Y	-121.3	-13.56	401.4	2677.1	1.03	2.98
US-L4-P150		-118.4	-13.18	509.4	2060.7	1.35	1.71
US-L4-P175		-116.8	-13.05	580.4	1347.5	1.57	0.16
L4 1.4-1.55 m		-117.6	-13.3	714.0	552.0	1.48	0.42
L4 1.55-1.7 m		-114.7	-13.04	745.0	21.9	1.54	<0.4
L4 1.7-1.85 m	Y	-113.2	-12.52	775.0	17.8	1.59	<0.4
L4 2.2-2.35 m		-114.6	-13.04	704.0	592.0	1.11	<0.4
L4 2.35-2.5 m		-	-	-	-	-	-
L4 2.5-2.65 m		-114.6	-12.98	755.0	209.0	1.48	<0.4
US-L5-P050		-112.8	-11.58	1161.9	6755.6	0.96	6.60
US-L5-P075		-116.9	-12.33	784.1	4986.8	1.01	6.11
US-L5-P100		-120.0	-13.12	607.3	3575.3	1.09	0.73
US-L5-P125	Y	-118.0	-13.08	561.4	2583.2	1.25	0.24
US-L5-P300C		-111.4	-11.91	716.1	168.7	1.73	BDL
L5 0.95-1.1 m		-113.2	-12.48	656.0	227.0	1.67	1.29
L5 1.1-1.25 m		-117.4	-12.98	580.0	1480.0	1.10	6.06
L5 1.25-1.4 m		-115.1	-12.95	620.0	226.0	1.30	1.33
L5 2.25-2.4 m		-122	-13.89	509.0	931.0	1.06	7.04
L5 2.4-2.55 m		-114.4	-12.61	601.0	18.5	1.40	0.52
L5 2.55-2.7 m		-113.9	-12.53	610.0	15.8	1.39	0.51
US-L6-P150		-108.6	-11.30	4476.3	3126.1	2.00	BDL
US-L6-P175		-111.2	-11.95	2402.3	2629.6	2.20	BDL
US-L6-P200		-111.8	-12.21	1960.5	1849.4	1.75	BDL
US-L6-P225		-114.0	-12.8	639.8	498.6	1.26	BDL
US-L6-P250		-114.3	-12.84	635.1	537.4	1.21	BDL
US-L6-P275		-112.6	-12.37	651.5	621.7	1.02	BDL
US-L6-P300		-111.2	-12.37	664.0	405.5	1.31	BDL
US-L6-P300C		-114.1	-12.49	658.5	305.7	1.40	BDL
L6 0.4-0.55 m		-	-	1000.0	706.0	2.04	0.49
L6 0.55-0.7 m		-	-	816.0	295.0	2.02	0.58
L6 0.7-0.85 m		-	-	-	-	-	-
L6 0.85-1.0 m		-118.4	-13.21	877.0	417.0	1.66	0.70
L6 1.0-1.15 m		-114.6	-12.78	664.0	85.1	1.97	<0.4
L6 1.15-1.3 m		-	-	620.0	2.4	1.77	<0.4

Table B-3. continued

Sample ID	Rep.	NO ₂ -N	PO ₄	Br
US-L1-P175		BDL	BDL	BDL
US-L1-P200		BDL	BDL	BDL
US-L1-P225	Y	BDL	BDL	BDL

L1 1.5-1.65 m		<0.2	<1	<0.4
L1 1.65-1.8 m		<0.2	<1	<0.4
L1 1.8-1.95 m		<0.2	<1	<0.4
L1 2.25-2.4 m		<0.2	<1	<0.4
L1 2.4-2.55 m		<0.2	<1	<0.4
L1 2.55-2.7 m		<0.2	<1	<0.4
L2 0.95-1.15 m		<0.2	<1	<0.4
L2 1.15-1.35 m	Y	<0.2	<1	<0.4
L2 1.35-1.5 m	Y	<0.2	<1	0.42
L2 2.15-2.3 m		<20	<100	<40
L2 2.3-2.45 m		<0.2	<1	<0.4
L2 2.45-2.6 m	Y	<0.2	<1	<0.4
US-L3-P300		BDL	BDL	BDL
US-L3-P300C	Y	BDL	BDL	BDL
L3 0.15-0.3 m		<0.2	<1	<0.4
L3 0.3-0.45 m		<0.2	<1	<0.4
L3 0.45-0.6 m		<0.2	<1	0.45
L3 0.9-1.05 m		<0.2	<1	<0.4
L3 1.05-1.2 m		<0.2	<1	0.45
L3 1.2-1.35 m		<0.2	<1	0.44
US-L4-P050		BDL	BDL	BDL
US-L4-P075		BDL	BDL	BDL
US-L4-P100		BDL	BDL	BDL
US-L4-P125	Y	BDL	BDL	BDL
US-L4-P150		BDL	BDL	BDL
US-L4-P175		BDL	BDL	BDL
L4 1.4-1.55 m		<0.2	<1	<0.4
L4 1.55-1.7 m		<0.2	<1	0.47
L4 1.7-1.85 m	Y	<0.2	<1	0.49
L4 2.2-2.35 m		<0.2	<1	<0.4
L4 2.35-2.5 m		-	-	-
L4 2.5-2.65 m		<0.2	<1	0.4
US-L5-P050		BDL	BDL	BDL
US-L5-P075		BDL	BDL	BDL
US-L5-P100		BDL	BDL	BDL
US-L5-P125	Y	BDL	BDL	BDL
US-L5-P300C		BDL	BDL	BDL
L5 0.95-1.1 m		<0.2	<1	<0.4
L5 1.1-1.25 m		<0.2	<1	<0.4
L5 1.25-1.4 m		<0.2	<1	<0.4
L5 2.25-2.4 m		<0.2	<1	<0.4
L5 2.4-2.55 m		<0.2	<1	<0.4
L5 2.55-2.7 m		<0.2	<1	<0.4
US-L6-P150		BDL	BDL	BDL
US-L6-P175		BDL	BDL	BDL
US-L6-P200		BDL	BDL	BDL

US-L6-P225	BDL	BDL	BDL
US-L6-P250	BDL	BDL	BDL
US-L6-P275	BDL	BDL	BDL
US-L6-P300	BDL	BDL	BDL
US-L6-P300C	BDL	BDL	BDL
L6 0.4-0.55 m	<0.2	<1	0.45
L6 0.55-0.7 m	<0.2	<1	0.41
L6 0.7-0.85 m	-	-	-
L6 0.85-1.0 m	<0.2	<1	0.43
L6 1.0-1.15 m	<0.2	<1	0.41
L6 1.15-1.3 m	<0.2	<1	0.45

APPENDIX C: SOLID PHASE GEOCHEMISTRY

Table C-1: Cation exchange capacity (CEC) and specific surface area (SSA) measurements on lysimeter CFT and petroleum coke samples taken from cores and bulk sample. The methylene blue titration method was used to estimate both values.

Sample ID	Sample Type	Methylene Blue Titration Method	
		CEC (meq 100g ⁻¹)	SSA (m ² /g)
L1 1.5-1.65 m	Coke/CFT	1.96	37.9
L1 1.8-1.95 m	Coke/CFT	4.83	93.0
L1 2.4-2.55 m	CFT	10.36	205.6
L2 1.15-1.35 m	CFT	9.82	192.1
L2 2.3-2.45 m	CFT	11.17	183.6
L3 0.3-0.45 m	CFT	9.55	190.9
L3 0.9-1.05 m	CFT	14.98	287.6
L4 1.7-1.85 m	CFT	10.36	205.6
L4 2.35-2.5 m	CFT	20.89	394.0
L5 2.25-2.4 m	CFT	6.43	140.7
L5 2.4-2.55 m	CFT	10.26	204.4
L6 0.55-0.7 m	CFT	9.41	170.3
L6 1.15-1.3 m	CFT	10.18	190.9
Syncrude Fluid Coke 1	Coke	0.38	19.3
Syncrude Fluid Coke 2	Coke	0.43	21.9

APPENDIX D: COLUMN EXPERIMENT PORE WATER CHEMISTRY

Table D-1: Laboratory column experiment pore water chemistry. Parameter reported include pH, E_{measured} (E; mV), electrical conductivity (EC; mS cm^{-1}), temperature (T; $^{\circ}\text{C}$), alkalinity as CaCO_3 (Alk.; mg L^{-1}), dissolved sulfide (S^{2-} ; $\mu\text{g L}^{-1}$), dissolved nitrogen reported as ammonia ($\text{NH}_3\text{-N}$; mg L^{-1}). Insufficient pore water data for measurement is indicated by a hyphen (-). Any samples below the detection limit of the instrument are labelled BDL.

Sample ID	Height in Column (m)	pH	E	EC	T
CC-SatC-0.2m-01	0.2	7.97	-153.3	5.75	21.4
CC-SatC-0.3m-01	0.3	7.78	-281.3	4.51	21.0
CC-SatC-0.4m-01	0.4	7.75	15	4.61	21.5
CC-SatC-0.5m-01	0.5	7.81	-287.2	4.26	21.2
CC-SatC-0.6m-01	0.6	7.74	-293	4.27	21.3
CC-SatC-0.7m-01	0.7	7.72	-302.5	4.61	21.1
CC-SatC-0.8m-01	0.8	7.89	-306.3	4.54	21.0
CC-SatC-0.9m-01	0.9	7.53	-278	6.06	21.5
CC-SatC-1.0m-01	1.0	6.64	73.2	6.33	20.9
CC-SatC-1.1m-01	1.1	6.26	100	3.41	20.4
CC-SatC-1.2m-01	1.2	6.6	110.4	2.66	21.2
CC-SatC-1.3m-01	1.3	6.56	114	2.70	20.3
CC-SatC-1.4m-01	1.4	6.51	117	1.32	20.5
CC-SatC-0.2m-02	0.2	7.85	60.2	3.90	22.6
CC-SatC-0.3m-02	0.3	7.75	-284	4.15	22.0
CC-SatC-0.4m-02	0.4	7.9	-272.6	4.18	22.9
CC-SatC-0.5m-02	0.5	7.97	-289.8	4.09	22.4
CC-SatC-0.6m-02	0.6	7.95	-287	4.19	22.5
CC-SatC-0.7m-02	0.7	7.98	-312	4.11	22.8
CC-SatC-0.8m-02	0.8	7.74	-310.6	4.12	21.9
CC-SatC-0.9m-02	0.9	7.95	-279.7	5.66	22.3
CC-SatC-1.0m-02	1.0	6.96	-13.3	5.03	21.9
CC-SatC-1.1m-02	1.1	6.65	22.2	3.08	21.7
CC-SatC-1.2m-02	1.2	6.87	21.5	2.45	21.9
CC-SatC-1.3m-02	1.3	6.87	22.9	1.45	21.9
CC-SatC-1.4m-02	1.4	6.93	32	0.35	22.0
CC-SatC-0.2m-03	0.2	7.95	-	4.83	21.5
CC-SatC-0.3m-03	0.3	-	-	-	-
CC-SatC-0.4m-03	0.4	7.93	-136.6	5.1	21.6
CC-SatC-0.5m-03	0.5	7.9	-15.7	4.44	21.6
CC-SatC-0.6m-03	0.6	7.86	-259	4.48	21.3
CC-SatC-0.7m-03	0.7	7.96	-169.8	3.97	21.5
CC-SatC-0.8m-03	0.8	7.8	-280	4.28	21.6
CC-SatC-0.9m-03	0.9	7.76	38.8	5.73	21.5
CC-SatC-1.0m-03	1.0	7.11	56	4.59	21.9
CC-SatC-1.1m-03	1.1	6.88	68.4	3.01	21.8

CC-SatC-1.2m-03	1.2	7.15	57.7	0.93	21.6
CC-SatC-1.3m-03	1.3	7.05	94.3	0.34	22.2
CC-SatC-1.4m-03	1.4	6.92	116.7	0.85	21.6
CC-SatC-0.2m-04	0.2	7.89	124.7	4.00	21.8
CC-SatC-0.3m-04	0.3	7.9	-169.8	4.02	21.6
CC-SatC-0.4m-04	0.4	7.82	-1.1	3.91	21.8
CC-SatC-0.5m-04	0.5	7.87	32.2	3.82	21.9
CC-SatC-0.6m-04	0.6	8.14	-9.9	3.84	21.9
CC-SatC-0.7m-04	0.7	7.82	135.5	4.71	21.8
CC-SatC-0.8m-04	0.8	7.88	-308.4	3.84	22.0
CC-SatC-0.9m-04	0.9	7.67	-305.4	3.96	21.3
CC-SatC-1.0m-04	1.0	7.34	146.3	3.41	21.6
CC-SatC-1.1m-04	1.1	7.1	141	2.28	21.4
CC-SatC-1.2m-04	1.2	7.27	126.2	0.57	21.6
CC-SatC-1.3m-04	1.3	7.18	20	0.17	22.0
CC-SatC-1.4m-04	1.4	7.43	-6.4	0.05	22.1
CC-SatC-0.2m-05	0.2	7.91	117.7	3.69	23.4
CC-SatC-0.3m-05	0.3	8	103	4.37	23.4
CC-SatC-0.4m-05	0.4	7.79	97.6	3.71	23.5
CC-SatC-0.5m-05	0.5	7.85	127	3.67	23.5
CC-SatC-0.6m-05	0.6	7.91	111.4	3.73	23.5
CC-SatC-0.7m-05	0.7	7.83	153.8	3.73	23.8
CC-SatC-0.8m-05	0.8	7.86	-261.4	3.64	23.6
CC-SatC-0.9m-05	0.9	7.71	58.6	3.31	23.5
CC-SatC-1.0m-05	1.0	7.27	122.7	2.66	23.6
CC-SatC-1.1m-05	1.1	7.03	144.2	2.12	23.6
CC-SatC-1.2m-05	1.2	7.25	140.6	0.54	23.4
CC-SatC-1.3m-05	1.3	7.06	155.9	0.18	23.8
CC-SatC-1.4m-05	1.4	6.98	177.2	0.04	23.5
CC-SatC-0.2m-06	0.2	7.73	166.7	3.74	21.8
CC-SatC-0.3m-06	0.3	7.91	171.3	3.80	21.8
CC-SatC-0.4m-06	0.4	7.84	171.5	3.83	21.3
CC-SatC-0.5m-06	0.5	7.74	167.4	3.64	21.2
CC-SatC-0.6m-06	0.6	7.71	170.4	3.74	21.3
CC-SatC-0.7m-06	0.7	7.78	177.3	3.75	21.4
CC-SatC-0.8m-06	0.8	7.83	-226.5	3.52	21.6
CC-SatC-0.9m-06	0.9	7.61	64.4	3.21	21.4
CC-SatC-1.0m-06	1.0	7.4	112.5	2.74	21.5
CC-SatC-1.1m-06	1.1	7.17	130.3	2.12	22.2
CC-SatC-1.2m-06	1.2	7.39	130.6	0.48	21.8
CC-SatC-1.3m-06	1.3	7.17	153.4	0.20	21.3
CC-SatC-1.4m-06	1.4	7.21	181.5	0.06	21.2
CC-SatC-0.2m-07	0.2	7.82	170.6	4.21	21.4
CC-SatC-0.3m-07	0.3	7.94	176.4	4.39	21.3
CC-SatC-0.4m-07	0.4	7.83	177	-	21.3
CC-SatC-0.5m-07	0.5	7.97	177.4	4.45	21.1

CC-SatC-0.6m-07	0.6	8	177.2	-	21.4
CC-SatC-0.7m-07	0.7	7.85	171.1	4.51	21.2
CC-SatC-0.8m-07	0.8	7.88	111.4	-	21.9
CC-SatC-0.9m-07	0.9	7.71	163.8	3.89	22.0
CC-SatC-1.0m-07	1.0	7.39	220.3	3.46	21.9
CC-SatC-1.1m-07	1.1	7.31	231.7	2.73	21.7
CC-SatC-1.2m-07	1.2	7.23	230	0.64	21.5
CC-SatC-1.3m-07	1.3	7.1	252.9	0.24	21.5
CC-SatC-1.4m-07	1.4	7.36	299.7	0.12	21.6
CC-SatC-0.2m-08	0.2	7.86	189.9	4.13	21.7
CC-SatC-0.3m-08	0.3	8.03	192.4	4.18	21.8
CC-SatC-0.4m-08	0.4	-	-	-	-
CC-SatC-0.5m-08	0.5	8.02	198	4.31	22.0
CC-SatC-0.6m-08	0.6	7.98	192.7	3.90	22.0
CC-SatC-0.7m-08	0.7	7.83	184	4.22	22.0
CC-SatC-0.8m-08	0.8	7.88	121.6	3.88	21.9
CC-SatC-0.9m-08	0.9	7.53	199.6	3.72	21.7
CC-SatC-1.0m-08	1.0	7.37	247.4	3.07	21.6
CC-SatC-1.1m-08	1.1	7.24	234.5	1.98	21.7
CC-SatC-1.2m-08	1.2	7.37	242.5	0.36	21.7
CC-SatC-1.3m-08	1.3	6.89	287.2	0.04	21.5
CC-SatC-1.4m-08	1.4	7.51	273.2	0.03	21.4
CC-UnsatC-0.2m-01	0.2	7.86	-245	4.31	21.7
CC-UnsatC-0.3m-01	0.3	7.85	-264.9	4.47	21.8
CC-UnsatC-0.4m-01	0.4	7.73	-278.8	4.77	21.2
CC-UnsatC-0.5m-01	0.5	7.8	-294.6	4.44	21.1
CC-UnsatC-0.6m-01	0.6	7.65	11.2	5.25	21.7
CC-UnsatC-0.8m-01	0.8	7.75	-186.6	4.55	21.7
CC-UnsatC-0.9m-01	0.9	8.05	61.8	4.29	21.4
CC-UnsatC-0.2m-02	0.2	7.9	-227.9	3.87	22.3
CC-UnsatC-0.3m-02	0.3	7.79	-268.5	4.14	22.1
CC-UnsatC-0.4m-02	0.4	7.75	-290.9	4.28	22.1
CC-UnsatC-0.5m-02	0.5	7.94	-319	4.37	22.8
CC-UnsatC-0.6m-02	0.6	7.87	-343.4	4.98	22.8
CC-UnsatC-0.8m-02	0.8	7.8	-302.2	4.73	22
CC-UnsatC-0.9m-02	0.9	-	-	-	-
CC-UnsatC-0.2m-03	0.2	7.85	95.4	6.4	21.8
CC-UnsatC-0.3m-03	0.3	7.94	-221	4.25	21.7
CC-UnsatC-0.4m-03	0.4	8.06	-22.3	4.5	21.8
CC-UnsatC-0.5m-03	0.5	7.97	-290.8	4.35	21.8
CC-UnsatC-0.6m-03	0.6	7.88	-351.8	4.53	21.7
CC-UnsatC-0.8m-03	0.8	8.12	-133.5	4.31	21.5
CC-UnsatC-0.9m-03	0.9	-	-	-	-
CC-UnsatC-0.2m-04	0.2	7.88	20.6	3.72	21.7
CC-UnsatC-0.3m-04	0.3	7.89	-124.1	3.64	21.9

CC-UnsatC-0.4m-04	0.4	7.92	-0.1	3.69	22.7
CC-UnsatC-0.5m-04	0.5	7.97	-57.2	3.67	22.3
CC-UnsatC-0.6m-04	0.6	-	-	-	-
CC-UnsatC-0.8m-04	0.8	8.03	10	3.6	21.9
CC-UnsatC-0.9m-04	0.9	-	-	-	-
CC-UnsatC-0.2m-05	0.2	7.87	112.4	3.74	23.4
CC-UnsatC-0.3m-05	0.3	7.88	116.6	3.57	23.7
CC-UnsatC-0.4m-05	0.4	7.83	111.3	3.49	23.6
CC-UnsatC-0.5m-05	0.5	7.82	75.3	3.5	23.6
CC-UnsatC-0.6m-05	0.6	7.79	74.4	3.47	23.7
CC-UnsatC-0.8m-05	0.8	7.89	71.3	3.39	24
CC-UnsatC-0.9m-05	0.9	-	-	-	-
CC-UnsatC-0.2m-06	0.2	7.93	165	3.34	20.7
CC-UnsatC-0.3m-06	0.3	7.95	177.2	3.03	20.6
CC-UnsatC-0.4m-06	0.4	7.97	168.6	3.03	20.9
CC-UnsatC-0.5m-06	0.5	7.92	189.1	3.01	21.9
CC-UnsatC-0.6m-06	0.6	7.85	171.6	3.04	21.7
CC-UnsatC-0.8m-06	0.8	7.89	171.6	3.48	20.8
CC-UnsatC-0.9m-06	0.9	-	-	-	-

Table D-1. continued

Sample ID	Height in Column (m)	Alk.	S ²⁻	NH ₃ -N
CC-SatC-0.2m-01	0.2	1461.0	28800	14.10
CC-SatC-0.3m-01	0.3	1387.4	23350	15.10
CC-SatC-0.4m-01	0.4	1425.2	38800	13.40
CC-SatC-0.5m-01	0.5	1494.0	20400	14.70
CC-SatC-0.6m-01	0.6	1527.5	28900	14.70
CC-SatC-0.7m-01	0.7	1360.8	35950	15.10
CC-SatC-0.8m-01	0.8	1527.8	37750	14.60
CC-SatC-0.9m-01	0.9	934.4	3250	21.30
CC-SatC-1.0m-01	1.0	35.0	0	0.05
CC-SatC-1.1m-01	1.1	11.0	0	0.02
CC-SatC-1.2m-01	1.2	34.1	0	0.00
CC-SatC-1.3m-01	1.3	22.9	0	1.89
CC-SatC-1.4m-01	1.4	7.9	0	1.24
CC-SatC-0.2m-02	0.2	1560.0	-	13.60
CC-SatC-0.3m-02	0.3	1440.0	28800	14.20
CC-SatC-0.4m-02	0.4	1616.8	910	14.60
CC-SatC-0.5m-02	0.5	1573.7	49	14.20
CC-SatC-0.6m-02	0.6	1402.8	91	14.30
CC-SatC-0.7m-02	0.7	1640.0	36	14.20
CC-SatC-0.8m-02	0.8	1676.6	52500	14.10
CC-SatC-0.9m-02	0.9	780.0	7	9.91

CC-SatC-1.0m-02	1.0	92.0	0	0.05
CC-SatC-1.1m-02	1.1	35.9	2	0.03
CC-SatC-1.2m-02	1.2	57.9	2	0.02
CC-SatC-1.3m-02	1.3	44.0	4	0.00
CC-SatC-1.4m-02	1.4	16.0	0	0.02
CC-SatC-0.2m-03	0.2	-	-	13.80
CC-SatC-0.3m-03	0.3	-	5600	0.00
CC-SatC-0.4m-03	0.4	1611.6	95	14.50
CC-SatC-0.5m-03	0.5	1581.8	376	13.90
CC-SatC-0.6m-03	0.6	1618.9	9650	13.80
CC-SatC-0.7m-03	0.7	1641.8	20950	13.70
CC-SatC-0.8m-03	0.8	1639.6	38800	14.60
CC-SatC-0.9m-03	0.9	907.6	1020	8.33
CC-SatC-1.0m-03	1.0	93.5	1	0.14
CC-SatC-1.1m-03	1.1	52.4	0	0.13
CC-SatC-1.2m-03	1.2	107.1	24	0.05
CC-SatC-1.3m-03	1.3	33.9	1	0.08
CC-SatC-1.4m-03	1.4	24.3	-	0.05
CC-SatC-0.2m-04	0.2	1414.7	10	14.10
CC-SatC-0.3m-04	0.3	1491.1	900	14.60
CC-SatC-0.4m-04	0.4	1488.9	10	13.90
CC-SatC-0.5m-04	0.5	1408.7	12	14.30
CC-SatC-0.6m-04	0.6	1461.0	2105	14.20
CC-SatC-0.7m-04	0.7	1510.0	10	14.50
CC-SatC-0.8m-04	0.8	1565.3	37800	14.90
CC-SatC-0.9m-04	0.9	794.0	12760	7.95
CC-SatC-1.0m-04	1.0	221.4	3	0.22
CC-SatC-1.1m-04	1.1	70.0	2	0.21
CC-SatC-1.2m-04	1.2	116.1	2	0.08
CC-SatC-1.3m-04	1.3	55.3	0	0.05
CC-SatC-1.4m-04	1.4	8.9	0	BDL
CC-SatC-0.2m-05	0.2	1556.7	21	15.00
CC-SatC-0.3m-05	0.3	1643.4	0	15.20
CC-SatC-0.4m-05	0.4	1460.0	21	15.30
CC-SatC-0.5m-05	0.5	1229.8	27	15.40
CC-SatC-0.6m-05	0.6	1449.3	53	15.50
CC-SatC-0.7m-05	0.7	1218.6	16	15.00
CC-SatC-0.8m-05	0.8	1510.8	13800	15.50
CC-SatC-0.9m-05	0.9	860.0	10	7.68
CC-SatC-1.0m-05	1.0	213.7	1	0.17
CC-SatC-1.1m-05	1.1	121.7	0	0.17
CC-SatC-1.2m-05	1.2	122.8	1	0.07
CC-SatC-1.3m-05	1.3	61.2	1	0.08
CC-SatC-1.4m-05	1.4	13.5	1	BDL
CC-SatC-0.2m-06	0.2	1811.0	14	14.90
CC-SatC-0.3m-06	0.3	1780.6	10	15.30

CC-SatC-0.4m-06	0.4	1732.0	8	15.30
CC-SatC-0.5m-06	0.5	1744.7	10	15.00
CC-SatC-0.6m-06	0.6	1732.3	10	14.90
CC-SatC-0.7m-06	0.7	1750.9	6	14.80
CC-SatC-0.8m-06	0.8	1741.3	22950	15.10
CC-SatC-0.9m-06	0.9	1129.9	755	6.68
CC-SatC-1.0m-06	1.0	281.5	1	0.21
CC-SatC-1.1m-06	1.1	137.6	1	0.13
CC-SatC-1.2m-06	1.2	122.7	0	0.07
CC-SatC-1.3m-06	1.3	45.7	0	0.11
CC-SatC-1.4m-06	1.4	18.7	0	BDL
CC-SatC-0.2m-07	0.2	1763.7	17	15.00
CC-SatC-0.3m-07	0.3	1848.5	20	15.30
CC-SatC-0.4m-07	0.4	1474.0	6	16.20
CC-SatC-0.5m-07	0.5	1750.8	16	15.70
CC-SatC-0.6m-07	0.6	1704.2	6	15.80
CC-SatC-0.7m-07	0.7	1703.5	16	15.20
CC-SatC-0.8m-07	0.8	1791.5	350	14.00
CC-SatC-0.9m-07	0.9	1072.8	8000	5.74
CC-SatC-1.0m-07	1.0	319.4	1	0.18
CC-SatC-1.1m-07	1.1	173.2	1	0.13
CC-SatC-1.2m-07	1.2	125.2	1	0.08
CC-SatC-1.3m-07	1.3	28.6	1	0.12
CC-SatC-1.4m-07	1.4	11.3	1	BDL
CC-SatC-0.2m-08	0.2	1713.0	-	15.40
CC-SatC-0.3m-08	0.3	1435.8	-	15.40
CC-SatC-0.4m-08	0.4	-	-	-
CC-SatC-0.5m-08	0.5	1736.3	-	15.30
CC-SatC-0.6m-08	0.6	1346.6	-	15.50
CC-SatC-0.7m-08	0.7	1680.0	-	14.70
CC-SatC-0.8m-08	0.8	1646.3	-	13.70
CC-SatC-0.9m-08	0.9	978.9	-	5.26
CC-SatC-1.0m-08	1.0	308.7	-	0.20
CC-SatC-1.1m-08	1.1	174.0	-	0.13
CC-SatC-1.2m-08	1.2	121.6	-	0.08
CC-SatC-1.3m-08	1.3	-	-	0.03
CC-SatC-1.4m-08	1.4	9.0	-	0.00
CC-UnsatC-0.2m-01	0.2	1403.1	21450	15.1
CC-UnsatC-0.3m-01	0.3	1340.0	35100	15.9
CC-UnsatC-0.4m-01	0.4	1447.1	37500	15.2
CC-UnsatC-0.5m-01	0.5	1425.7	35900	15
CC-UnsatC-0.6m-01	0.6	1450.9	31650	19.2
CC-UnsatC-0.8m-01	0.8	1077.8	27950	16.9
CC-UnsatC-0.9m-01	0.9	1211.4	17950	13.3
CC-UnsatC-0.2m-02	0.2	1536.9	18	14.5
CC-UnsatC-0.3m-02	0.3	1673.3	139	14.5

CC-UnsatC-0.4m-02	0.4	1640.0	125	14.2
CC-UnsatC-0.5m-02	0.5	1640.0	15450	16
CC-UnsatC-0.6m-02	0.6	1836.3	34000	16.3
CC-UnsatC-0.8m-02	0.8	1576.8	14150	16.1
CC-UnsatC-0.9m-02	0.9	-	-	-
CC-UnsatC-0.2m-03	0.2	1457.0	33	14.3
CC-UnsatC-0.3m-03	0.3	1415.1	53	13.9
CC-UnsatC-0.4m-03	0.4	1527.4	42	14.3
CC-UnsatC-0.5m-03	0.5	1578.9	2600	13.8
CC-UnsatC-0.6m-03	0.6	1750.4	35200	14.6
CC-UnsatC-0.8m-03	0.8	1271.2	20	14.9
CC-UnsatC-0.9m-03	0.9	-	-	-
CC-UnsatC-0.2m-04	0.2	1518.5	20	15.1
CC-UnsatC-0.3m-04	0.3	1470.0	20	14.9
CC-UnsatC-0.4m-04	0.4	1326.3	48	14.5
CC-UnsatC-0.5m-04	0.5	1449.1	5000	15
CC-UnsatC-0.6m-04	0.6	-	-	-
CC-UnsatC-0.8m-04	0.8	1398.1	-	BDL
CC-UnsatC-0.9m-04	0.9	-	-	-
CC-UnsatC-0.2m-05	0.2	1396.5	18	15.1
CC-UnsatC-0.3m-05	0.3	1482.4	18	15.4
CC-UnsatC-0.4m-05	0.4	1425.4	21	15.9
CC-UnsatC-0.5m-05	0.5	1452.3	19	16.6
CC-UnsatC-0.6m-05	0.6	1476.8	25	15.4
CC-UnsatC-0.8m-05	0.8	1275.5	25	15
CC-UnsatC-0.9m-05	0.9	-	-	-
CC-UnsatC-0.2m-06	0.2	1259.4	17	15.7
CC-UnsatC-0.3m-06	0.3	1404.7	9	14.3
CC-UnsatC-0.4m-06	0.4	1287.1	21	16.6
CC-UnsatC-0.5m-06	0.5	1467.7	21	16.6
CC-UnsatC-0.6m-06	0.6	1629.7	20	16.4
CC-UnsatC-0.8m-06	0.8	1656.3	24	14.7
CC-UnsatC-0.9m-06	0.9	-	-	-

Table D-2: Major cations measured by Inductively Coupled Plasma-Optical Emission Spectroscopy (ICP-OES). All values are reported in mg L⁻¹. Sample concentrations below the detection limit (BDL) of the instrument are labeled accordingly. Cd was not included in this table, as all concentrations measured were below the detectable limit.

Sample ID	Height in Column (m)	As	Ba	Fe	P	S	Mo
CC-SatC-0.2m-01	0.2	0.410	0.334	BDL	0.163	145.4	0.58
CC-SatC-0.3m-01	0.3	0.072	0.262	BDL	0.142	96.6	0.16

CC-SatC-0.4m-01	0.4	0.147	0.522	BDL	0.114	89.9	0.13
CC-SatC-0.5m-01	0.5	0.022	0.381	BDL	0.164	64.0	0.03
CC-SatC-0.6m-01	0.6	BDL	0.499	BDL	0.187	68.1	BDL
CC-SatC-0.7m-01	0.7	0.017	0.393	BDL	0.147	164.8	BDL
CC-SatC-0.8m-01	0.8	BDL	0.438	BDL	0.172	124.3	BDL
CC-SatC-0.9m-01	0.9	BDL	0.147	BDL	0.123	787.6	BDL
CC-SatC-1.0m-01	1.0	BDL	0.021	BDL	0.069	1575.0	1.25
CC-SatC-1.1m-01	1.1	BDL	0.024	BDL	0.067	705.6	1.26
CC-SatC-1.2m-01	1.2	BDL	0.025	BDL	0.063	331.8	0.66
CC-SatC-1.3m-01	1.3	0.016	0.034	BDL	0.063	324.5	0.82
CC-SatC-1.4m-01	1.4	BDL	0.019	BDL	0.061	66.5	0.18
CC-SatC-0.2m-02	0.2	BDL	0.678	BDL	0.049	37.1	0.02
CC-SatC-0.3m-02	0.3	BDL	0.763	BDL	0.176	85.7	BDL
CC-SatC-0.4m-02	0.4	BDL	0.625	BDL	0.175	155.2	BDL
CC-SatC-0.5m-02	0.5	BDL	0.712	BDL	0.197	26.5	BDL
CC-SatC-0.6m-02	0.6	BDL	0.717	BDL	0.212	82.7	BDL
CC-SatC-0.7m-02	0.7	BDL	0.583	BDL	0.127	64.6	BDL
CC-SatC-0.8m-02	0.8	BDL	0.805	BDL	0.166	262.3	BDL
CC-SatC-0.9m-02	0.9	BDL	0.132	BDL	0.092	1059.1	0.13
CC-SatC-1.0m-02	1.0	BDL	0.018	BDL	0.031	1014.4	1.51
CC-SatC-1.1m-02	1.1	BDL	0.023	BDL	0.023	664.4	1.91
CC-SatC-1.2m-02	1.2	BDL	0.023	BDL	0.025	471.2	1.54
CC-SatC-1.3m-02	1.3	BDL	0.020	BDL	0.026	220.7	1.16
CC-SatC-1.4m-02	1.4	BDL	0.017	BDL	0.022	38.6	0.16
CC-SatC-0.2m-03	0.2	0.019	0.671	BDL	0.075	23.8	BDL
CC-SatC-0.3m-03	0.3	BDL	0.514	BDL	0.136	62.4	BDL
CC-SatC-0.4m-03	0.4	BDL	0.723	BDL	0.100	11.0	BDL
CC-SatC-0.5m-03	0.5	BDL	0.707	BDL	0.138	18.3	BDL
CC-SatC-0.6m-03	0.6	BDL	0.732	BDL	0.213	21.8	BDL
CC-SatC-0.7m-03	0.7	BDL	0.706	BDL	0.130	15.4	BDL
CC-SatC-0.8m-03	0.8	BDL	0.763	BDL	0.184	80.5	BDL
CC-SatC-0.9m-03	0.9	BDL	0.094	BDL	0.031	867.7	0.36
CC-SatC-1.0m-03	1.0	BDL	0.021	BDL	0.044	1079.3	1.97
CC-SatC-1.1m-03	1.1	BDL	0.020	BDL	0.031	509.6	1.69
CC-SatC-1.2m-03	1.2	BDL	0.028	BDL	0.033	86.6	0.71
CC-SatC-1.3m-03	1.3	BDL	0.021	BDL	0.025	14.2	0.14
CC-SatC-1.4m-03	1.4	BDL	0.003	BDL	0.023	4.8	0.02
CC-SatC-0.2m-04	0.2	BDL	0.753	BDL	0.151	24.7	BDL
CC-SatC-0.3m-04	0.3	BDL	0.713	BDL	0.210	11.3	BDL
CC-SatC-0.4m-04	0.4	BDL	0.710	BDL	0.154	13.7	BDL
CC-SatC-0.5m-04	0.5	BDL	0.551	BDL	0.141	12.8	BDL
CC-SatC-0.6m-04	0.6	0.021	0.617	BDL	0.209	14.5	BDL
CC-SatC-0.7m-04	0.7	BDL	0.727	BDL	0.090	17.9	BDL
CC-SatC-0.8m-04	0.8	BDL	0.763	BDL	0.204	353.0	BDL
CC-SatC-0.9m-04	0.9	BDL	0.085	BDL	0.088	818.4	0.13
CC-SatC-1.0m-04	1.0	BDL	0.018	BDL	0.057	945.2	1.99

CC-SatC-1.1m-04	1.1	BDL	0.020	BDL	0.040	581.5	2.16
CC-SatC-1.2m-04	1.2	BDL	0.058	BDL	0.026	61.6	0.56
CC-SatC-1.3m-04	1.3	BDL	0.023	BDL	0.033	5.1	0.17
CC-SatC-1.4m-04	1.4	BDL	0.001	BDL	0.031	2.2	0.03
CC-SatC-0.2m-05	0.2	0.020	0.800	0.0121	0.219	10.6	BDL
CC-SatC-0.3m-05	0.3	0.016	0.602	0.0032	0.204	7.1	BDL
CC-SatC-0.4m-05	0.4	0.021	0.802	0.0188	0.229	11.3	BDL
CC-SatC-0.5m-05	0.5	0.018	0.770	0.0207	0.219	13.9	0.00
CC-SatC-0.6m-05	0.6	0.019	0.713	0.0135	0.225	8.4	0.00
CC-SatC-0.7m-05	0.7	0.021	0.744	0.0182	0.149	15.8	BDL
CC-SatC-0.8m-05	0.8	0.023	0.689	BDL	0.203	142.5	BDL
CC-SatC-0.9m-05	0.9	0.012	0.084	0.0199	0.044	477.9	0.30
CC-SatC-1.0m-05	1.0	0.013	0.023	BDL	0.065	786.4	2.12
CC-SatC-1.1m-05	1.1	0.013	0.024	BDL	0.043	521.2	2.04
CC-SatC-1.2m-05	1.2	BDL	0.130	BDL	0.030	28.4	0.40
CC-SatC-1.3m-05	1.3	0.006	0.034	BDL	0.032	5.0	0.18
CC-SatC-1.4m-05	1.4	BDL	0.002	BDL	0.023	1.5	0.02
CC-SatC-0.2m-06	0.2	0.041	0.787	0.0120	0.230	9.8	BDL
CC-SatC-0.3m-06	0.3	0.016	0.658	0.0099	0.208	7.1	BDL
CC-SatC-0.4m-06	0.4	0.037	0.753	0.0242	0.242	8.7	BDL
CC-SatC-0.5m-06	0.5	0.045	0.792	0.0283	0.217	7.4	BDL
CC-SatC-0.6m-06	0.6	0.034	0.741	0.0141	0.246	8.2	BDL
CC-SatC-0.7m-06	0.7	0.024	0.744	0.0053	0.174	15.7	BDL
CC-SatC-0.8m-06	0.8	0.031	0.702	BDL	0.191	33.3	BDL
CC-SatC-0.9m-06	0.9	0.031	0.099	0.0122	0.042	295.4	0.16
CC-SatC-1.0m-06	1.0	0.016	0.024	BDL	0.079	640.6	1.91
CC-SatC-1.1m-06	1.1	0.010	0.023	BDL	0.046	422.2	1.81
CC-SatC-1.2m-06	1.2	0.011	0.096	BDL	0.030	22.0	0.40
CC-SatC-1.3m-06	1.3	0.007	0.040	0.2653	0.034	4.5	0.13
CC-SatC-1.4m-06	1.4	0.009	0.002	BDL	0.022	2.4	0.04
CC-SatC-0.2m-07	0.2	BDL	0.778	0.0360	0.227	6.2	BDL
CC-SatC-0.3m-07	0.3	BDL	0.632	0.0180	0.222	6.0	BDL
CC-SatC-0.4m-07	0.4	BDL	0.764	0.0330	0.264	7.3	BDL
CC-SatC-0.5m-07	0.5	BDL	0.671	0.0280	0.214	7.3	BDL
CC-SatC-0.6m-07	0.6	BDL	0.631	0.0230	0.230	8.3	BDL
CC-SatC-0.7m-07	0.7	BDL	0.720	0.0100	0.202	15.5	BDL
CC-SatC-0.8m-07	0.8	BDL	0.639	0.0030	0.182	25.5	BDL
CC-SatC-0.9m-07	0.9	BDL	0.085	0.0580	0.100	317.7	0.24
CC-SatC-1.0m-07	1.0	BDL	0.024	BDL	0.095	559.4	1.68
CC-SatC-1.1m-07	1.1	BDL	0.024	0.0020	0.080	363.7	1.57
CC-SatC-1.2m-07	1.2	BDL	0.097	BDL	0.041	20.7	0.37
CC-SatC-1.3m-07	1.3	BDL	0.025	0.0030	0.059	4.8	0.10
CC-SatC-1.4m-07	1.4	BDL	0.002	0.0070	0.042	3.6	0.05
CC-SatC-0.2m-08	0.2	0.044	0.607	0.0253	0.223	5.8	BDL
CC-SatC-0.3m-08	0.3	0.081	0.719	0.0125	0.311	6.6	BDL
CC-SatC-0.4m-08	0.4	0.069	0.732	BDL	0.244	13.1	BDL

CC-SatC-0.5m-08	0.5	0.071	0.643	BDL	0.210	17.1	BDL
CC-SatC-0.6m-08	0.6	0.047	0.095	0.0045	0.087	280.5	0.33
CC-SatC-0.7m-08	0.7	0.014	0.027	BDL	0.071	446.7	1.63
CC-SatC-0.8m-08	0.8	0.016	0.027	BDL	0.050	270.6	1.44
CC-SatC-0.9m-08	0.9	0.010	0.084	BDL	0.023	14.9	0.32
CC-SatC-1.0m-08	1.0	BDL	0.004	BDL	0.014	2.1	0.03
CC-SatC-1.1m-08	1.1	BDL	0.002	BDL	0.010	1.6	0.02
CC-SatC-1.2m-08	1.2	0.044	0.607	0.0253	0.223	5.8	BDL
CC-SatC-1.3m-08	1.3	0.081	0.719	0.0125	0.311	6.6	BDL
CC-SatC-1.4m-08	1.4	0.069	0.732	BDL	0.244	13.1	BDL
CC-UnsatC-0.2m-01	0.2	BDL	0.497	BDL	0.228	91.6	BDL
CC-UnsatC-0.3m-01	0.3	BDL	0.345	BDL	0.151	117.3	BDL
CC-UnsatC-0.4m-01	0.4	BDL	0.408	BDL	0.187	98.4	BDL
CC-UnsatC-0.5m-01	0.5	BDL	0.434	BDL	0.182	76.1	BDL
CC-UnsatC-0.6m-01	0.6	BDL	0.186	BDL	0.167	364.9	BDL
CC-UnsatC-0.8m-01	0.8	BDL	0.320	BDL	0.166	142.9	BDL
CC-UnsatC-0.9m-01	0.9	BDL	0.421	0.0271	0.117	88.2	0.00
CC-UnsatC-0.2m-02	0.2	BDL	0.619	BDL	0.250	14.9	BDL
CC-UnsatC-0.3m-02	0.3	BDL	0.776	BDL	0.200	120.6	BDL
CC-UnsatC-0.4m-02	0.4	BDL	0.603	BDL	0.173	219.2	BDL
CC-UnsatC-0.5m-02	0.5	BDL	0.535	BDL	0.160	161.4	BDL
CC-UnsatC-0.6m-02	0.6	BDL	1.030	BDL	0.177	861.2	BDL
CC-UnsatC-0.8m-02	0.8	BDL	0.764	BDL	0.267	199.3	BDL
CC-UnsatC-0.9m-02	0.9	-	-	-	-	-	-
CC-UnsatC-0.2m-03	0.2	BDL	0.646	BDL	0.218	11.7	BDL
CC-UnsatC-0.3m-03	0.3	BDL	0.604	BDL	0.059	10.4	BDL
CC-UnsatC-0.4m-03	0.4	BDL	0.701	BDL	0.096	6.6	BDL
CC-UnsatC-0.5m-03	0.5	BDL	0.735	BDL	0.150	19.2	BDL
CC-UnsatC-0.6m-03	0.6	BDL	0.881	BDL	0.072	356.7	BDL
CC-UnsatC-0.8m-03	0.8	BDL	0.693	BDL	0.092	9.0	BDL
CC-UnsatC-0.9m-03	0.9	-	-	-	-	-	-
CC-UnsatC-0.2m-04	0.2	BDL	0.706	BDL	0.274	7.1	BDL
CC-UnsatC-0.3m-04	0.3	0.017	0.713	0.0395	0.185	11.3	BDL
CC-UnsatC-0.4m-04	0.4	0.026	0.727	BDL	0.189	5.8	BDL
CC-UnsatC-0.5m-04	0.5	BDL	0.732	BDL	0.201	14.2	BDL
CC-UnsatC-0.6m-04	0.6	-	-	-	-	-	-
CC-UnsatC-0.8m-04	0.8	0.020	0.702	BDL	0.215	10.0	BDL
CC-UnsatC-0.9m-04	0.9	-	-	-	-	-	-
CC-UnsatC-0.2m-05	0.2	0.019	0.761	0.0419	0.293	5.6	BDL
CC-UnsatC-0.3m-05	0.3	0.018	0.780	0.0174	0.235	8.2	BDL
CC-UnsatC-0.4m-05	0.4	0.021	0.744	0.0077	0.243	4.9	BDL
CC-UnsatC-0.5m-05	0.5	0.019	0.769	0.0012	0.234	12.4	BDL
CC-UnsatC-0.6m-05	0.6	0.021	0.765	BDL	0.181	9.8	BDL
CC-UnsatC-0.8m-05	0.8	0.016	0.683	0.0093	0.257	11.6	BDL

CC-UnsatC-0.9m-05	0.9	-	-	-	-	-	-
CC-UnsatC-0.2m-06	0.2	0.032	0.765	0.0513	0.325	5.0	BDL
CC-UnsatC-0.3m-06	0.3	0.029	0.791	0.0256	0.271	7.7	BDL
CC-UnsatC-0.4m-06	0.4	0.030	0.788	0.0128	0.275	4.6	BDL
CC-UnsatC-0.5m-06	0.5	0.024	0.755	0.0041	0.251	12.4	BDL
CC-UnsatC-0.6m-06	0.6	0.036	0.805	0.0036	0.247	11.1	BDL
CC-UnsatC-0.8m-06	0.8	0.028	0.687	0.0061	0.277	12.8	BDL
CC-UnsatC-0.9m-06	0.9	-	-	-	-	-	-

Table D-2. continued

Sample ID	Height in Column (m)	Al	Se	Ca	K	Mg	Na
CC-SatC-0.2m-01	0.2	BDL	BDL	49.8	23.97	29.94	994.7
CC-SatC-0.3m-01	0.3	BDL	BDL	45.0	14.95	19.95	941.9
CC-SatC-0.4m-01	0.4	BDL	BDL	56.4	21.35	25.80	914.7
CC-SatC-0.5m-01	0.5	BDL	BDL	44.2	16.24	19.76	906.9
CC-SatC-0.6m-01	0.6	BDL	BDL	55.7	20.38	24.88	895.3
CC-SatC-0.7m-01	0.7	BDL	BDL	94.3	23.50	33.45	972.8
CC-SatC-0.8m-01	0.8	BDL	BDL	68.2	22.05	29.85	936.0
CC-SatC-0.9m-01	0.9	BDL	BDL	227.5	32.41	140.78	1156.4
CC-SatC-1.0m-01	1.0	BDL	0.0469	460.1	28.79	467.43	721.0
CC-SatC-1.1m-01	1.1	BDL	0.0132	345.7	12.64	158.94	301.3
CC-SatC-1.2m-01	1.2	BDL	BDL	194.1	71.21	82.10	104.1
CC-SatC-1.3m-01	1.3	BDL	BDL	172.9	6.11	91.53	99.1
CC-SatC-1.4m-01	1.4	BDL	BDL	31.5	1.40	18.62	23.2
CC-SatC-0.2m-02	0.2	BDL	BDL	49.5	30.26	26.78	937.3
CC-SatC-0.3m-02	0.3	BDL	BDL	55.4	19.23	26.08	945.1
CC-SatC-0.4m-02	0.4	BDL	BDL	48.8	50.96	21.70	922.2
CC-SatC-0.5m-02	0.5	BDL	BDL	53.5	36.35	24.92	927.4
CC-SatC-0.6m-02	0.6	BDL	BDL	54.1	61.30	24.10	922.4
CC-SatC-0.7m-02	0.7	BDL	BDL	45.5	17.72	18.36	942.8
CC-SatC-0.8m-02	0.8	BDL	BDL	64.6	19.25	26.10	939.9
CC-SatC-0.9m-02	0.9	BDL	BDL	324.9	25.86	244.34	969.5
CC-SatC-1.0m-02	1.0	BDL	BDL	390.5	16.63	259.45	484.5
CC-SatC-1.1m-02	1.1	BDL	BDL	346.2	10.75	159.16	231.0
CC-SatC-1.2m-02	1.2	BDL	BDL	270.8	7.35	130.11	127.6
CC-SatC-1.3m-02	1.3	BDL	BDL	133.5	3.88	66.06	54.6
CC-SatC-1.4m-02	1.4	BDL	BDL	19.5	1.09	10.20	15.2
CC-SatC-0.2m-03	0.2	BDL	BDL	45.1	18.57	25.67	941.3
CC-SatC-0.3m-03	0.3	BDL	BDL	36.8	13.08	18.80	955.8
CC-SatC-0.4m-03	0.4	BDL	BDL	53.4	18.53	25.78	932.9
CC-SatC-0.5m-03	0.5	BDL	BDL	51.7	18.28	25.24	922.4
CC-SatC-0.6m-03	0.6	BDL	BDL	54.7	18.48	25.05	935.4
CC-SatC-0.7m-03	0.7	BDL	BDL	54.1	17.43	24.04	925.3
CC-SatC-0.8m-03	0.8	BDL	BDL	58.8	18.63	26.20	924.2

CC-SatC-0.9m-03	0.9	BDL	BDL	306.3	24.70	224.08	965.2
CC-SatC-1.0m-03	1.0	BDL	BDL	466.6	17.23	265.43	489.4
CC-SatC-1.1m-03	1.1	BDL	BDL	275.4	8.18	126.22	167.1
CC-SatC-1.2m-03	1.2	BDL	BDL	60.5	2.95	30.26	38.5
CC-SatC-1.3m-03	1.3	BDL	BDL	13.5	0.88	6.65	8.4
CC-SatC-1.4m-03	1.4	BDL	BDL	2.3	0.20	1.12	4.3
CC-SatC-0.2m-04	0.2	BDL	BDL	55.2	18.96	27.02	938.6
CC-SatC-0.3m-04	0.3	BDL	BDL	50.4	18.18	26.42	938.6
CC-SatC-0.4m-04	0.4	BDL	BDL	52.7	17.42	24.83	920.2
CC-SatC-0.5m-04	0.5	BDL	BDL	41.2	13.91	19.64	909.9
CC-SatC-0.6m-04	0.6	BDL	BDL	43.1	18.67	25.47	936.4
CC-SatC-0.7m-04	0.7	BDL	BDL	52.7	18.84	26.29	960.2
CC-SatC-0.8m-04	0.8	BDL	BDL	56.7	19.31	27.21	969.6
CC-SatC-0.9m-04	0.9	BDL	BDL	273.9	21.86	186.27	819.8
CC-SatC-1.0m-04	1.0	BDL	BDL	468.3	15.94	226.80	497.9
CC-SatC-1.1m-04	1.1	BDL	BDL	330.7	9.48	150.28	204.4
CC-SatC-1.2m-04	1.2	BDL	BDL	53.3	2.47	26.80	28.4
CC-SatC-1.3m-04	1.3	BDL	BDL	13.6	0.56	7.21	4.7
CC-SatC-1.4m-04	1.4	BDL	BDL	1.2	0.18	0.53	3.6
CC-SatC-0.2m-05	0.2	BDL	BDL	54.4	20.71	29.30	965.8
CC-SatC-0.3m-05	0.3	BDL	BDL	34.5	22.53	30.55	1037.5
CC-SatC-0.4m-05	0.4	BDL	BDL	58.0	20.02	28.68	955.7
CC-SatC-0.5m-05	0.5	BDL	BDL	56.8	19.96	28.01	944.3
CC-SatC-0.6m-05	0.6	BDL	BDL	47.2	20.39	28.81	955.4
CC-SatC-0.7m-05	0.7	BDL	BDL	51.1	19.91	27.35	928.1
CC-SatC-0.8m-05	0.8	BDL	BDL	47.0	19.69	28.09	930.2
CC-SatC-0.9m-05	0.9	BDL	BDL	159.8	20.95	135.60	776.3
CC-SatC-1.0m-05	1.0	BDL	BDL	363.0	14.90	190.02	443.8
CC-SatC-1.1m-05	1.1	BDL	BDL	263.8	10.02	136.34	225.6
CC-SatC-1.2m-05	1.2	BDL	BDL	41.0	2.20	22.33	15.5
CC-SatC-1.3m-05	1.3	BDL	BDL	13.5	0.61	7.82	3.7
CC-SatC-1.4m-05	1.4	BDL	BDL	1.1	0.24	0.47	3.2
CC-SatC-0.2m-06	0.2	BDL	BDL	53.3	20.45	29.10	962.4
CC-SatC-0.3m-06	0.3	BDL	BDL	41.6	20.77	29.42	970.5
CC-SatC-0.4m-06	0.4	BDL	BDL	52.9	20.41	29.18	949.8
CC-SatC-0.5m-06	0.5	BDL	BDL	57.7	20.33	28.18	942.7
CC-SatC-0.6m-06	0.6	BDL	BDL	51.3	20.16	28.34	957.8
CC-SatC-0.7m-06	0.7	BDL	BDL	50.9	19.91	27.46	941.3
CC-SatC-0.8m-06	0.8	BDL	BDL	48.6	19.53	27.87	921.2
CC-SatC-0.9m-06	0.9	BDL	BDL	104.4	18.93	97.92	768.6
CC-SatC-1.0m-06	1.0	BDL	BDL	294.7	13.82	159.40	437.2
CC-SatC-1.1m-06	1.1	BDL	BDL	216.8	9.36	112.73	228.7
CC-SatC-1.2m-06	1.2	BDL	BDL	38.5	1.99	21.64	13.0
CC-SatC-1.3m-06	1.3	BDL	BDL	11.3	0.53	6.46	3.6
CC-SatC-1.4m-06	1.4	BDL	BDL	1.5	0.30	0.76	3.4
CC-SatC-0.2m-07	0.2	BDL	BDL	57.8	20.35	27.79	967.4

CC-SatC-0.3m-07	0.3	BDL	BDL	42.7	20.48	27.42	985.5
CC-SatC-0.4m-07	0.4	0.012	BDL	58.0	20.09	27.46	963.6
CC-SatC-0.5m-07	0.5	BDL	BDL	47.6	20.20	27.01	981.8
CC-SatC-0.6m-07	0.6	BDL	BDL	42.6	20.13	26.52	965.2
CC-SatC-0.7m-07	0.7	BDL	BDL	52.7	19.52	26.01	960.6
CC-SatC-0.8m-07	0.8	BDL	BDL	46.5	19.21	25.78	914.8
CC-SatC-0.9m-07	0.9	BDL	BDL	121.7	17.34	92.76	703.7
CC-SatC-1.0m-07	1.0	BDL	BDL	257.9	12.71	125.96	416.6
CC-SatC-1.1m-07	1.1	BDL	BDL	190.3	8.62	87.06	216.1
CC-SatC-1.2m-07	1.2	BDL	BDL	40.9	1.94	19.79	12.1
CC-SatC-1.3m-07	1.3	BDL	BDL	8.9	0.51	4.43	3.6
CC-SatC-1.4m-07	1.4	BDL	BDL	2.3	0.41	1.21	3.8
CC-SatC-0.2m-08	0.2	3.175	BDL	38.8	54.85	27.19	782.0
CC-SatC-0.3m-08	0.3	5.356	BDL	48.0	38.07	28.40	969.5
CC-SatC-0.4m-08	0.4	5.197	BDL	50.4	19.39	26.85	976.4
CC-SatC-0.5m-08	0.5	1.431	BDL	42.7	18.94	27.10	793.5
CC-SatC-0.6m-08	0.6	0.766	BDL	112.9	16.37	92.91	657.3
CC-SatC-0.7m-08	0.7	0.545	BDL	208.9	11.51	113.62	377.6
CC-SatC-0.8m-08	0.8	0.409	BDL	148.3	7.68	74.35	195.5
CC-SatC-0.9m-08	0.9	0.428	BDL	35.1	1.75	18.23	12.8
CC-SatC-1.0m-08	1.0	0.546	BDL	2.3	0.30	1.36	3.3
CC-SatC-1.1m-08	1.1	0.550	BDL	1.2	0.22	0.68	3.1
CC-SatC-1.2m-08	1.2	3.175	BDL	38.8	54.85	27.19	782.0
CC-SatC-1.3m-08	1.3	5.356	BDL	48.0	38.07	28.40	969.5
CC-SatC-1.4m-08	1.4	5.197	BDL	50.4	19.39	26.85	976.4
CC-UnsatC-0.2m-01	0.2	BDL	BDL	52.2	19.53	23.79	883.5
CC-UnsatC-0.3m-01	0.3	BDL	BDL	58.6	17.11	24.05	951.3
CC-UnsatC-0.4m-01	0.4	BDL	BDL	65.4	21.74	27.95	920.9
CC-UnsatC-0.5m-01	0.5	BDL	BDL	59.5	20.79	26.22	901.3
CC-UnsatC-0.6m-01	0.6	BDL	BDL	140.4	27.24	47.75	1017.4
CC-UnsatC-0.8m-01	0.8	BDL	BDL	52.2	16.16	22.19	927.2
CC-UnsatC-0.9m-01	0.9	BDL	BDL	39.3	17.00	18.31	812.4
CC-UnsatC-0.2m-02	0.2	BDL	BDL	46.0	30.18	21.71	899.2
CC-UnsatC-0.3m-02	0.3	BDL	BDL	61.7	43.45	25.22	926.3
CC-UnsatC-0.4m-02	0.4	BDL	BDL	43.4	22.11	21.57	933.9
CC-UnsatC-0.5m-02	0.5	BDL	BDL	38.8	14.13	18.29	923.6
CC-UnsatC-0.6m-02	0.6	BDL	BDL	84.0	20.96	32.11	967.1
CC-UnsatC-0.8m-02	0.8	BDL	BDL	56.8	19.04	24.80	911.2
CC-UnsatC-0.9m-02	0.9	-	-	-	-	-	-
CC-UnsatC-0.2m-03	0.2	BDL	BDL	48.1	17.53	23.22	897.5
CC-UnsatC-0.3m-03	0.3	BDL	BDL	45.9	15.81	21.58	884.2
CC-UnsatC-0.4m-03	0.4	BDL	BDL	51.7	17.95	24.18	893.3
CC-UnsatC-0.5m-03	0.5	BDL	BDL	55.2	18.67	24.43	921.9
CC-UnsatC-0.6m-03	0.6	BDL	BDL	71.3	19.41	28.94	909.9
CC-UnsatC-0.8m-03	0.8	BDL	BDL	52.2	17.94	23.52	886.6

CC-UnsatC-0.9m-03	0.9	-	-	-	-	-	-
CC-UnsatC-0.2m-04	0.2	BDL	BDL	55.8	17.93	24.87	928.6
CC-UnsatC-0.3m-04	0.3	BDL	BDL	56.8	17.93	24.91	926.5
CC-UnsatC-0.4m-04	0.4	BDL	BDL	56.5	17.84	24.59	928.4
CC-UnsatC-0.5m-04	0.5	BDL	BDL	55.6	18.46	25.31	945.1
CC-UnsatC-0.6m-04	0.6	-	-	-	-	-	-
CC-UnsatC-0.8m-04	0.8	BDL	BDL	54.8	17.48	23.18	891.7
CC-UnsatC-0.9m-04	0.9	-	-	-	-	-	-
CC-UnsatC-0.2m-05	0.2	BDL	BDL	55.4	19.65	27.68	944.5
CC-UnsatC-0.3m-05	0.3	BDL	BDL	60.8	19.53	27.31	946.5
CC-UnsatC-0.4m-05	0.4	BDL	BDL	55.3	19.19	27.01	934.3
CC-UnsatC-0.5m-05	0.5	BDL	BDL	55.8	19.50	27.29	930.8
CC-UnsatC-0.6m-05	0.6	BDL	BDL	59.1	19.65	27.99	920.9
CC-UnsatC-0.8m-05	0.8	BDL	BDL	53.2	18.54	24.02	915.5
CC-UnsatC-0.9m-05	0.9	-	-	-	-	-	-
CC-UnsatC-0.2m-06	0.2	BDL	BDL	54.9	19.85	28.35	942.8
CC-UnsatC-0.3m-06	0.3	BDL	BDL	60.7	20.28	27.90	971.0
CC-UnsatC-0.4m-06	0.4	BDL	BDL	57.1	20.03	27.79	946.9
CC-UnsatC-0.5m-06	0.5	BDL	BDL	52.1	19.98	28.21	954.6
CC-UnsatC-0.6m-06	0.6	BDL	BDL	61.6	19.84	28.49	949.6
CC-UnsatC-0.8m-06	0.8	BDL	BDL	49.8	18.05	24.45	900.9
CC-UnsatC-0.9m-06	0.9	-	-	-	-	-	-

Table D-3: Inorganic anions measured by ion chromatography. All values reported in mg L⁻¹.

Sample ID	Height in Column (m)	F	Br	SO ₄	Cl
CC-SatC-0.2m-01	0.2	1.51	<0.4	353.00	495.00
CC-SatC-0.3m-01	0.3	1.52	<0.4	379.00	460.00
CC-SatC-0.4m-01	0.4	1.58	<0.4	254.00	472.00
CC-SatC-0.5m-01	0.5	1.59	<0.4	178.00	468.00
CC-SatC-0.6m-01	0.6	1.62	<0.4	177.00	467.00
CC-SatC-0.7m-01	0.7	1.51	<0.4	466.00	454.00
CC-SatC-0.8m-01	0.8	1.55	<0.4	336.00	459.00
CC-SatC-0.9m-01	0.9	1.23	<0.4	2260.00	344.00
CC-SatC-1.0m-01	1.0	0.21	<0.4	4450.00	51.50
CC-SatC-1.1m-01	1.1	<0.1	<0.4	2100.00	1.05
CC-SatC-1.2m-01	1.2	0.14	<0.4	1310.00	0.93
CC-SatC-1.3m-01	1.3	<0.1	<0.4	1270.00	0.52
CC-SatC-1.4m-01	1.4	<0.1	<0.4	294.00	0.63
CC-SatC-0.2m-02	0.2	1.66	<0.4	113.00	458.00
CC-SatC-0.3m-02	0.3	1.17	<0.4	9.38	460.00
CC-SatC-0.4m-02	0.4	1.52	<0.4	116.00	461.00
CC-SatC-0.5m-02	0.5	1.58	<0.4	96.10	466.00
CC-SatC-0.6m-02	0.6	1.14	<0.4	6.76	465.00

CC-SatC-0.7m-02	0.7	1.54	<0.4	137.00	462.00
CC-SatC-0.8m-02	0.8	1.57	<0.4	175.00	450.00
CC-SatC-0.9m-02	0.9	1.26	<0.4	2230.00	338.00
CC-SatC-1.0m-02	1.0	0.4	<0.4	99.30	77.90
CC-SatC-1.1m-02	1.1	<0.1	<0.4	1980.00	5.84
CC-SatC-1.2m-02	1.2	0.27	<0.4	1430.00	1.00
CC-SatC-1.3m-02	1.3	0.18	<0.4	800.00	1.66
CC-SatC-1.4m-02	1.4	<0.1	<0.4	134.00	0.68
CC-SatC-0.2m-03	0.2	1.65	<0.4	57.80	457.00
CC-SatC-0.3m-03	0.3	1.56	<0.4	11.20	457.00
CC-SatC-0.4m-03	0.4	1.58	<0.4	22.10	463.00
CC-SatC-0.5m-03	0.5	1.49	<0.4	53.90	462.00
CC-SatC-0.6m-03	0.6	1.58	<0.4	7.57	463.00
CC-SatC-0.7m-03	0.7	1.57	<0.4	49.20	458.00
CC-SatC-0.8m-03	0.8	1.58	<0.4	164.00	436.00
CC-SatC-0.9m-03	0.9	1.3	<0.4	2540.00	228.00
CC-SatC-1.0m-03	1.0	0.47	<0.4	3120.00	79.10
CC-SatC-1.1m-03	1.1	0.19	<0.4	1810.00	9.02
CC-SatC-1.2m-03	1.2	0.4	<0.4	256.00	1.64
CC-SatC-1.3m-03	1.3	0.14	<0.4	40.80	0.74
CC-SatC-1.4m-03	1.4	<0.1	<0.4	12.60	<0.2
CC-SatC-0.2m-04	0.2	1.66	<0.4	55.60	460.00
CC-SatC-0.3m-04	0.3	1.59	<0.4	3.89	458.00
CC-SatC-0.4m-04	0.4	1.68	<0.4	34.30	463.00
CC-SatC-0.5m-04	0.5	1.53	<0.4	40.20	461.00
CC-SatC-0.6m-04	0.6	1.44	<0.4	9.47	464.00
CC-SatC-0.7m-04	0.7	1.7	<0.4	45.50	454.00
CC-SatC-0.8m-04	0.8	1.23	<0.4	10.80	411.00
CC-SatC-0.9m-04	0.9	0.87	<0.8	2090.00	211.00
CC-SatC-1.0m-04	1.0	0.68	<0.4	2830.00	109.00
CC-SatC-1.1m-04	1.1	0.27	<0.4	1770.00	29.70
CC-SatC-1.2m-04	1.2	0.24	<0.4	196.00	3.64
CC-SatC-1.3m-04	1.3	0.16	<0.4	13.40	1.27
CC-SatC-1.4m-04	1.4	<0.1	<0.4	5.72	0.50
CC-SatC-0.2m-05	0.2	1.49	<0.4	17.80	456.00
CC-SatC-0.3m-05	0.3	1.66	<0.4	8.38	508.00
CC-SatC-0.4m-05	0.4	1.47	<0.4	21.20	460.00
CC-SatC-0.5m-05	0.5	1.24	<0.4	29.50	476.00
CC-SatC-0.6m-05	0.6	1.58	<0.4	7.00	462.00
CC-SatC-0.7m-05	0.7	1.63	<0.4	35.80	467.00
CC-SatC-0.8m-05	0.8	1.69	<0.4	16.30	387.00
CC-SatC-0.9m-05	0.9	0.95	<0.4	1340.00	235.00
CC-SatC-1.0m-05	1.0	0.69	<0.4	2160.00	118.00
CC-SatC-1.1m-05	1.1	0.3	<0.4	1480.00	58.90
CC-SatC-1.2m-05	1.2	0.29	<0.4	80.00	6.41
CC-SatC-1.3m-05	1.3	0.11	<0.4	12.70	1.51

CC-SatC-1.4m-05	1.4	<0.1	<0.4	3.28	0.50
CC-SatC-0.2m-06	0.2	1.57	<0.4	30.60	454.00
CC-SatC-0.3m-06	0.3	1.54	<0.4	9.61	466.00
CC-SatC-0.4m-06	0.4	1.48	<0.4	14.60	463.00
CC-SatC-0.5m-06	0.5	1.5	<0.4	11.20	463.00
CC-SatC-0.6m-06	0.6	1.58	<0.4	12.30	458.00
CC-SatC-0.7m-06	0.7	1.63	<0.4	33.80	438.00
CC-SatC-0.8m-06	0.8	1.69	<0.4	15.80	371.00
CC-SatC-0.9m-06	0.9	1.17	<0.4	849.00	236.00
CC-SatC-1.0m-06	1.0	0.79	<0.4	1790.00	125.00
CC-SatC-1.1m-06	1.1	0.37	<0.4	1220.00	70.40
CC-SatC-1.2m-06	1.2	0.22	<0.4	61.90	8.33
CC-SatC-1.3m-06	1.3	<0.1	<0.4	10.90	1.39
CC-SatC-1.4m-06	1.4	<0.1	<0.4	5.48	0.58
CC-SatC-0.2m-07	0.2	1.52	<0.4	7.16	455.00
CC-SatC-0.3m-07	0.3	1.47	<0.4	6.47	454.00
CC-SatC-0.4m-07	0.4	1.46	<0.4	9.46	450.00
CC-SatC-0.5m-07	0.5	1.53	<0.4	9.25	459.00
CC-SatC-0.6m-07	0.6	1.64	<0.4	12.30	488.00
CC-SatC-0.7m-07	0.7	1.61	<0.4	30.10	437.00
CC-SatC-0.8m-07	0.8	1.69	<0.4	28.80	362.00
CC-SatC-0.9m-07	0.9	1.18	<0.4	920.00	230.00
CC-SatC-1.0m-07	1.0	0.7	<0.4	1410.00	119.00
CC-SatC-1.1m-07	1.1	0.53	<0.4	1030.00	75.30
CC-SatC-1.2m-07	1.2	0.23	<0.4	56.70	9.28
CC-SatC-1.3m-07	1.3	<0.1	<0.4	11.90	1.57
CC-SatC-1.4m-07	1.4	<0.1	<0.4	7.37	0.81
CC-SatC-0.2m-08	0.2	1.53	<0.4	6.82	455.00
CC-SatC-0.3m-08	0.3	1.49	<0.4	4.73	463.00
CC-SatC-0.4m-08	0.4	-	-	-	-
CC-SatC-0.5m-08	0.5	1.48	<0.4	6.47	458.00
CC-SatC-0.6m-08	0.6	1.55	<0.4	8.44	454.00
CC-SatC-0.7m-08	0.7	1.62	<0.4	26.40	429.00
CC-SatC-0.8m-08	0.8	1.73	<0.4	39.40	345.00
CC-SatC-0.9m-08	0.9	1.11	<0.4	818.00	206.00
CC-SatC-1.0m-08	1.0	0.67	<0.4	1250.00	118.00
CC-SatC-1.1m-08	1.1	0.55	<0.4	780.00	68.30
CC-SatC-1.2m-08	1.2	0.25	<0.4	31.70	5.95
CC-SatC-1.3m-08	1.3	<0.1	<0.4	4.31	0.53
CC-SatC-1.4m-08	1.4	<0.1	<0.4	3.48	0.45
CC-UnsatC-0.2m-01	0.2	1.55	<0.4	255.00	475.00
CC-UnsatC-0.3m-01	0.3	1.5	<0.4	430.00	467.00
CC-UnsatC-0.4m-01	0.4	1.55	<0.4	264.00	467.00
CC-UnsatC-0.5m-01	0.5	1.56	<0.4	201.00	467.00
CC-UnsatC-0.6m-01	0.6	1.18	<0.4	1100.00	443.00
CC-UnsatC-0.8m-01	0.8	1.03	<0.4	551.00	461.00

CC-UnsatC-0.9m-01	0.9	1.75	<0.4	256.00	472.00
CC-UnsatC-0.2m-02	0.2	1.24	<0.4	5.70	472.00
CC-UnsatC-0.3m-02	0.3	1.12	<0.4	19.90	468.00
CC-UnsatC-0.4m-02	0.4	1.21	<0.4	5.30	464.00
CC-UnsatC-0.5m-02	0.5	1.16	<0.4	9.41	492.00
CC-UnsatC-0.6m-02	0.6	1.5	<0.4	343.00	453.00
CC-UnsatC-0.8m-02	0.8	1.21	<0.4	6.76	462.00
CC-UnsatC-0.9m-02	0.9	-	-	-	-
CC-UnsatC-0.2m-03	0.2	1.6	<0.4	26.90	477.00
CC-UnsatC-0.3m-03	0.3	1.64	<0.4	27.60	476.00
CC-UnsatC-0.4m-03	0.4	1.6	<0.4	<0.4	466.00
CC-UnsatC-0.5m-03	0.5	1.6	<0.4	50.40	468.00
CC-UnsatC-0.6m-03	0.6	1.5	<0.4	231.00	456.00
CC-UnsatC-0.8m-03	0.8	1.68	<0.4	10.80	457.00
CC-UnsatC-0.9m-03	0.9	-	-	-	-
CC-UnsatC-0.2m-04	0.2	1.6	<0.4	14.60	471.00
CC-UnsatC-0.3m-04	0.3	1.63	<0.4	23.40	470.00
CC-UnsatC-0.4m-04	0.4	1.62	<0.4	<0.4	469.00
CC-UnsatC-0.5m-04	0.5	1.66	<0.4	33.60	462.00
CC-UnsatC-0.6m-04	0.6	-	-	-	-
CC-UnsatC-0.8m-04	0.8	1.74	<0.4	20.50	456.00
CC-UnsatC-0.9m-04	0.9	-	-	-	-
CC-UnsatC-0.2m-05	0.2	1.53	<0.4	5.86	468.00
CC-UnsatC-0.3m-05	0.3	1.59	<0.4	11.90	463.00
CC-UnsatC-0.4m-05	0.4	1.56	<0.4	<0.4	465.00
CC-UnsatC-0.5m-05	0.5	1.65	<0.4	24.90	460.00
CC-UnsatC-0.6m-05	0.6	1.54	<0.4	16.30	456.00
CC-UnsatC-0.8m-05	0.8	1.73	<0.4	22.30	453.00
CC-UnsatC-0.9m-05	0.9	-	-	-	-
CC-UnsatC-0.2m-06	0.2	1.53	<0.4	4.72	466.00
CC-UnsatC-0.3m-06	0.3	1.62	<0.4	11.40	463.00
CC-UnsatC-0.4m-06	0.4	1.58	<0.4	<0.4	460.00
CC-UnsatC-0.5m-06	0.5	1.6	<0.4	25.10	460.00
CC-UnsatC-0.6m-06	0.6	1.45	<0.4	20.60	448.00
CC-UnsatC-0.8m-06	0.8	1.63	<0.4	25.90	445.00
CC-UnsatC-0.9m-06	0.9	-	-	-	-

Table D-3. continued

Sample ID	Height in Column (m)	NO ₂	NO ₃	PO ₄
CC-SatC-0.2m-01	0.2	<0.2	<0.4	1.14
CC-SatC-0.3m-01	0.3	<0.2	<0.4	1.13
CC-SatC-0.4m-01	0.4	<0.2	<0.4	<1

CC-SatC-0.5m-01	0.5	<0.2	<0.4	1.15
CC-SatC-0.6m-01	0.6	<0.2	<0.4	1.16
CC-SatC-0.7m-01	0.7	<0.2	<0.4	<1
CC-SatC-0.8m-01	0.8	<0.2	<0.4	<1
CC-SatC-0.9m-01	0.9	<0.2	<0.4	<1
CC-SatC-1.0m-01	1.0	<0.2	1.68	<1
CC-SatC-1.1m-01	1.1	<0.2	<0.4	<1
CC-SatC-1.2m-01	1.2	<0.2	<0.4	<1
CC-SatC-1.3m-01	1.3	<0.2	<0.4	<1
CC-SatC-1.4m-01	1.4	<0.2	8.3	<1
CC-SatC-0.2m-02	0.2	<0.2	<0.4	<1
CC-SatC-0.3m-02	0.3	<0.2	<0.4	1.18
CC-SatC-0.4m-02	0.4	<0.2	<0.4	1.06
CC-SatC-0.5m-02	0.5	<0.2	<0.4	1.18
CC-SatC-0.6m-02	0.6	<0.2	<0.4	1.21
CC-SatC-0.7m-02	0.7	<0.2	<0.4	<1
CC-SatC-0.8m-02	0.8	<0.2	<0.4	<1
CC-SatC-0.9m-02	0.9	<0.2	1.77	<1
CC-SatC-1.0m-02	1.0	<0.2	4.89	<1
CC-SatC-1.1m-02	1.1	<0.2	0.43	<1
CC-SatC-1.2m-02	1.2	<0.2	1.31	<1
CC-SatC-1.3m-02	1.3	<0.2	1.1	<1
CC-SatC-1.4m-02	1.4	<0.2	2.45	<1
CC-SatC-0.2m-03	0.2	<0.2	<0.4	<1
CC-SatC-0.3m-03	0.3	<0.2	<0.4	1.17
CC-SatC-0.4m-03	0.4	<0.2	<0.4	<1
CC-SatC-0.5m-03	0.5	<0.2	<0.4	1.11
CC-SatC-0.6m-03	0.6	<0.2	<0.4	1.22
CC-SatC-0.7m-03	0.7	<0.2	<0.4	1.16
CC-SatC-0.8m-03	0.8	<0.2	<0.4	<1
CC-SatC-0.9m-03	0.9	<0.2	<0.4	<1
CC-SatC-1.0m-03	1.0	<0.2	9.59	<1
CC-SatC-1.1m-03	1.1	<0.2	1.31	<1
CC-SatC-1.2m-03	1.2	<0.2	4.59	<1
CC-SatC-1.3m-03	1.3	<0.2	1.66	<1
CC-SatC-1.4m-03	1.4	<0.2	<0.4	<1
CC-SatC-0.2m-04	0.2	<0.2	<0.4	1.15
CC-SatC-0.3m-04	0.3	<0.2	<0.4	1.26
CC-SatC-0.4m-04	0.4	<0.2	<0.4	1.15
CC-SatC-0.5m-04	0.5	<0.2	<0.4	1.19
CC-SatC-0.6m-04	0.6	<0.2	<0.4	1.23
CC-SatC-0.7m-04	0.7	<0.2	0.81	1.12
CC-SatC-0.8m-04	0.8	<0.2	<0.4	<1
CC-SatC-0.9m-04	0.9	<0.4	0.93	<2
CC-SatC-1.0m-04	1.0	<0.2	19.9	<1
CC-SatC-1.1m-04	1.1	<0.2	5.53	<1

CC-SatC-1.2m-04	1.2	<0.2	10.5	<1
CC-SatC-1.3m-04	1.3	1.43	6.72	<1
CC-SatC-1.4m-04	1.4	1.24	0.42	<1
CC-SatC-0.2m-05	0.2	<0.2	<0.4	<1
CC-SatC-0.3m-05	0.3	<0.2	<0.4	<1
CC-SatC-0.4m-05	0.4	<0.2	<0.4	<1
CC-SatC-0.5m-05	0.5	<0.2	<0.4	<1
CC-SatC-0.6m-05	0.6	<0.2	<0.4	<1
CC-SatC-0.7m-05	0.7	<0.2	<0.4	<1
CC-SatC-0.8m-05	0.8	<0.2	0.47	<1
CC-SatC-0.9m-05	0.9	<0.2	<0.4	<1
CC-SatC-1.0m-05	1.0	<0.2	25.60	<1
CC-SatC-1.1m-05	1.1	<0.2	17.00	<1
CC-SatC-1.2m-05	1.2	0.59	16.10	<1
CC-SatC-1.3m-05	1.3	0.52	8.49	<1
CC-SatC-1.4m-05	1.4	<0.2	0.89	<1
CC-SatC-0.2m-06	0.2	<0.2	<0.4	<1
CC-SatC-0.3m-06	0.3	<0.2	<0.4	<1
CC-SatC-0.4m-06	0.4	<0.2	<0.4	<1
CC-SatC-0.5m-06	0.5	<0.2	<0.4	<1
CC-SatC-0.6m-06	0.6	<0.2	<0.4	<1
CC-SatC-0.7m-06	0.7	<0.2	<0.4	<1
CC-SatC-0.8m-06	0.8	<0.2	<0.4	<1
CC-SatC-0.9m-06	0.9	<0.2	<0.4	<1
CC-SatC-1.0m-06	1.0	<0.2	28.30	<1
CC-SatC-1.1m-06	1.1	<0.2	22.90	<1
CC-SatC-1.2m-06	1.2	0.58	17.90	<1
CC-SatC-1.3m-06	1.3	0.40	6.68	<1
CC-SatC-1.4m-06	1.4	<0.2	0.89	<1
CC-SatC-0.2m-07	0.2	<0.2	<0.4	<1
CC-SatC-0.3m-07	0.3	<0.2	<0.4	<1
CC-SatC-0.4m-07	0.4	<0.2	<0.4	<1
CC-SatC-0.5m-07	0.5	<0.2	<0.4	<1
CC-SatC-0.6m-07	0.6	<0.2	<0.4	2.34
CC-SatC-0.7m-07	0.7	<0.2	<0.4	1.96
CC-SatC-0.8m-07	0.8	<0.2	<0.4	1.89
CC-SatC-0.9m-07	0.9	<0.2	<0.4	<1
CC-SatC-1.0m-07	1.0	<0.2	32.60	<1
CC-SatC-1.1m-07	1.1	<0.2	32.40	<1
CC-SatC-1.2m-07	1.2	0.79	18.90	<1
CC-SatC-1.3m-07	1.3	0.27	5.14	<1
CC-SatC-1.4m-07	1.4	<0.2	1.49	<1
CC-SatC-0.2m-08	0.2	<0.2	<0.4	1.89
CC-SatC-0.3m-08	0.3	<0.2	<0.4	1.95
CC-SatC-0.4m-08	0.4	-	-	-
CC-SatC-0.5m-08	0.5	<0.2	<0.4	1.70

CC-SatC-0.6m-08	0.6	<0.2	<0.4	1.87
CC-SatC-0.7m-08	0.7	<0.2	<0.4	1.78
CC-SatC-0.8m-08	0.8	<0.2	<0.4	1.78
CC-SatC-0.9m-08	0.9	<0.2	<0.4	<1
CC-SatC-1.0m-08	1.0	<0.2	33.80	<1
CC-SatC-1.1m-08	1.1	<0.2	33.40	<1
CC-SatC-1.2m-08	1.2	0.24	15.50	1.57
CC-SatC-1.3m-08	1.3	<0.2	0.56	<1
CC-SatC-1.4m-08	1.4	<0.2	<0.4	<1
CC-UnsatC-0.2m-01	0.2	<0.2	<0.4	1.20
CC-UnsatC-0.3m-01	0.3	<0.2	<0.4	1.12
CC-UnsatC-0.4m-01	0.4	<0.2	<0.4	1.06
CC-UnsatC-0.5m-01	0.5	<0.2	<0.4	1.14
CC-UnsatC-0.6m-01	0.6	<0.2	<0.4	<1
CC-UnsatC-0.8m-01	0.8	<0.2	<0.4	1.16
CC-UnsatC-0.9m-01	0.9	<0.2	<0.4	1.14
CC-UnsatC-0.2m-02	0.2	<0.2	<0.4	1.25
CC-UnsatC-0.3m-02	0.3	<0.2	<0.4	1.18
CC-UnsatC-0.4m-02	0.4	<0.2	<0.4	1.25
CC-UnsatC-0.5m-02	0.5	<0.2	<0.4	1.25
CC-UnsatC-0.6m-02	0.6	<0.2	<0.4	<1
CC-UnsatC-0.8m-02	0.8	<0.2	<0.4	1.32
CC-UnsatC-0.9m-02	0.9	-	-	-
CC-UnsatC-0.2m-03	0.2	<0.2	<0.4	1.25
CC-UnsatC-0.3m-03	0.3	<0.2	<0.4	<1
CC-UnsatC-0.4m-03	0.4	<0.2	<0.4	<1
CC-UnsatC-0.5m-03	0.5	<0.2	<0.4	<1
CC-UnsatC-0.6m-03	0.6	<0.2	<0.4	<1
CC-UnsatC-0.8m-03	0.8	<0.2	<0.4	<1
CC-UnsatC-0.9m-03	0.9	-	-	-
CC-UnsatC-0.2m-04	0.2	<0.2	<0.4	1.36
CC-UnsatC-0.3m-04	0.3	<0.2	<0.4	1.14
CC-UnsatC-0.4m-04	0.4	<0.2	<0.4	1.17
CC-UnsatC-0.5m-04	0.5	<0.2	<0.4	1.25
CC-UnsatC-0.6m-04	0.6	-	-	-
CC-UnsatC-0.8m-04	0.8	<0.2	<0.4	1.15
CC-UnsatC-0.9m-04	0.9	-	-	-
CC-UnsatC-0.2m-05	0.2	<0.2	<0.4	<1
CC-UnsatC-0.3m-05	0.3	<0.2	<0.4	<1
CC-UnsatC-0.4m-05	0.4	<0.2	<0.4	<1
CC-UnsatC-0.5m-05	0.5	<0.2	<0.4	<1
CC-UnsatC-0.6m-05	0.6	<0.2	<0.4	<1
CC-UnsatC-0.8m-05	0.8	<0.2	<0.4	<1
CC-UnsatC-0.9m-05	0.9	-	-	-

CC-UnsatC-0.2m-06	0.2	<0.2	<0.4	1.04
CC-UnsatC-0.3m-06	0.3	<0.2	<0.4	<1
CC-UnsatC-0.4m-06	0.4	<0.2	<0.4	<1
CC-UnsatC-0.5m-06	0.5	<0.2	<0.4	<1
CC-UnsatC-0.6m-06	0.6	<0.2	<0.4	<1
CC-UnsatC-0.8m-06	0.8	<0.2	<0.4	<1
CC-UnsatC-0.9m-06	0.9	-	-	-

APPENDIX E: PHREEQC OUTPUT AND CORRELATION ANALYSIS

Table E-1: Pearson correlation matrix and p-values of major lysimeter pore water constituents. Top right triangle represents raw data, while the bottom left triangle represents centred log-ratio transformed data. Green represents significant correlations ($p < 0.05$), red represents strong negative correlations ($R < -0.6$), and blue represents strong positive correlations ($R > 0.6$)

	Alkalinity	NH ₃ -N	F	Cl	SO ₄	Ba	Ca	K	Mg	Na
Alkalinity	NT	-0.21953	0.116118	-0.08131	-0.49733	0.286749	-0.60911	-0.3923	-0.57287	-0.2878
	CLRT	0.114	0.408	0.562	0.000152	0.0374	1.3E-06	0.00367	7.37E-06	0.0366
NH ₃ -N	0.152963		0.024145	-0.21033	-0.06074	-0.05515	0.122208	0.284556	0.174888	0.027319
	0.274		0.864	0.131	0.666	0.695	0.383	0.0389	0.21	0.846
F	0.714178	0.284778		0.093039	-0.224	0.287728	-0.33099	-0.16658	-0.25671	-0.12715
	1.92E-09	0.0388		0.508	0.107	0.0367	0.0155	0.233	0.0635	0.364
Cl	0.306855	-0.10308	0.133209		0.202099	-0.09233	-0.08119	0.113729	0.012613	0.449422
	0.0254	0.463	0.342		0.147	0.511	0.563	0.417	0.921	0.000736
SO ₄	-0.51541	-0.50923	-0.57421	-0.36747		-0.46665	0.750712	0.590511	0.779788	0.653943
	7.84E-05	9.86E-05	6.94E-06	0.00679		0.000428	9.6E-11	3.25E-06	5.97E-12	1.1E-07
Ba	0.647343	0.457404	0.705882	0.199296	-0.60688		-0.60467	-0.45058	-0.54993	-0.4515
	1.62E-07	0.000574	3.56E-09	0.153	1.46E-06		1.63E-06	0.00071	0.00002	0.00069
Ca	-0.67626	-0.49167	-0.67476	-0.30365	0.365742	-0.80228		0.626667	0.957157	0.539248
	2.74E-08	0.000185	3.02E-08	0.0271	0.00708	5.13E-13		5.17E-07	4.11E-29	0.000031
K	-0.37703	-2.3E-05	-0.33605	-0.15722	-0.09911	-0.41788	0.399517		0.691039	0.693309
	0.00539	0.999	0.0139	0.261	0.48	0.00185	0.00304		1.02E-08	8.72E-09
Mg	-0.77285	-0.41036	-0.69481	-0.32812	0.344772	-0.78347	0.930543	0.461563		0.662808
	1.2E-11	0.00227	7.85E-09	0.0165	0.0115	4.07E-12	6.68E-24	0.000504		6.41E-08
Na	0.455759	-0.10026	0.375847	0.37794	-0.42371	0.093171	-0.24737	0.205397	-0.24967	NT
	0.000605	0.475	0.00555	0.00527	0.00157	0.507	0.0741	0.14	0.0714	CLRT

Table E-2: PHREEQC output for select column experiment samples. Charge balance error (CBE) and saturation indices of specific minerals are reported.

Sample ID	Saturation Indices (SI)						
	CBE (%)	Pyrite	Gypsum	Calcite	Dolomite (D)	Dolomite	Siderite
CC-SatC-0.2 m-01	-0.79	19.47	-1.63	1.05	1.64	2.20	-3.34
CC-SatC-0.3 m-01	-2.57	14.73	-1.62	0.81	1.01	1.57	-3.41
CC-SatC-0.4 m-01	-1.05	24.76	-1.69	0.91	1.23	1.79	-3.89
CC-SatC-0.5 m-01	-2.37	14.57	-1.93	0.89	1.19	1.75	-3.23
CC-SatC-0.6 m-01	-2.37	14.23	-1.84	0.93	1.26	1.83	-3.60
CC-SatC-0.7 m-01	1.72	13.87	-1.25	1.04	1.38	1.94	-3.87
CC-SatC-0.8 m-01	-2.51	14.08	-1.51	1.13	1.64	2.21	-3.68
CC-SatC-0.9 m-01	0.06	13.89	-0.43	0.93	1.38	1.94	-2.51
CC-SatC-1.0 m-01	-1.10	-1000.00	0.01	-1.18	-2.63	-2.06	-4.57
CC-SatC-1.1 m-01	-0.37	-1000.00	-0.18	-2.03	-4.68	-4.11	-5.29
CC-SatC-1.2 m-01	-13.50	-1000.00	-0.47	-1.34	-3.34	-2.77	-4.44

CC-SatC-1.3 m-01	-17.18	-1000.00	-0.52	-1.61	-3.79	-3.22	-4.65
CC-SatC-1.4 m-01	-26.95	-1000.00	-1.51	-2.61	-5.74	-5.17	-4.94
CC-SatC-0.3 m-02	6.29	14.52	-3.09	0.95	1.35	1.91	-3.60
CC-SatC-0.4 m-02	-1.24	13.72	-2.09	1.08	1.59	2.15	-1.80
CC-SatC-0.5 m-02	0.35	10.75	-2.13	1.17	1.79	2.35	-1.74
CC-SatC-0.6 m-02	6.96	11.40	-3.24	1.14	1.70	2.27	-1.76
CC-SatC-0.7 m-02	-2.69	9.70	-2.05	1.13	1.64	2.20	-1.73
CC-SatC-0.8 m-02	-2.30	13.58	-1.80	1.03	1.42	1.98	-4.09
CC-SatC-0.9 m-02	6.64	9.44	-0.30	1.43	2.48	3.04	-2.00
CC-SatC-1.0 m-02	84.04	-1000.00	-1.38	-0.16	-0.74	-0.18	-3.52
CC-SatC-1.1 m-02	-2.45	15.81	-0.20	-1.09	-2.79	-2.23	-4.35
CC-SatC-1.2 m-02	-2.52	16.50	-0.35	-0.71	-2.00	-1.43	-3.88
CC-SatC-1.3 m-02	-12.46	17.24	-0.73	-1.02	-2.62	-2.06	-3.90
CC-SatC-1.4 m-02	-15.10	-1000.00	-1.93	-1.99	-4.52	-3.96	-4.07
CC-SatC-0.4 m-03	1.17	16.55	-2.75	1.15	1.74	2.30	-1.78
CC-SatC-0.5 m-03	0.43	21.41	-2.38	1.10	1.64	2.20	-2.23
CC-SatC-0.6 m-03	1.41	15.57	-3.20	1.09	1.59	2.16	-2.55
CC-SatC-0.7 m-03	-0.54	18.87	-2.40	1.18	1.76	2.32	-3.03
CC-SatC-0.8 m-03	-1.90	14.77	-1.86	1.04	1.48	2.05	-3.76
CC-SatC-0.9 m-03	-0.48	23.46	-0.28	1.25	2.10	2.67	-3.03
CC-SatC-1.0 m-03	-3.02	17.48	-0.02	-0.19	-0.89	-0.32	-3.72
CC-SatC-1.1 m-03	-14.57	-1000.00	-0.29	-0.78	-2.17	-1.61	-4.02
CC-SatC-1.2 m-03	-4.54	20.65	-1.34	-0.55	-1.67	-1.11	-3.39
CC-SatC-1.3 m-03	-1.85	18.66	-2.51	-1.63	-3.81	-3.25	-4.14
CC-SatC-0.2 m-04	5.48	20.84	-2.33	1.08	1.61	2.17	-4.47
CC-SatC-0.3 m-04	4.71	17.34	-3.52	1.07	1.62	2.19	-1.82
CC-SatC-0.4 m-04	2.87	18.60	-2.55	1.01	1.46	2.03	-2.34
CC-SatC-0.5 m-04	3.00	19.39	-2.57	0.94	1.32	1.89	-2.89
CC-SatC-0.6 m-04	4.50	22.79	-3.21	1.22	1.98	2.55	-2.71
CC-SatC-0.7 m-04	4.46	21.10	-2.44	1.02	1.49	2.05	-4.49
CC-SatC-0.8 m-04	6.27	13.95	-3.03	1.11	1.67	2.23	-3.66
CC-SatC-0.9 m-04	0.31	13.65	-0.36	1.09	1.74	2.30	-3.26
CC-SatC-1.0 m-04	-3.93	20.56	-0.04	0.43	0.27	0.83	-4.68
CC-SatC-1.1 m-04	-2.65	20.16	-0.24	-0.36	-1.33	-0.77	-4.70
CC-SatC-1.2 m-04	-9.11	19.98	-1.47	-0.43	-1.42	-0.86	-4.41
CC-SatC-1.3 m-04	-12.41	-1000.00	-2.98	-1.27	-3.07	-2.51	-3.31
CC-SatC-0.2 m-05	4.75	22.18	-2.84	1.14	1.81	2.37	-3.33
CC-SatC-0.3 m-05	3.73	-1000.00	-3.38	1.05	1.83	2.39	-3.81
CC-SatC-0.4 m-05	6.47	22.15	-2.73	1.04	1.57	2.12	-2.59
CC-SatC-0.5 m-05	10.80	22.85	-2.58	1.03	1.54	2.10	-3.24
CC-SatC-0.6 m-05	6.46	22.91	-3.30	1.07	1.71	2.27	-3.21
CC-SatC-0.7 m-05	10.08	22.78	-2.53	0.97	1.46	2.01	-3.72
CC-SatC-0.8 m-05	5.99	15.41	-2.93	1.03	1.63	2.19	-2.81
CC-SatC-0.9 m-05	2.42	20.91	-0.69	1.03	1.76	2.32	-2.02
CC-SatC-1.0 m-05	-1.22	18.94	-0.20	0.31	0.10	0.66	-4.24
CC-SatC-1.1 m-05	-3.16	-1000.00	-0.38	-0.23	-0.98	-0.43	-4.46

CC-SatC-1.2 m-05	-8.93	19.40	-1.90	-0.46	-1.41	-0.85	-4.64
CC-SatC-1.3 m-05	-17.94	19.62	-3.01	-1.33	-3.11	-2.56	-4.88
CC-SatC-0.2 m-06	-1.28	23.10	-2.63	0.99	1.49	2.05	-3.70
CC-SatC-0.3 m-06	-0.72	22.61	-3.24	1.05	1.72	2.29	-4.21
CC-SatC-0.4 m-06	-0.10	22.96	-2.94	1.08	1.65	2.22	-3.69
CC-SatC-0.5 m-06	-0.48	23.27	-3.02	1.02	1.48	2.05	-3.35
CC-SatC-0.6 m-06	0.26	23.03	-3.03	0.94	1.38	1.94	-3.65
CC-SatC-0.7 m-06	-0.89	22.20	-2.59	1.01	1.50	2.07	-4.33
CC-SatC-0.8 m-06	0.75	16.67	-2.94	1.04	1.59	2.15	-3.24
CC-SatC-0.9 m-06	0.78	24.91	-0.99	0.89	1.49	2.05	-1.97
CC-SatC-1.0 m-06	-1.70	19.03	-0.31	0.47	0.41	0.97	-4.09
CC-SatC-1.1 m-06	-3.08	19.29	-0.49	-0.11	-0.76	-0.20	-4.34
CC-SatC-1.2 m-06	-10.34	-1000.00	-2.03	-0.36	-1.22	-0.66	-4.66
CC-SatC-1.3 m-06	-13.19	-1000.00	-3.13	-1.45	-3.40	-2.83	-2.65
CC-SatC-0.2 m-07	0.55	23.78	-3.22	1.10	1.65	2.21	-3.46
CC-SatC-0.3 m-07	-1.14	23.60	-3.40	1.10	1.76	2.33	-4.07
CC-SatC-0.4 m-07	7.08	22.96	-3.07	1.06	1.54	2.11	-3.70
CC-SatC-0.5 m-07	0.76	23.61	-3.19	1.15	1.81	2.38	-3.97
CC-SatC-0.6 m-07	-0.26	22.58	-3.12	1.13	1.81	2.37	-4.13
CC-SatC-0.7 m-07	1.13	23.18	-2.63	1.08	1.60	2.17	-4.09
CC-SatC-0.8 m-07	-1.10	24.18	-2.70	1.08	1.67	2.23	-3.65
CC-SatC-0.9 m-07	-2.39	29.23	-0.90	1.03	1.69	2.25	-3.17
CC-SatC-1.0 m-07	0.34	20.85	-0.42	0.50	0.44	1.00	-5.85
CC-SatC-1.1 m-07	-6.83	21.42	-0.57	0.09	-0.42	0.15	-5.85
CC-SatC-1.2 m-07	-11.56	21.19	-2.03	-0.48	-1.54	-0.98	-6.06
CC-SatC-1.3 m-07	-11.16	22.08	-3.16	-1.80	-4.17	-3.61	-6.38
CC-UnsatC-0.9 m-01	-3.43	27.51	-1.81	0.99	1.40	1.97	-2.39
CC-UnsatC-0.8 m-01	0.34	17.87	-1.41	0.73	0.84	1.41	-3.71
CC-UnsatC-0.6 m-01	-6.40	24.43	-0.82	1.10	1.48	2.04	-3.79
CC-UnsatC-0.5 m-01	-0.01	14.30	-1.75	0.99	1.36	1.92	-3.77
CC-UnsatC-0.4 m-01	-0.46	14.70	-1.61	0.95	1.28	1.85	-3.87
CC-UnsatC-0.3 m-01	-1.22	15.38	-1.47	0.97	1.32	1.88	-3.70
CC-UnsatC-0.2 m-01	-2.57	16.09	-1.71	0.98	1.38	1.95	-3.24
CC-UnsatC-0.8 m-02	1.56	13.99	-3.23	1.05	1.50	2.07	-2.90
CC-UnsatC-0.6 m-02	-5.94	12.70	-1.45	1.28	1.92	2.48	-3.49
CC-UnsatC-0.5 m-02	-2.00	13.65	-3.25	1.04	1.53	2.09	-2.78
CC-UnsatC-0.4 m-02	0.11	11.20	-3.45	0.91	1.27	1.84	-1.89
CC-UnsatC-0.3 m-02	0.51	12.11	-2.74	1.10	1.57	2.13	-1.86
CC-UnsatC-0.2 m-02	0.89	11.92	-3.39	1.05	1.55	2.12	-1.79
CC-UnsatC-0.8 m-03	7.41	15.61	-3.04	1.24	1.89	2.46	-1.71
CC-UnsatC-0.6 m-03	-5.90	12.48	-1.66	1.21	1.79	2.35	-3.55
CC-UnsatC-0.5 m-03	0.48	14.10	-2.38	1.19	1.79	2.35	-1.85
CC-UnsatC-0.4 m-03	1.33	19.25	-4.80	1.24	1.93	2.49	-2.37
CC-UnsatC-0.3 m-03	1.84	13.21	-2.69	1.05	1.54	2.11	-1.78
CC-UnsatC-0.2 m-03	1.86	21.42	-2.69	1.00	1.44	2.01	-3.88
CC-UnsatC-0.5 m-04	5.37	22.32	-2.55	1.17	1.77	2.33	-2.17

CC-UnsatC-0.4 m-04	8.14	19.83	-4.75	1.12	1.65	2.21	-2.55
CC-UnsatC-0.3 m-04	3.98	17.16	-2.69	1.11	1.63	2.19	-0.22
CC-UnsatC-0.2 m-04	3.08	19.63	-2.90	1.10	1.62	2.18	-2.70
CC-UnsatC-0.8m-05	8.64	21.37	-2.72	1.06	1.58	2.13	-2.72
CC-UnsatC-0.6 m-05	4.69	20.60	-2.83	1.06	1.59	2.14	-3.48
CC-UnsatC-0.5 m-05	5.24	20.44	-2.67	1.05	1.59	2.14	-3.48
CC-UnsatC-0.4 m-05	6.38	21.94	-4.77	1.06	1.60	2.15	-3.30
CC-UnsatC-0.3 m-05	5.66	22.18	-2.96	1.15	1.76	2.31	-3.12
CC-UnsatC-0.2 m-05	7.34	22.55	-3.30	1.08	1.66	2.21	-2.66
CC-UnsatC-0.8m-06	-1.22	23.35	-2.71	1.08	1.60	2.16	-4.38
CC-UnsatC-0.6 m-06	2.93	22.86	-2.73	1.14	1.70	2.26	-4.57
CC-UnsatC-0.5 m-06	5.88	23.15	-2.70	1.10	1.70	2.26	-5.01
CC-UnsatC-0.4 m-06	10.88	23.39	-4.74	1.13	1.70	2.27	-4.28
CC-UnsatC-0.3 m-06	8.64	23.17	-2.97	1.16	1.73	2.30	-4.04
CC-UnsatC-0.2 m-06	10.92	23.83	-3.38	1.07	1.59	2.16	-3.54

Table E-3: PHREEQC output for select lysimeter samples. Charge balance error (CBE) and saturation indices of specific minerals are reported.

Sample ID	CBE (%)	Saturation Indices (SI)					
		Pyrite	Gypsum	Calcite	Dolomite (D)	Dolomite	Siderite
US-L1-P175	-5.99	19.79	-0.06	0.68	0.84	1.41	-1.55
US-L1-P200	-3.01	22.54	-0.23	0.80	1.13	1.68	-3.46
US-L1-P225	-4.98	17.31	-0.51	0.95	1.53	2.08	-0.55
L1 1.65-1.8 m (interface)	1.76	19.52	-0.33	0.53	0.68	1.24	0.65
L1 1.8-1.95 m (interface)	-6.14	21.28	-0.49	0.70	0.95	1.52	0.63
L1 2.4-2.55 m	4.24	14.47	-2.59	0.23	-0.11	0.45	-3.52
L1 2.55-2.7 m	4.93	15.52	-2.57	0.49	0.38	0.95	-2.97
L2 1.15-1.35 m	2.82	20.48	-2.74	0.54	0.48	1.05	-2.65
L2 1.35-1.5 m	6.95	17.21	-1.76	0.21	-0.16	0.40	-2.66
L2 2.15-2.3 m	30.36	17.30	-3.10	0.48	0.35	0.92	-1.52
L2 2.3-2.45 m	0.79	16.28	-3.39	0.52	0.43	0.99	-2.94
L2 2.45-2.6 m	-0.97	16.19	-3.58	0.46	0.31	0.87	-3.07
US-L3-P300C	11.66	22.49	-1.26	0.67	0.56	1.13	-3.16
US-L3-P300	-23.31	20.82	-1.16	0.26	-0.25	0.30	-3.30
L3 0.15-0.3 m	18.06	23.53	-0.98	0.79	1.05	1.61	-3.11
L3 0.3-0.45 m	-20.14	22.01	-2.51	0.52	0.48	1.04	-5.10
US-L4-P050	-0.55	23.11	-0.14	0.69	0.70	1.26	-0.85
US-L4-P075	-9.75	22.65	-0.26	-0.10	-0.97	-0.41	0.26
US-L4-P100	-4.61	22.63	-0.31	0.61	0.60	1.17	-2.48
US-L4-P125	-2.48	19.88	-0.37	0.61	0.81	1.36	-3.11
US-L4-P150	-1.40	24.67	-0.59	0.96	1.62	2.17	-1.56
US-L4-P175	3.86	16.95	-0.91	0.85	1.30	1.86	-0.57
L4 1.4-1.55 m	6.60	19.38	-1.62	0.51	0.57	1.13	-2.07
L4 1.55-1.7 m	2.50	19.48	-3.37	0.41	0.25	0.82	-1.99

L4 1.7-1.85 m	1.94	17.79	-3.48	0.52	0.48	1.05	-1.91
L4 2.2-2.35 m	5.70	17.86	-1.57	0.70	0.78	1.35	-2.03
L4 2.5-2.65 m	6.29	16.62	-2.17	0.66	0.75	1.32	-1.98
US-L5-P050	10.03	19.35	0.05	0.79	1.32	1.86	-1.65
US-L5-P075	5.70	-1000.00	-0.01	0.31	0.24	0.78	-1000.00
US-L5-P100	3.27	21.43	-0.18	0.71	1.00	1.54	-0.20
US-L5-P125	4.02	17.72	-0.48	1.31	2.21	2.76	-1.05
US-L5-P300C	0.52	13.77	-2.29	0.94	1.70	2.24	-1.63
L5 1.25-1.4 m	1.37	18.95	-2.17	0.41	0.26	0.82	0.42
L5 2.25-2.4 m	7.22	18.80	-1.00	0.68	0.68	1.24	0.01
L5 2.4-2.55 m	0.61	17.07	-3.31	0.35	0.12	0.69	-1.02
L5 2.55-2.7 m	3.45	15.19	-3.37	0.45	0.29	0.86	-2.87
US-L6-P300C	4.42	26.24	-1.73	0.32	-0.27	0.28	-1.10
US-L6-P300	-5.24	24.65	-1.56	0.29	-0.36	0.18	-2.20
US-L6-P275	-4.19	22.59	-0.98	0.52	0.15	0.69	0.57
US-L6-P250	-5.63	22.69	-1.11	0.56	0.46	1.00	0.42
US-L6-P225	10.45	25.58	-1.29	1.07	1.70	2.23	-2.70
US-L6-P200	0.02	13.27	-1.02	0.65	0.99	1.52	-0.35
US-L6-P175	-47.83	18.23	-0.94	0.51	0.76	1.29	-1.17
US-L6-P150	-0.69	22.62	-0.84	0.98	1.63	2.18	-4.81